공학박사학위논문

디젤 엔진 EGR 쿨러의 파울링 특성에 관한 연구

A Study on Fouling Characteristics of EGR Coolers in Diesel Engine

2014 년 2 월

서울대학교 대학원

기계항공공학부

이 준

디젤 엔진 EGR 쿨러의 파울링 특성에 관한 연구

A Study on Fouling Characteristics of EGR Coolers in Diesel Engine

지도교수 민 경 덕

이 논문을 공학박사 학위논문으로 제출함

2014 년 2 월

서울대학교 대학원
기계항공공학부
이 준

이준의 공학박사 학위논문을 인준함

2013 년 12 월

위 원 장	고 상 근	(인)
부위원장	민 경 덕	(인)
위 원	이 동 준	(인)
위 원	송 한 호	(인)
위 원	이 진 욱	(인)

Acknowledgements

This project on my Ph.D thesis would not be happened without the advices and helps of following people.

First and foremost, I would like to express my respect and gratitude to my advisor, Professor Kyoungdoug Min. During the graduate course, my knowledge were grown up with his invaluable advices. He gave the inspirations of this study and his guidance and encouragement were the source of power overcoming many difficulties during the project.

I would like to special thanks to the project members who offered assistance, valuable discussions and beautiful memories of friendship. Minje Kim, Seunghyun Lee, Seungha Lee, Jeongwoo Lee, Namho Kim, Joohan Kim, Hwanyoung Oh, jungyeon Lee, Seokwon Cho, Dongsu Kim, Minje Park, Jaeman Park, Yunwoo Lee, Jinhi Kim and Gyujin Kim assisted lots of the study. This work would never have been achieved without their efforts and patients. Also, I'd like to thanks to all of my graduate schoolmates for unforgettably joyful lab life.

I would like to present my deepest love and gratitude to my wife, Yeonsook Yoo, for her great sacrifice, thoughtful consideration, unimaginable patience, and endless love. My daughters and son-in-law, Sua Lee, Hyunah Lee, and Heuiwon Han, were my emotional anchor. And my honorable Father-in law, Dr. Heungkun Yoo, gave me the direction of life during my life. It was, it is, and it will be the greatest happiness in my life to be with my family. *I love you*.

Abstract

A Study on Fouling Characteristics
of EGR Coolers in Diesel Engine

Joon Lee

Department of Mechanical and Aerospace Engineering

The Graduate School

Seoul National University

In recent years, HSDI (high speed direct injection) diesel engines have been largely applied to RV, SUV and passenger cars due to good fuel economy, high thermal efficiency and very low carbon dioxide emissions. However, worldwide environmental issues such as global warming have led to ever tightening exhaust emission legislations for passenger diesel vehicles, especially on NO_x and PM emissions. For example, Euro-6 emission legislation enforced since 2014 mandates that NO_x emissions should be reduced by 56% more than the current Euro-5.

An exhaust gas recirculation (EGR) system has been widely applied to diesel engines to reduce NO_x emissions without a large modification on the engine body. The principle of EGR is to reduce the temperatures of flame and the oxygen concentration of working fluid in a combustion chamber; thereby, reducing NO_x emissions. The existing EGR system uses only EGR valve to reduce NO_x emissions, resulting in increase in PM emissions. Therefore, modification on the system is required to avoid the PM penalty. Recently, numerous researches have been actively conducted to reduce NO_x emissions as

well as to overcome the disadvantages of deteriorating PM and fuel consumption through a new EGR cooler system.

In order to satisfy the strict Euro-6 NO_x emission standard, the use of a high EGR rate becomes more crucial. If a high EGR rate is applied, PM emissions will be inevitably increased. Practically, high concentration of PM in the exhaust gas is relatively easy to be deposited on the surface of an EGR cooler. This is so-called fouling which deteriorates the thermal effectiveness of an EGR cooler and increases the pressure drop through it. As a result, the NO_x reduction rate and the performance of an engine will be decreased. On the other hand, recent combustion technologies of HSDI diesel engine such as LTC (low temperature combustion) diesel engine and ultra-high pressure fuel injection system lead to severe fouling phenomena because smaller sized particles deposit on the inner surface of an EGR cooler. Accordingly, many studies have been conducted in the field of EGR cooler fouling. However, there are few researches concerning the cross correlation on the fouling phenomena between a test rig and a real engine.

In this study, the design features of existing and modified EGR coolers were reviewed to maintain desired performance against fouling resistance. The behavior of fluid such as velocity vector, temperature and pressure contour of exhaust gases in EGR cooler was analyzed through 3-D CFD (Computational Fluid Dynamics). The results which consist of outlet temperatures, heat transfer effectiveness and pressure drops and so on were obtained by using 2 kinds of EGR coolers in production and another 2 kinds of modified EGR coolers.

Then, the characteristics of the above EGR coolers on a test rig were investigated at clean and fouled conditions. During this step, fouling resistances which are directly related to the heat transfer effectiveness were verified with gas velocities. In addition, the characteristics of EGR coolers on engine dynamometers were evaluated at clean and fouled conditions. The fouling test

mode was made on the basis of ESC 13 mode and proposal from an EGR cooler manufacturer. The characteristics of heat transfer effectiveness and pressure drop were examined with EGR mass flow rates. For the further analyses on the emission level of NO_x and PM were performed according to EGR ratio. This work has the advantages to identify the change rate of NO_x and PM for the purpose of evaluation of EGR coolers.

The fouling characteristics of each step, such as design review, rig test and engine test were evaluated through the aforementioned studies. On the basis of these results, the improved design specification was proposed. The effectiveness of improved EGR cooler was confirmed through CFD analysis. From these, it is possible to suggest proper methodology to obtain good characteristics against fouling of EGR cooler.

Keywords: Exhaust gas recirculation (EGR), High speed direct injection (HSDI) diesel engine, NO_x emission, PM emission, EGR cooler, Fouling, Heat transfer effectiveness

Student Number: 2011-30207

List of Tables

List of Figures

xiii

xvii

Acronym

AFR	Air Fuel Ratio
CAD	Crank Angle Degree
CFD	Computational Fluid Dynamics
DI	Direct Injection
DPF	Diesel Particulate Filter
EGR	Exhaust Gas Recirculation
ESC	European Stationary Cycle
FIE	Fuel Injection Equipment
FR	Fouling Resistance
HC	Hydrocarbon
HSDI	High Speed Direct Injection
LTC	Low Temperature Combustion
NO_x	Nitrogen Oxides
PM	Particulate Matter
S&T	Shell and Tube
SOF	Soluble Organic Fraction

Chapter 1. Introduction

1.1 Background and Technical review

1.1.1 Emission legislations

Diesel engine has several advantages such as high thermal efficiency, good fuel economy, and excellent durability over the gasoline engine. It also emits less carbon dioxide (CO_2), carbon monoxide (CO) and hydrocarbons (HCs) than the gasoline engine. Recently, high speed direct injection (HSDI) diesel engine is under the spotlight as countermeasures for realization of low emissions and good fuel economy. This engine achieved higher specific power and fuel efficiency than the previous engines using high pressure injection system and variable geometry turbo system [1, 2]. However, it is also the major source of more nitrogen oxides (NO_x) which is one of the important air pollutants and particulate matter (PM) [3]. Nitrogen oxides are a critical precursor for other substances of much higher toxicity, including NO_2 and ground level ozone. Exposures to NO_x concentrations of 100ppm are very dangerous, exposures to 200ppm may be fatal [4]. In response, governments are introducing stricter environmental regulations as shown in Figure 1.1. The representative regulation is European emissions legislation called Euro. The suggested Euro VI will put the law into effect in 2014. In accordance with Euro VI, NO_x should be reduced by 56 %, while PM has to be maintained compared to the Euro V level as shown in Table 1.1.

The widely used measure to reduce NO_x emissions in diesel engines is to return some part of the exhaust gas to the intake of the engine. Exhaust gas recirculation (EGR) is a good method to reduce intake air temperature and oxygen concentration for reduction of NO_x as shown in Figure 1.2 [5, 6]. However, as the

oxygen concentration is reduced, the reaction rate slows down and the flame temperature decreases. Consequently, PM formation is increased. This is NO_x-PM trade off as shown in Figure 1.3 [7].

The important effects of EGR are lowering the flame temperature and oxygen concentration of the working fluid in the combustion chamber. Mixing the intake air with hot exhaust recirculation gas increases the temperature of intake air and affects the combustion temperature and NO_x formation [8, 9]. The increased temperature of intake charge air reduces the mass of air drawn into the cylinder and lowers the heat capacity resulting in higher combustion temperature. These negative effects can be recovered by EGR cooler.

High concentration of particulate matter in the exhaust gases deposit on the EGR cooler tubes to form an insulating layer known as the fouling layer, which adds to thermal resistance between the coolant and the hot exhaust gases [10]. The fouling layer decreases the thermal effectiveness and increases the pressure drop in the EGR cooler. Accordingly, the efficiency deterioration of EGR cooler has an adverse effect on NO_x reduction rate [11, 12].

Recently, to cope with stringent exhaust emission regulations, many engine manufacturers are developing new combustion technology, such as low temperature combustion (LTC) engine and extreme high pressure diesel common rail system [13-15]. As a result of the application of these techniques, the SOF contents in soot were increased and the mean particle was decreased [16-18]. This causes the thermophoretic deposits on the tube wall of the EGR cooler. Therefore, many researchers have pay attention to the fouling phenomena in the EGR cooler.

1.1.2 Previous researches on fouling phenomena

Exhaust Gas Recirculation (EGR) is one of the key factors that influence on the exhaust gas emission characteristics of diesel engines since the EGR changes the combustion parameters such as valve timing, fuel injection timing, ignition delay, flame temperature, combustion speed [19-23].

Grillot et al. validated that the results concerning the mass accumulation and the heat exchanger (asymptotic) fouling resistance behavior outline the role of the soot particle thermophoresis and the fluid velocity. The proposed model, which explains the probe mass accumulation kinetics, emphasizes the modification of the deposit thermal conductivity during the deposition [24].

Storey et al. investigated the results of a study of fundamental aspects of EGR cooler fouling. The geometry of the EGR coolers also can influence its performance as they have to meet several technical requirements such as minimal deposition, least pressure drop and maximum effectiveness [25].

Kim et al. showed that the thermal effectiveness of various EGR coolers experimentally. Plate & fin heat exchangers turned out to be more efficient than shell & tube heat exchangers [26].

Zhang et al. investigated the influence of particulate matter in the exhaust gases of a diesel engine on the performance of an EGR cooler [27].

Zahn et al. measured particulate fouling of full scale EGR coolers with various exhaust treatment devices located upstream of the cooler [28].

Table 1.1 EU Emission Standards for Passenger Cars [29].

Stage	Date	CO	HC+NOx	NOx	PM	PN
		g/km				#/km
Euro 1†	1992.07	2.72 (3.16)	0.97 (1.13)	-	0.14 (0.18)	-
Euro 2, IDI	1996.01	1.0	0.7	-	0.08	-
Euro 2, DI	1996.01[a]	1.0	0.9	-	0.10	-
Euro 3	2000.01	0.64	0.56	0.50	0.05	-
Euro 4	2005.01	0.50	0.30	0.25	0.025	-
Euro 5a	2009.09[b]	0.50	0.23	0.18	0.005[d]	-
Euro 5b	2011.09[c]	0.50	0.23	0.18	0.005[d]	6.0×10^{11}
Euro 6	2014.09	0.50	0.17	0.08	0.005[d]	6.0×10^{11}

† Values in brackets are conformity of production (COP) limits

a. until 1999.09.30 (after that date DI engines must meet the IDI limits)

b. 2011.01 for all models

c. 2013.01 for all models

d. 0.0045 g/km using the PMP measurement procedure

Global Regulation Timeline by Region				*Phase in **Proposed	CVS – Commercial Vehicle Systems LVS – Light Vehicle Systems		
	2008	**2009**	**2010**	**2011**	**2012**	**2013**	**2014**
U.S.	Locomotive & Marine Tiers0-2	CA CVS Retrofit**	US-10 CVS On-highway Motorcycle Rule Tier22	US off-road diesel Tier-4A*	Locomotive & Marine Tier 3 CA LEV 3	US Tier 3LVS** Locomotive & Marine Tier 4	US off-road diesel Tier-4B*
EUROPE	EU Euro-5 CVS	EU Euro-5 LVS*	Netherlands Marine 0E/Retrofit	EU off-road Stage 3B*	EU CO_2/GHG 120g PM # LVS	EU-6 CVS**	EU off-road Stage 4 EU Euro-6 LVS*
CHINA	Euro-3 Two-wheel Beijing Euro-4 LVS	Beijing CVS Yellow Label		Euro-4 LVS/CVS	Euro-5 LVS*		Euro-5 CVS*
JAPAN	Cold-start restrictions LVS	Japan-09 LVS/CVS		NOx reductions LVS		JP-13 CVS	

Stricter Emission Regulations
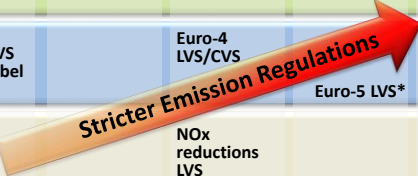
Figure 1.1 Trend and comparison of worldwide exhaust emission standards [30].
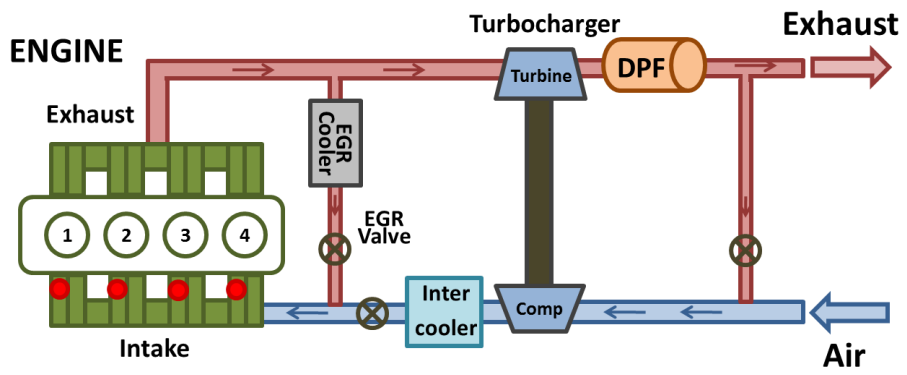
Figure 1.2 The layout of EGR system in diesel engines.
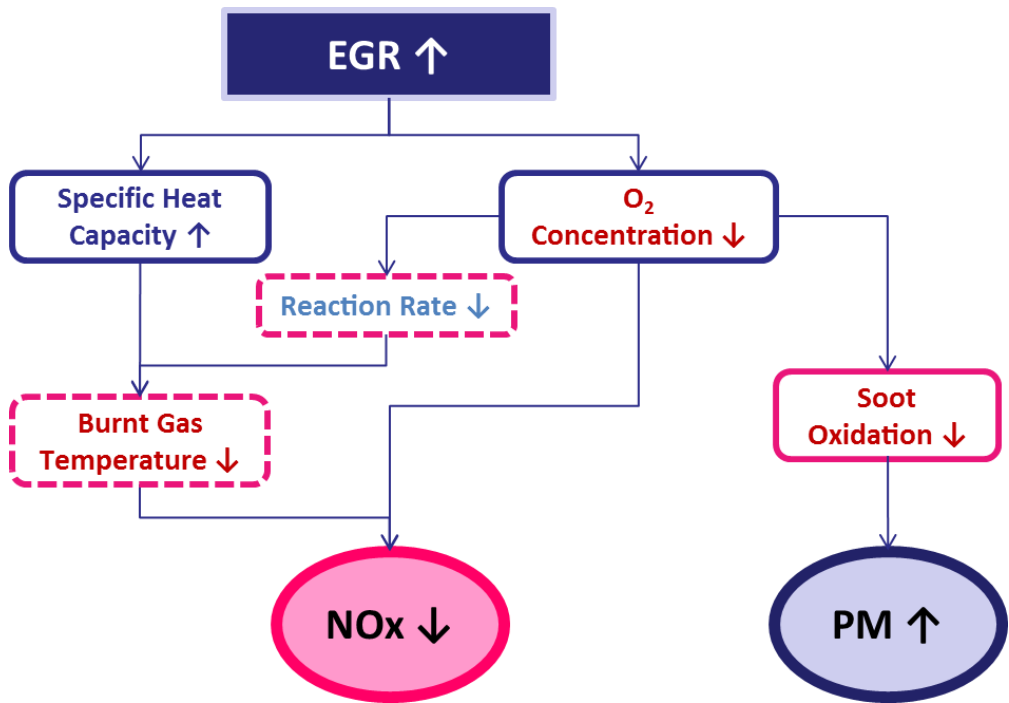
Figure 1.3 The effects of EGR on NOx and PM emissions in Diesel engines.

1.2 Objectives

In this study, the design geometry of EGR cooler was reviewed and then the characteristics of fouling phenomena and correlation analysis on a test rig and engine dynamometer was evaluated. Finally proper design of EGR cooler which is less sensitive to fouling was proposed.

The detailed objectives of this study are:

1. Reviewing the design of existing and modified EGR coolers to keep the good characteristics against fouling resistance,

2. Evaluating the characteristics of fouling phenomena on both rig and engine, and

3. Suggesting a methodology to maintain heat transfer effectiveness.

Chapter 2. Theoretical basis

In this chapter, the theoretical basis on the fouling mechanism is described.

2.1 Fouling mechanism

The particles in exhaust gas are normally exposed to external forces. The external forces lead the particles to retreat from the main exhaust gas stream [31, 32]. As a result, particles are deposited on the tube wall in EGR cooler. The resulting deposit of PM in EGR coolers can produce critical problems. These problems include fouling, which has been extensively investigated. Fouling refers to the attachment of PM, SOF and HC deposits to the inside of an EGR cooler during engine operation [33-35]. This fouling mechanism is due to thermophoresis in a field with temperature gradient, gravitational settling, condensation of hydro carbons and Brownian diffusion [36].

In a thermal gradient field, the particles in the exhaust gas are driven to move to cold zone. This phenomenon is known as thermophoresis. The cause of EGR cooler fouling is known to the occurrence of ingredients, such as the design of cooler, the operation mode, the temperatures of inlet gas and outlet gas, the corrosion by soluble organic fraction and PM and so on. This phenomenon not only reduces the heat transfer efficiency and NO_x reduction capability of the cooler but also causes corrosion [37, 38].

2.1.1 Thermophoresis by temperature gradient

According to the research shown by Talbot et al., thermophoresis is the term describing the phenomenon wherein small particles, such as soot particles, aerosols or the like, when suspended in a gas in which there exists a temperature gradient

∇T, experience a force in the direction opposite to that of ∇T. The fundamental physical processes for the thermophoresis were first investigated by Maxwell. He showed that gas molecules on a small element of area will deliver more tangential momentum force to the wall if they come from the hotter zone than the colder zone. The net tangential momentum force is that a shear stress is exerted by the gas on the wall in the direction opposite to $\partial T/\partial s$, the temperature gradient parallel to the wall in the gas. Also, since an equal and opposite shear stress is exerted by the wall upon the gas, a flow of the gas adjacent to the wall occurs in the direction toward the hotter zone [36]. This is known as the main mechanism of particle deposition. The thermal force, $\boldsymbol{F}_{th}$, on a particle is,

$$\boldsymbol{F}_{th} = \frac{-p\lambda d_p{}^2 \nabla T}{T} \tag{2.1.1}$$

Where, T : absolute temperature of exhaust gas

     p : exhaust gas pressure

     λ : mean free path

     d_p : particle of diameter

     ∇T : temperature gradient

2.1.2 Condensation and diffusion

The EGR cooler feed gas in a diesel engine consists of several HC species. Heavier HCs are more likely to condense at the coolant temperatures, 30-90℃ typically encountered in diesel engine EGR coolers. The condensation would cause a lower concentration, resulting in a concentration gradient to drive diffusion. In a free stream of a gas at the condition of a certain pressure and temperature, a condensate film will be formed as shown in Figure 2.1.1.

10

The mass condensation flux ($J_{g,i}$) from the gas stream to the surface is defined as [39],

$$J_{g,i}(x,\,t) = K_g(x,\,t)\ \rho_g(t)\ \ln\left(\frac{1-y_{i,int}(x,t)}{1-y_{i,gas}(x,t)}\right) \tag{2.1.2}$$

Where, $y_{i,gas}$: mole fraction of the vapor in the gas stream

$y_{i,int}$: mole fraction of the vapor at the gas/liquid interface

$K_g(x,\,t) = \left(\frac{h(x,t)}{\rho_g(t)Cp_g(t)}\right)\left(\frac{Pr(t)}{Sc_{g,i}}\right)^{2/3}$: the mass transfer coefficient

h : heat transfer coefficient

ρ_g : gas density

Cp_g : heat capacity

Pr : Prandtl number

Sc : Schemidt number
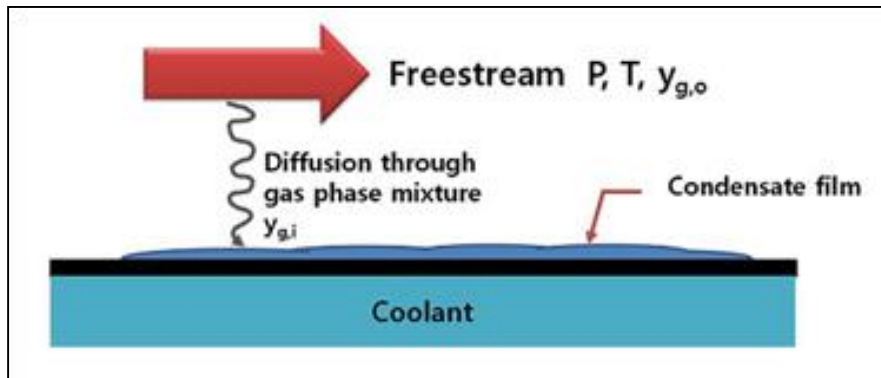
Figure 2.1 Condensation film forms on a surface of EGR cooler [36].

2.2 Principle of heat exchanger

Heat exchangers are normally classified by a flow arrangement and a type of construction. The simplest heat exchanger is one for which the hot and cold fluids move in the same or opposite direction in a concentric tube (or double-pipe) construction. In the parallel flow, the hot and cold fluids enter at the same end, flow in the same direction, and leave at the same end. In the counter flow, the fluids enter at opposite ends, flow in opposite direction, and leave at opposite ends. On the other hand, the fluids can enter in cross flow by the finned and unfinned heat exchangers. Another common heat exchanger is the shell and tube type [40-44]. Specific forms differ according to the number of shell and tube passes. A special class of configuration is compact heat exchanger which has a very large heat transfer surface area per unit volume [45].

2.2.1 Overall heat transfer coefficient

An essential part of any heat exchanger analysis is decision of the overall heat transfer coefficient. This coefficient is determined by accounting for conduction and convection resistance between fluids separated by plans and walls. The overall heat transfer coefficient may be expressed as [46],

$$\frac{1}{UA} = \frac{1}{U_c A_c} = \frac{1}{U_h A_h}$$

$$= \frac{1}{(\eta_0 h A)_c} + \frac{R''_{f,c}}{(\eta_0 A)_c} + R_w + \frac{R''_{f,h}}{(\eta_0 A)_h} + \frac{1}{(\eta_0 h A)_h} \qquad (2.1.3)$$

Where, *c, h* : cold and hot fluids, respectively

       U : overall heat transfer coefficient

       A : total surface area

h : convection heat transfer coefficient

R_w : conduction resistance of wall separating cold and hot sides

R_f'' : fouling factor

η_0 : overall surface efficiency of a finned surface

$$\eta_0 = 1- \frac{A_f}{A} \left(1 - \eta_f\right) \tag{2.1.4}$$

Where, A_f : entire fin area

η_f : efficiency of a single fin

$$\eta_f = \frac{\tan h \, (mL)}{mL} \tag{2.1.5}$$

Where, $m = (2h/kt)^{1/2}$

t : fin thickness

k : thermal conductivity

2.2.2 The effectiveness of EGR cooler

To define the effectiveness of a heat exchanger, we must first determine the maximum possible heat transfer (Q_{max}).

To write the general expression as below,

$$Q_{max} = C_{min}\left(T_{g,i} - T_{c,i}\right) \tag{2.2.1}$$

Where, C_{min} is equal to C_g or C_c.

    C_g and C_c are the exhaust gas and coolant heat capacity rates, respectively.

It is logical to define the effectiveness (ε) as the ratio of the actual heat transfer rate for a EGR cooler (Q) to the maximum possible heat transfer rate (Q_{max}):

$$\varepsilon = \frac{Q}{Q_{max}} = \frac{C_g\left(T_{g,i} - T_{g,o}\right)}{C_{min}\left(T_{g,i} - T_{c,i}\right)} \tag{2.2.2}$$

Where, $T_{g,i}$: the temperature of exhaust gas inlet

    $T_{g,o}$: the temperature of exhaust gas outlet

    $T_{c,i}$: the temperature of coolant inlet

The actual heat transfer rate can be determined from the expression as below,

$$Q = \varepsilon\, C_{min}\left(T_{g,i} - T_{c,i}\right) \tag{2.2.3}$$

The number of transfer units (NTU) is a dimensionless parameter that is widely used for that heat exchanger analysis and is defined as below,

$$\text{NTU} \equiv \frac{UA}{C_{min}} \tag{2.2.4}$$

Where, U : the overall heat transfer coefficient of the EGR cooler

A : the surface area of the EGR cooler

The effectiveness of the EGR cooler (ε) is determined by the heat exchanger effectiveness relation with for mixed flow C_{max} and C_{min} for the unmixed flow geometry proposed by Holman [47].

$$\varepsilon = (1/C_r)(1 - exp\{-C_r[1 - exp(-NTU)]\}) \tag{2.2.5}$$

Where, $C_r = \dfrac{C_{min}}{C_{max}}$

C_{min} and C_{max}: the minimum and maximum capacity rates, respectively

For $C_{min} = C_g$,

$$\varepsilon = \frac{T_{g,i} - T_{g,o}}{T_{g,i} - T_{c,i}} \tag{2.2.6}$$

Chapter 3. Design review for EGR coolers

The objectives of this chapter are to design EGR coolers by Pro-engineer CAD software and to perform CFD analysis by Fluent software as shown in Table 3.1 for the design review.

3.1 CFD analysis

3.1.1 3-D Modeling

Using 3-D full modeling by Pro-engineer, the gas tube, coolant passage and external housing were meshed [48, 49]. These modeling were performed about 2 different kinds of each EGR coolers, such as two kinds of shell & tube type with I-flow for 1.6L engine, and one kind of shell & tube type and another kind of wavy fin type with U-flow for 2.2L engine. Each heat transfer areas for 4 kinds of EGR coolers are shown in table 4.2 and 4.3. Figure   and Table 3.4 show 3-D model of shell & tube type EGR cooler for 1.6L engine. Figure .2 and Table 3.5 show 3-D model of shell & tube type and fin type EGR cooler for 2.2L engine. The shell & tube type EGR cooler has a lot of spiral shapes which can induce rotating gas flow inside of tube as shown in Figure 3.3 [50-52]. The rotating turbulent flow prevents boundary layer in which hot exhaust gas gets in contact with cold tube and cooled gas contents and hence results in improvement of heat transfer. Consequently, high velocity rotating flow reduces fouling by improved self-cleaning effect. On the other hand, the fin type EGR cooler has a lot of wavy shaped fins which can induce turbulence gas flow inside of oval tube as shown in Figure 4. The waving turbulent flow which is much stronger than the rotating turbulent flow in shell & tube can

impact on the deposited soot on the fin surfaces can also reduce fouling by improved self-cleaning effect [53-57].

3.1.2 CFD analysis condition

K-ε model was used for turbulence model and simple algorithm was used for pressure-velocity coupling. The boundary conditions are like follows. The mass flow rate is 30 kg/h at the condition of inlet gas temperature, 400℃ for a 1.6L diesel engine. On the other hand, the mass flow rate is 30kg/h at the condition of inlet gas temperature, 450℃ for a 2.2L diesel engine. Figure 3.5 shows the general view of CFD geometry and mesh for shell & tube type and fin type EGR cooler.

3.2 The results of analysis

Figure 3.6 shows the computational mesh of I-flow (shell & tube type) EGR cooler. Figure 3.7 shows the visualization of the velocity vector representing the conditions of exhaust gas flow in gas tube. Figure 3.8 shows the temperature decrease of gas in section of gas tubes. The hot inlet gas is cooled by thermal exchange with the coolant and getting out to the exit. Figure 3.9 shows the coolant flow inside of the EGR cooler. The inlet coolant is cooling the gas tubes by turns and getting out to the exit.

In case of U flow (shell & tube type) EGR cooler for 2.2L engine, Figure 3.10, Figure 3.11, 3.12 and 3.13 show the computational mesh, the visualization of the velocity vector representing the conditions of exhaust gas flow in gas tube, the

temperature contour of gas in section of gas tubes and the pressure contour of gas in section of gas tubes, respectively.

In case of U flow (fin type) EGR cooler for 2.2L engine, Figure 3.14, Figure 3.15, 3.16 and 3.17 show the computational mesh, the visualization of the velocity vector representing the conditions of exhaust gas flow in gas tube, the temperature contour of gas in section of gas tubes and the pressure contour of gas in section of gas tubes, respectively.

The CFD input conditions and the results of I-flow (shell & tube type, ø8.0 and ø7.5) EGR coolers were shown in Table 3.2. In addition, the CFD input conditions and the results of U-flow (shell & tube type and fin type) EGR coolers were shown in Table 3.2.

In case of I-flow EGR coolers, the effectiveness of base specification #1(ø8) is about 4% higher than that of modified specification #2(ø7.5). In case of U-flow EGR coolers, the effectiveness of base specification #3(S & T type) is about 3% lower than that of modified specification #4(Fin type). In conclusion, the effectiveness of modified specification #4(Fin type) is the best among them.

Table 3.1 CFD analysis conditions.

Description	Specification
3-D modeling	Pro-engineer wildfire 5.0
Modeler	Gambit 2.2.30
Solver	Fluent 6.2.16
Meshing	Body pipe & gas tube (HEX/Cooper) Coolant pipe (HEX/Cooper) Flange (Hex/Map)
Mesh number	500,000 elements

Table 3.2 Input conditions and CFD results

Input conditions		
Gas inlet temperature	400℃	
Gas mass flow	30 kg/h	
Coolant inlet temperature	90℃	
Results		
Specification	#1 (ø 8.0)	#2 (ø 7.5)
Gas temperature difference	248℃	235℃
Gas pressure drop	1.0kPa	1.3kPa
Gas outlet temperature	152℃	165℃
Effectiveness	80%	76%

Table 3.3 Input conditions and CFD results

Input conditions		
Gas inlet temperature	450℃	
Gas mass flow	30 kg/h	
Coolant inlet temperature	90℃	
Results		
Specification	#3 (ø 8.0, S&T)	#4 (Fin)
Gas temperature difference	299℃	311℃
Gas pressure drop	3.6kPa	4.9kPa
Gas outlet temperature	151℃	139℃
Effectiveness	83%	86%

Table 3.4 Specifications of shell & tube type EGR cooler for 1.6L engine.

Specification	Pitch (A)	Radius (R)	Diameter (B)	Length
# 1	5.5 mm	0.8 mm	⌀ 8.0 mm	230 mm
# 2	5.3 mm	0.8 mm	⌀ 7.5 mm	230 mm
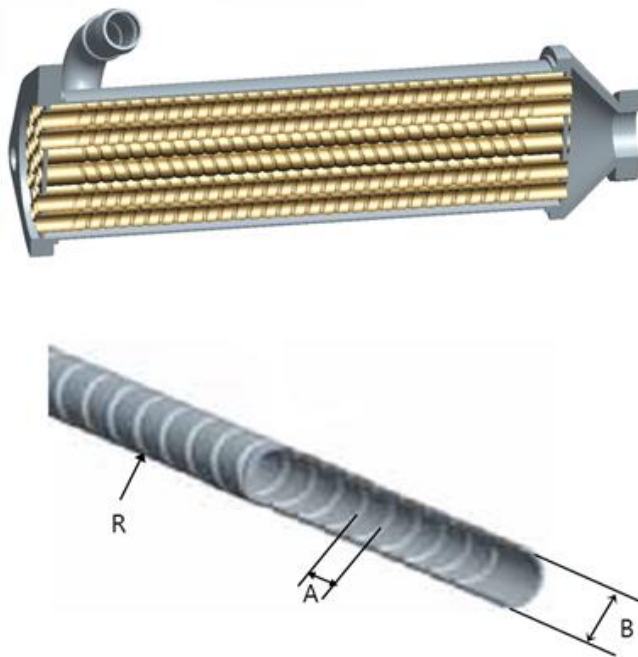
Figure 3.1 3-D model of shell & tube type EGR cooler with I-flow for 1.6L engine.

Table 3.5 Specifications of shell & tube type and fin type EGR cooler with U-
flow for 2.2L engine.

Shell & tube type	Fin type
Length:210 mm	Length: 210 mm
Diameter: ∅ 8.0 mm	Height: 7.5 mm
Spiral tube: 42 EA	Oval tube: 6 EA
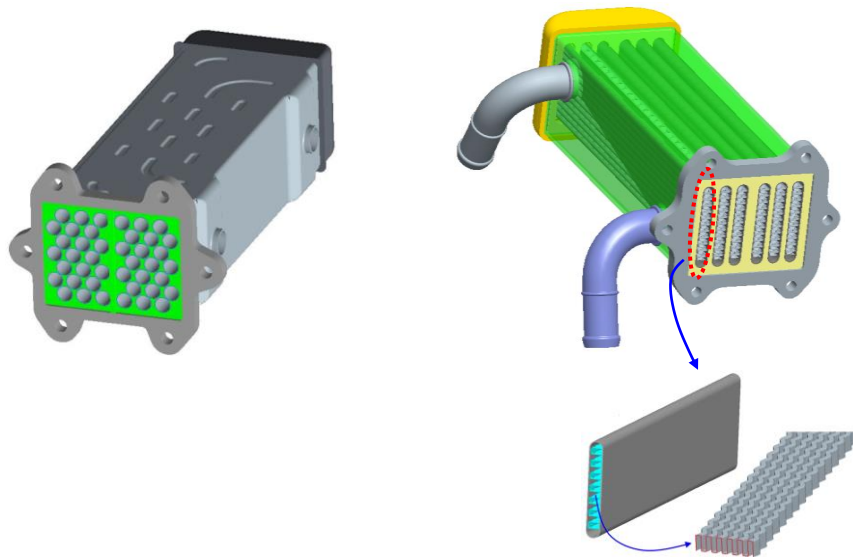
Figure 3.2 3-D models of shell & tube type and fin type EGR cooler with U-
flow for 2.2L engine.
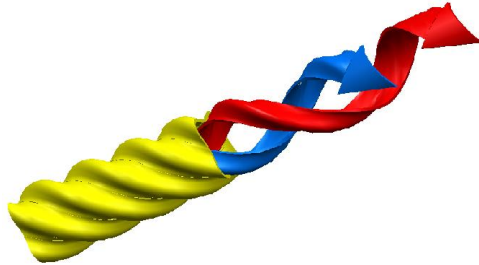
Figure 3.3 The rotating turbulent flow inside of shell & tube
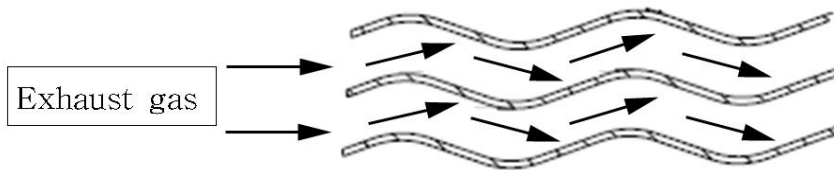
Figure 3.4 The waving turbulent flow inside of wavy fin channel.
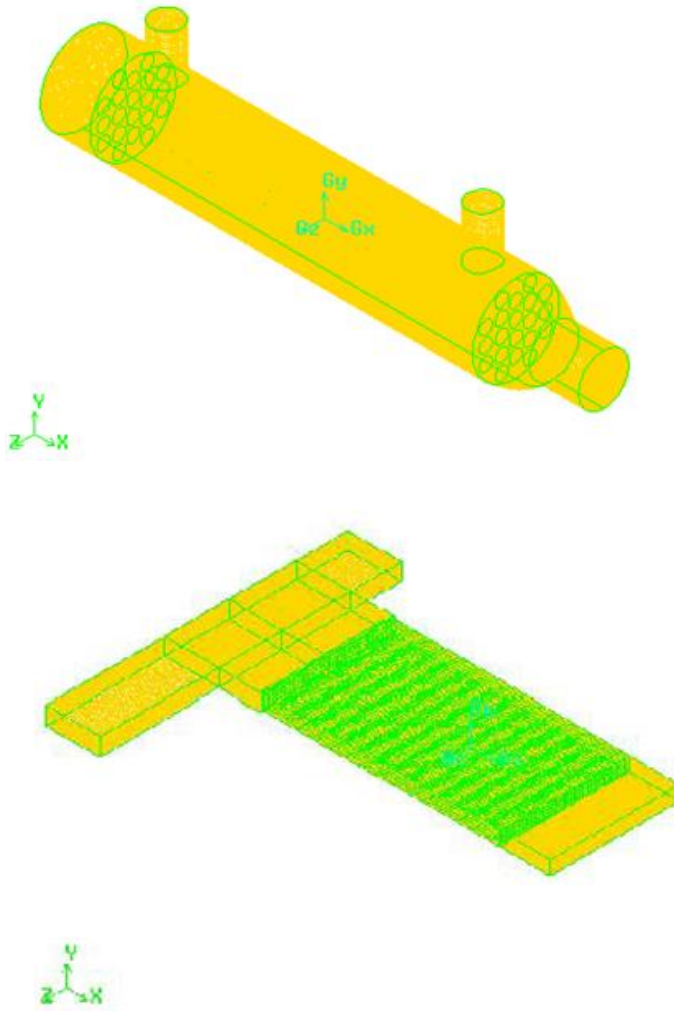
Figure 3.5 General view of CFD Geometry and mesh for shell & tube
type and fin type.
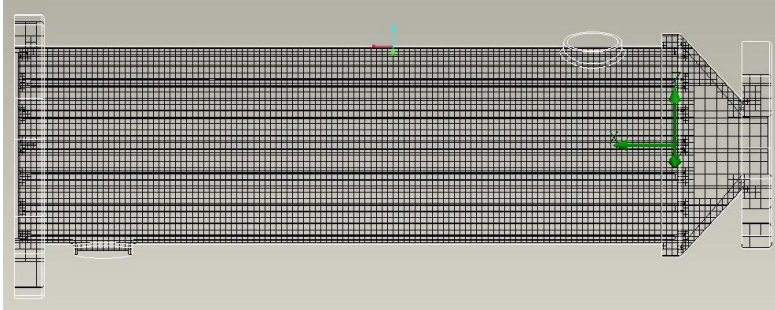
Figure 3.6 Computational mesh of I-flow EGR cooler.
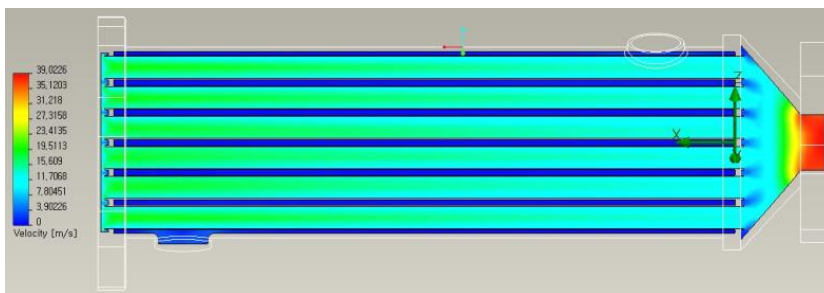
Figure 3.7 Velocity vector of gas inside of I-flow EGR cooler.
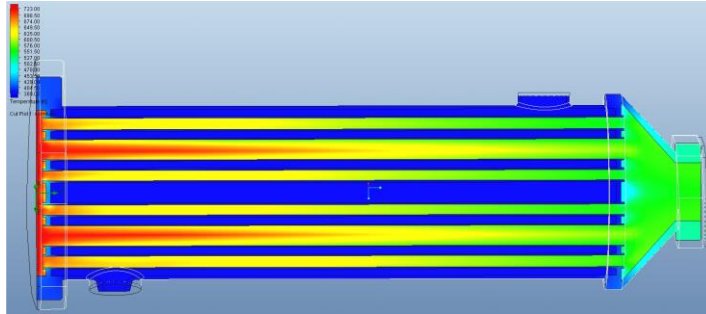
Figure 3.8 Temperature contour of exhaust gas.
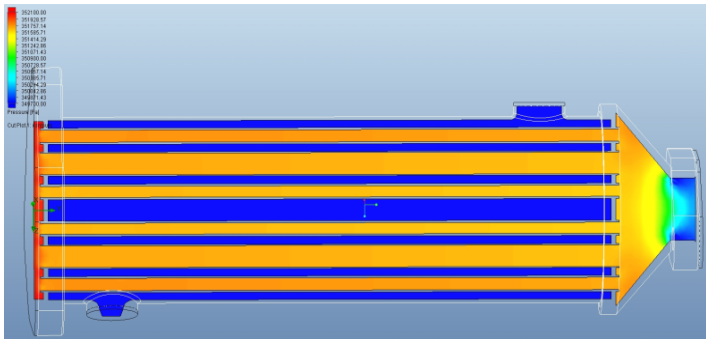
Figure 3.9 Pressure contour of exhaust gas
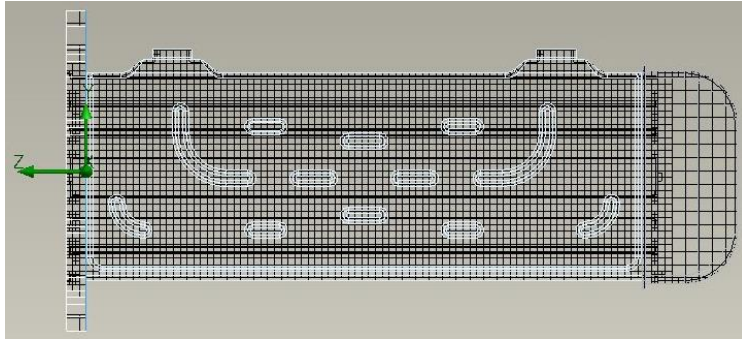
Figure 3.10 Computational mesh of U-flow (S&T) EGR cooler.
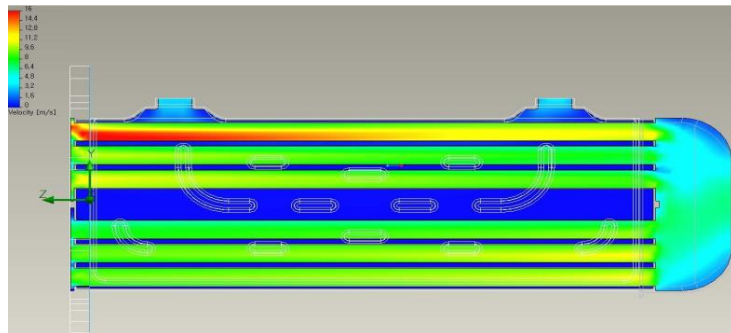
Figure 3.11 Velocity vector of gas inside of U-flow (S&T) EGR cooler.
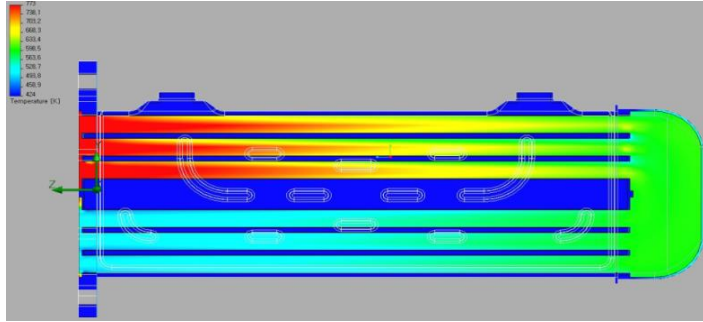
Figure 3.12 Temperature contour of gas in U-flow (S&T) EGR cooler.
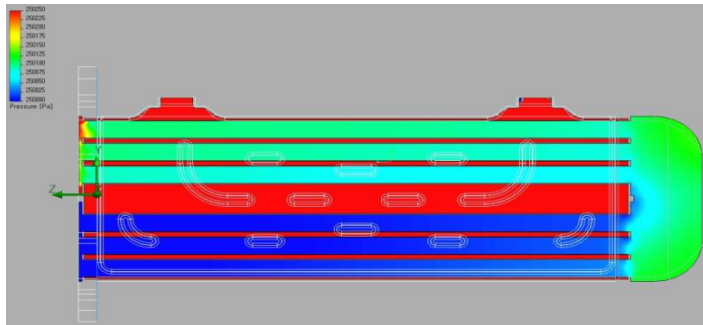
Figure 3.13 Pressure contour of gas in U-flow (S&T) EGR cooler
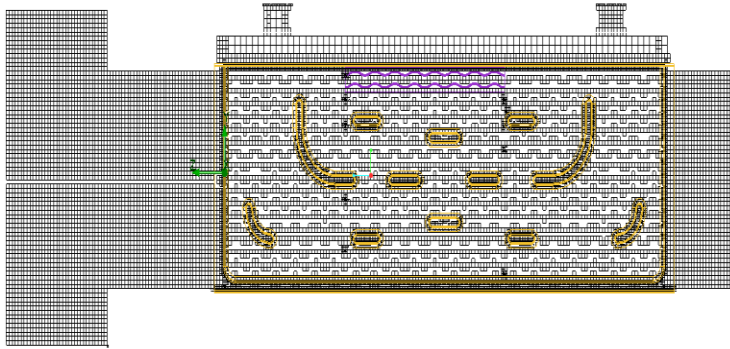
Figure3.14 Computational mesh of U-flow (Fin) EGR cooler.
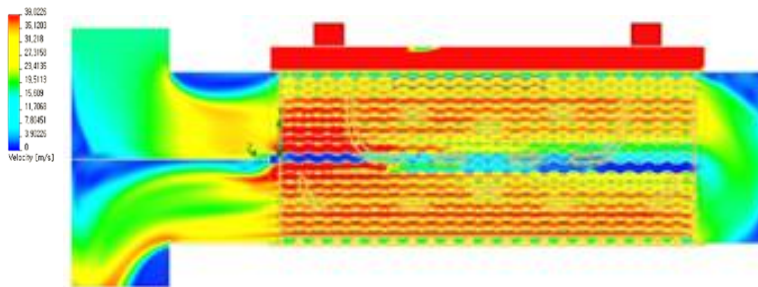
Figure 3.15 Velocity vector of gas inside of U-flow (Fin) EGR cooler.
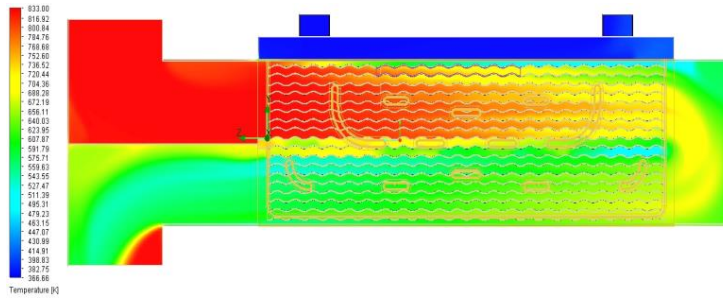
Figure 3.16 Temperature contour of gas in U-flow (Fin) EGR cooler.
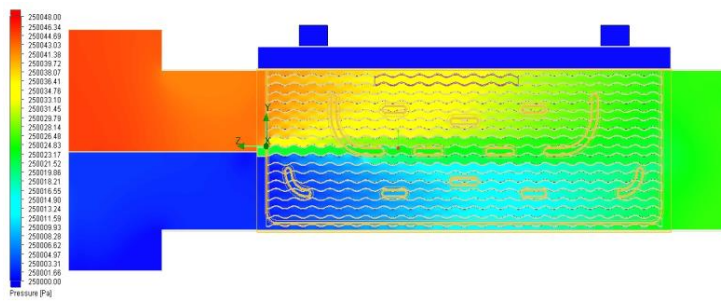
Figure 3.17 Pressure contour of gas in U-flow (Fin) EGR cooler.

Chapter 4. Experimental test on a test rig

The objectives of this chapter are to test the effectiveness of EGR coolers by a test rig.

4.1 Experimental setup

4.1.1 Experimental apparatus

The overall system of experimental test rig consist of dump combustor to generate high temperature exhaust gas and controller, PM feeder to supply particulate constantly, coolant temperature controller, differential pressure meter and thermal mass flow meter as shown in Table 4.1, Figure 4.1 and Figure 4.2.

In order to maintain stably the high temperature of exhaust gas, the total air flow rate in test rig was kept equally and the equivalence ratio in dump combustor was also maintained approximately at 0.7.

The carbon black similar to the characteristics of PM was used to simulate the fouling phenomena and was supplied with feeding rate, 0.7g/min into the section of the test rig constantly using PM feeder. The average particle diameter of carbon black was approximately 70nm.

To evaluate the performance of EGR cooler, a differential pressure meter was also installed to measure the pressure drop at front and rear side of the cooler. K-type thermocouple which would stand up to 1300℃ was used to measure hot exhaust gas. T-type thermocouple was also used to measure and control the temperature of coolant. Thermal mass flow meter (FTM500-iG, ABB) which can cover up to 450kg/h was installed to measure the mass flow rate of exhaust gas.

Exhaust gas is flowing into the EGR cooler through the furnace, DPF and PM feeder by turns.

All adjustment and measurement devices were controlled and monitored by using a personal computer. Data collection and analysis were performed through the data acquisition system.

Table 4.1 Specification of test rig.

Description	Specification
Temperature range of combustor	90~800℃
Temperature range of coolant	40~100℃
Particulate diameter, mass flow	30nm, 0.5~1.0g/min
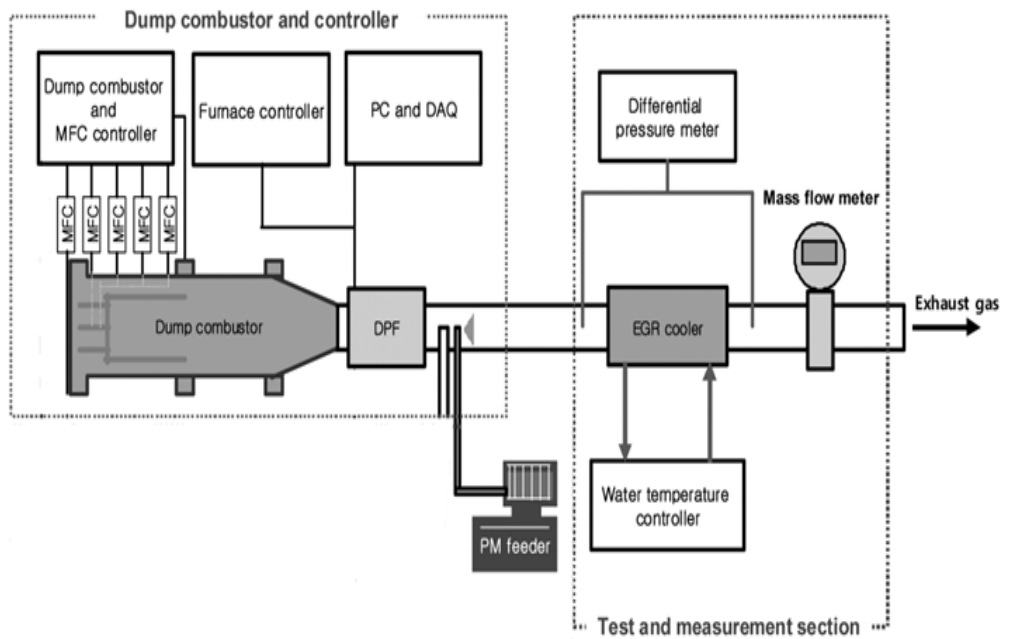
Figure 4.1 Schematic of a test rig set up.
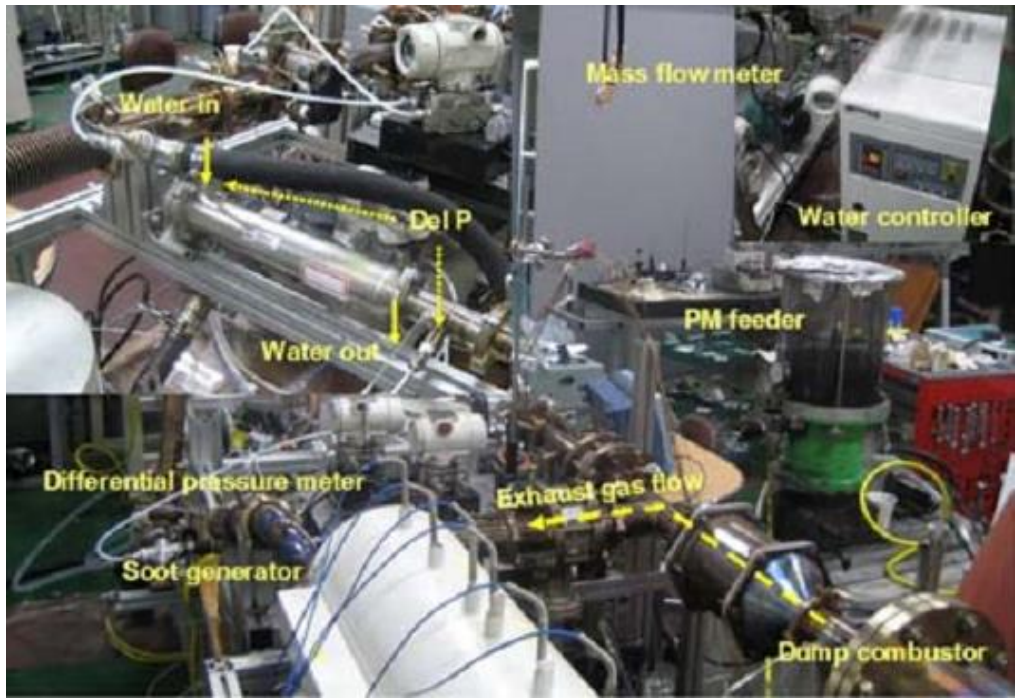
Figure 4.2 Pictures of test rig set up.

4.1.2 Experimental conditions

In this study, the temperature and mass flow rate of exhaust gas, the supply volume of PM, and the temperature and flow rate of coolant were controlled in order to simulate the fouling phenomena in EGR cooler. The EGR coolers, which were used in the experiments, were a shell and tube type for 1.6L diesel engine, a shell and tube type and a wavy fin type for 2.2L diesel engine as shown in Table 4.2 and Table 4.3.

The conditions for EGR mass flow effects are defined as 5 different operation points, such as 10, 20, 30, 40, and 50kg/h. Laboratory experiments were carried out to evaluate the effectiveness and the pressure drop of EGR cooler in test rig. The temperature of exhaust gas and coolant were adjusted at 500℃ and 90℃, respectively. The temperature deviations were controlled within ±2℃ and the flow rate of coolant was kept in 25L/min. The variables, such as the temperature of exhaust gas and coolant, were confirmed to be adjusted independently. To analyze the fouling characteristics of EGR cooler, carbon black was supplied by 0.7g/min to the exhaust gas.

The heat exchange effectiveness of EGR coolers based on the experimental conditions was analyzed by equation (2.3.6).

Table 4.2 Comparison of heat transfer area of EGRC for 1.6L engine

Spec	Status	Type	Gas tube	No. of tubes	Length (mm)	Heat transfer area (cm^2)	%
# 1	Base sample (in production)	Shell & tube, I - flow	φ8.0	28	230	1619	100
# 2	Modified sample	Shell & tube, I - flow	φ7.5	28	230	1517	94

Table 4.3 Comparison of heat transfer area of EGRC for 2.2L engine

Spec	Status	Type	Gas tube	No. of tubes	Length (mm)	Heat transfer area (cm^2)	%
# 3	Base sample (in production)	Shell & tube, U - flow	φ8.0	42	210	2217	100
# 4	Modified sample	Wavy fin, U - flow	direct	6	210	1393	218
			indirect			3438	

* direct : area between tubes and coolant
indirect : area between fins and gas

4.2 Experimental results

4.2.1 The effects of EGR mass flow

The experimental tests were performed to measure how PM fouling in EGR cooler changes the heat exchange effectiveness.

There were positive and negative effects in shell & tube type EGR cooler. The positive effect is due to the fact that the outer surface area of spiral grooves at tubes contacting the coolant was big and resulted in an improved heat transfer. The negative effect was occurred because the PM deposited inside the tube was accumulated and resulted in an enhanced thermal resistance.

The outlet temperature of exhaust gas in case of specification #2(ø7.5) was about 10℃ higher that in case of specification #1(ø8.0) as shown in Figure 4.3. This is due to the difference of heat transfer area. The pressure drops between 2 specifications were increased by 10% and 16% before and after fouling, respectively as shown in Figure 4.6 due to the difference of cross sectional areas.

4.2.2 The effects of PM feeding

For fouling test in case of 2 kinds of specification, #1(ø8.0) and #2(ø7.5), the carbon black was supplied with the feeding rate of 0.7g/min for 12.5 hours as shown in Figure 4.1 and Figure 4.2.

Figure 4.4 and 4.5 show the effectiveness changes of EGR cooler, which has specification #1(ø8.0) and specification #2(ø7.5), respectively before and after fouling. The effectiveness of specification #1(ø8.0) was decreased by 15%

approximately. The effectiveness of specification #2(ø7.5) was decreased by 18% approximately.

4.2.3 The heat exchange effectiveness

The pressure drop between the inlet and the outlet of exhaust gas is the quantitative index of the PM deposited inside the EGR cooler. The accumulation of PM deposit raised enhanced thermal resistance because of the increased pressure drop. The pressure drop of base specification #1(ø8.0) in production reached lower than that of modified specification #2(ø7.5), which means less PM deposited and smaller heat resistance as shown in Figure 4.6. Each pressure drop in case of specification #1(ø8.0) and specification #2(ø7.5) was increased by max 0.7kPa and max 1.0kPa, respectively at EGR mass flow, 50kg/h. The pressure drops between 2 specifications were increased by about 10% and 16% before and after fouling, respectively due to the difference of cross sectional areas. Figure 4.7 shows the effectiveness changes of EGR cooler as per EGR mass flow rate. The heat exchange effectiveness decreased gradually as the heat resistance increased.

Considering the above experimental results, the increase in exhaust gas outlet temperatures in 2 kinds of EGR cooler could be caused by PM deposited on the surface of shell & tubes. EGR cooler with specification #1(ø8.0) has lower pressure drop and lower gas outlet temperature and higher heat transfer effectiveness compared with EGR cooler with specification #2(ø7.5). The Thermal effectiveness of specification #1 is about 4% and 5% higher than that of specification #2 before and after fouling, respectively. The reduction of thermal effectiveness for both after fouling is 15~16% approximately.

In addition, for U-flow EGR coolers, the heat exchange effectiveness tests were also performed. One is shell and tube type with base specification #3(ø8.0) in

production and another is wavy-fin type with modified specification #4 as shown in Figure 3.2.

Figure 4.8 and 4.9 shows the pressure drop and thermal effectiveness of U-flow EGR coolers, respectively. Thermal effectiveness was decreased depending on the increase of EGR mass flow. Pressure drops between 2 specifications were increased by 12% and 17% before and after fouling, respectively due to the difference of cross sectional areas. Thermal effectiveness of specification #4(Fin) is about 8% and 12% higher than that of specification #3(S&T) before and after fouling, respectively.

In conclusion, the reduction of thermal effectiveness for fin type and shell & tube type is about 10% and 16%, respectively before and after fouling.
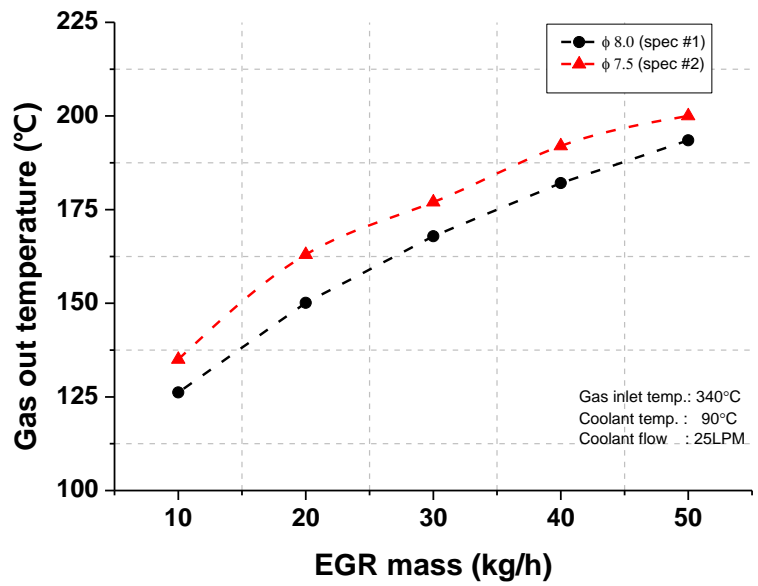
Figure 4.3 Outlet temperature of exhaust gas with EGR mass flow.
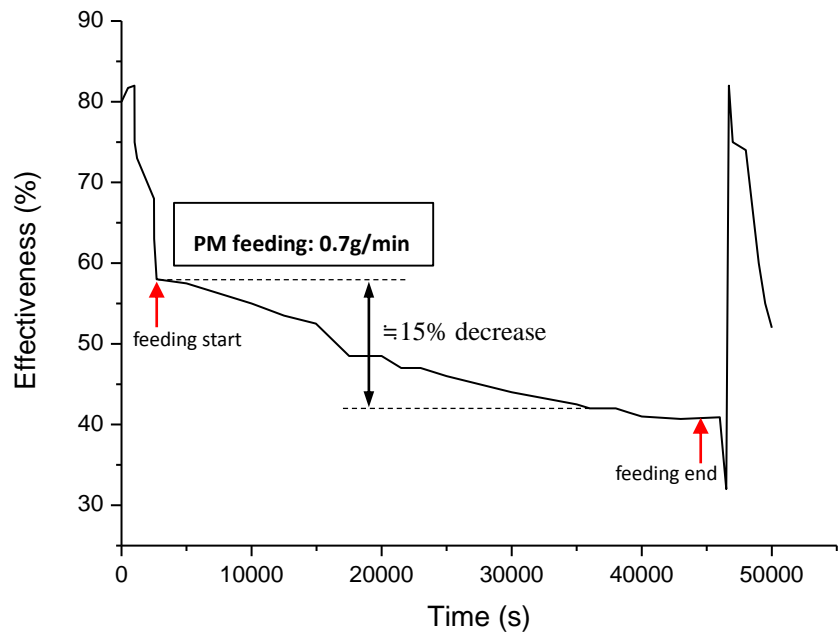
Figure 4.4 Effectiveness of EGR cooler (ø8.0) with time.
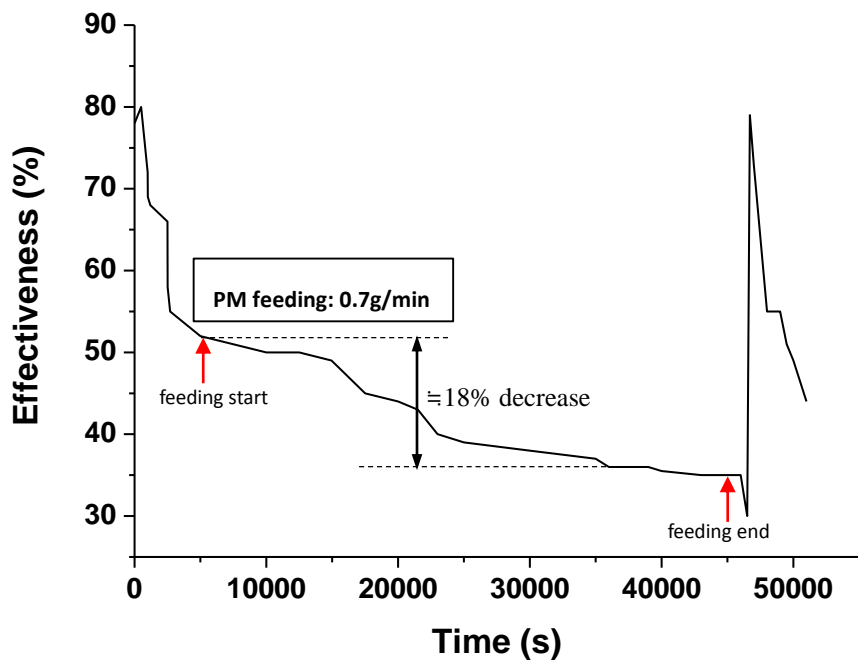
Figure 4.5 Effectiveness of EGR cooler (⌀7.5) with time
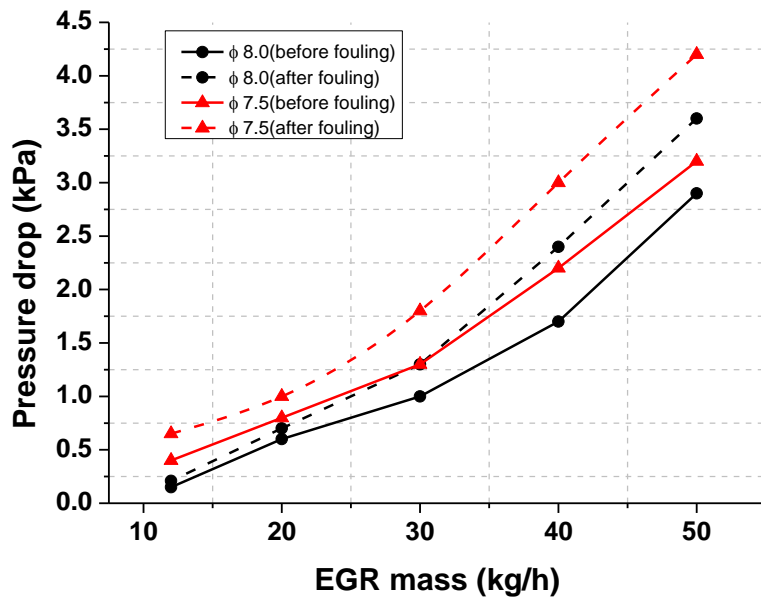
Figure 4.6 The pressure drop of I-flow EGR cooler with EGR mass.
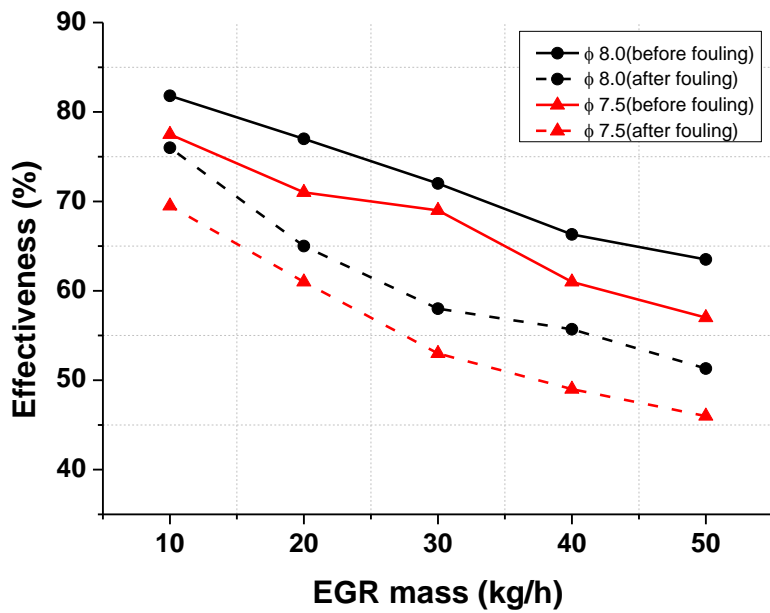
Figure 4.7 The effectiveness of I-flow EGR cooler with EGR mass.
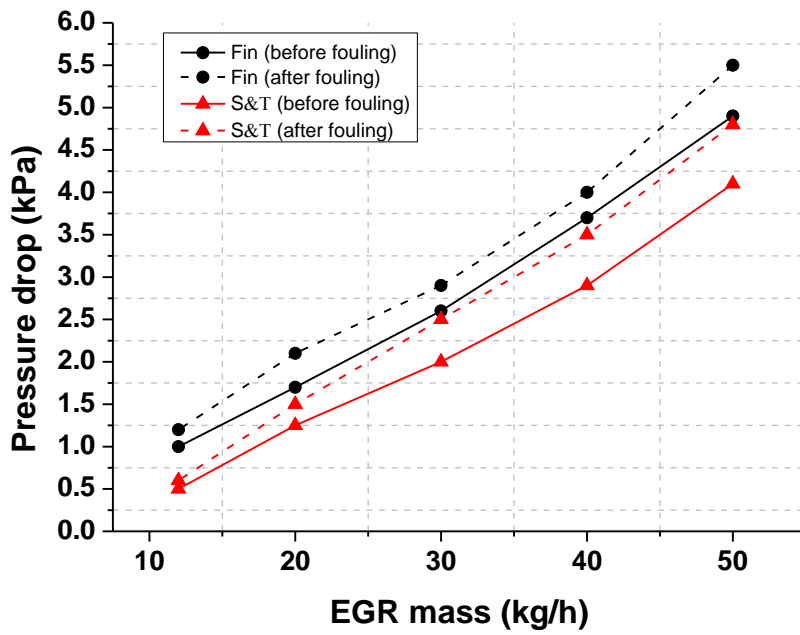
Figure 4.8 The pressure drop of U-flow EGR cooler with EGR mass.
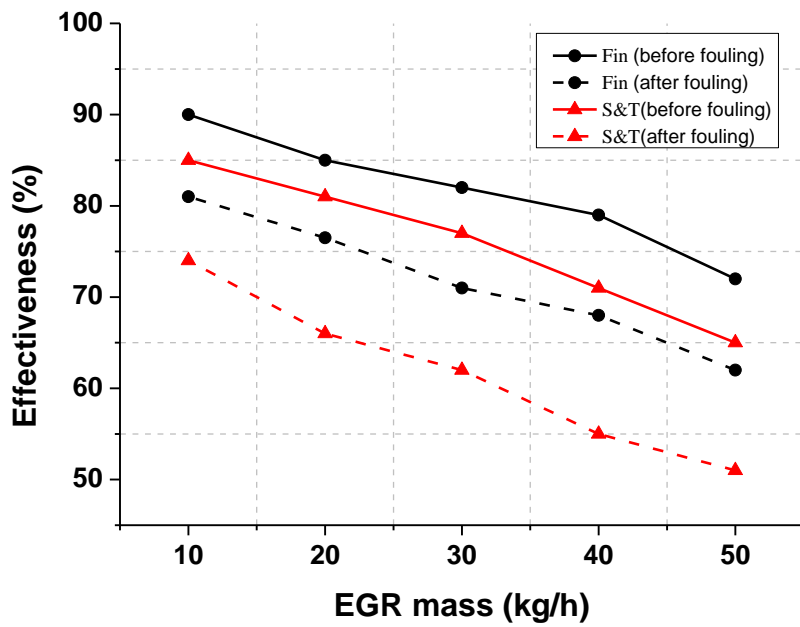
Figure 4.9 The effectiveness of U-flow EGR cooler with EGR mass.

4.3 Fouling mechanics of EGR cooler

Considering the fouling mechanics occurred inside of the tubes in EGR cooler, there is fouling resistance which is determined by two elements, such as the rates of mass deposition $(\dot{M}_d)$ and mass removal $(\dot{M}_r)$ of PM. Figure 4.10 shows the behavior of this.

Fouling resistance shows asymptotic behavior. At the stabilized condition, the rates of mass deposition $(\dot{M}_d)$ and mass removal $(\dot{M}_r)$ of PM are equal. The stabilized behavior is driven by the removal forces which are a function of gas flow velocity [58-62]. In particular, the removal forces are driven by the gas flow velocity near the tube wall of EGR cooler. The local gas flow velocity near the tube wall depends on the geometry shape of tubes, resulting in occurrence of wall shear stress as shown in Figure 4.11. Consequently, the shear force removes the PM deposition [63-66].

4.3.1 The equations for fouling resistance

According to the model and experiments reported by Abd-Elhady et al. [8], the forces acting on a particle of PM lying on x-axis and exposed to a shear flow are shown in Figure 4.12. Point O is the spot of rolling. In the figure, the various forces and symbols represents as follows,

F_{adh}: van der Waals adhesion force

F_b: buoyance force

F_d: drag force

F_g: gravity force

F_l: lift force

d: contact diameter

δ: deformation

r: particle radius

u: gas flow velocity

A hydrodynamic rolling moment is acting on a particle due to the drag force (F_d), which tends to roll the particle along the horizontal surface around point O [67-69].

This moment is given by Sharma et al. [70] as,

Hydrodynamic rolling moment = F_d (1.399 - δ)   (4.3.1)

Adhesion moment which tends to stick the particle to the surface exist as given by Hubbe [71] as,

Adhesion resting moment = ($F_{adh} + F_g − F_l − F_b$) d/2   (4.3.2)

The ratio between the hydrodynamic rolling moment and adhesion resting moment is defined by Zhang et al. [72] as the rolling moment ratio, RM.

$$RM = \frac{\text{Hydro}dynamic\ rolling\ moment}{Adhesion\ resting\ mopment}$$

$$= \frac{F_d\ (1.399r - \delta)}{\left(F_{adh} + F_g - F_l - F_b\right)d/2}$$ (4.3.3)

In case of the value of rolling moment ratio larger than 1, rolling of particle will arise. The rolling moment is a function of drag force. Drag force is also a function of velocity of the shear flow. The increase of flow velocity brings out the increase of rolling moment.

The fouling thermal resistance, R_f is expressed as,

$$R_f = R_{th}(t) - R_c \hspace{5cm} (4.3.4)$$

The overall thermal resistance, $R_{th}(t)$ is defined as,

$$R_{th}(t) = \frac{A_0 \times \text{LMTD}}{\dot{Q}} \hspace{4cm} (4.3.5)$$

R_c is the overall thermal resistance under clean conditions.

where, $\dot{Q} = U \cdot A \cdot \text{LMTD}$

$$= m_g C_p \left(T_{gas,in} - T_{gas,out} \right)$$

where, U : overall heat transfer coefficient, [W/m^2 K]

A : area, [m^2]

$\text{LMTD} = \dfrac{\Delta T_2 - \Delta T_1}{\ln(\Delta T_2 / \Delta T_1)}$: logarithmic mean temperature difference

For counter flow heat exchanger,

$\Delta T_1 = T_{gas,in} - T_{coolant,out}$, $\Delta T_2 = T_{gas,out} - T_{coolant,in}$

m_g : mass flow rate of exhaust gas, [kg/h]

C_p : specific heat

50

The gas velocity, V through the EGR cooler is controlled by changing the rate of mass flow. The gas velocity through EGR cooler is calculated from the measured mass flow rate of the flowing gases and the cross sectional area, A_{cr} of the tubes of EGR cooler as below.

$$V = \frac{m_g}{\rho A_{cr}}$$
(4.3.6)
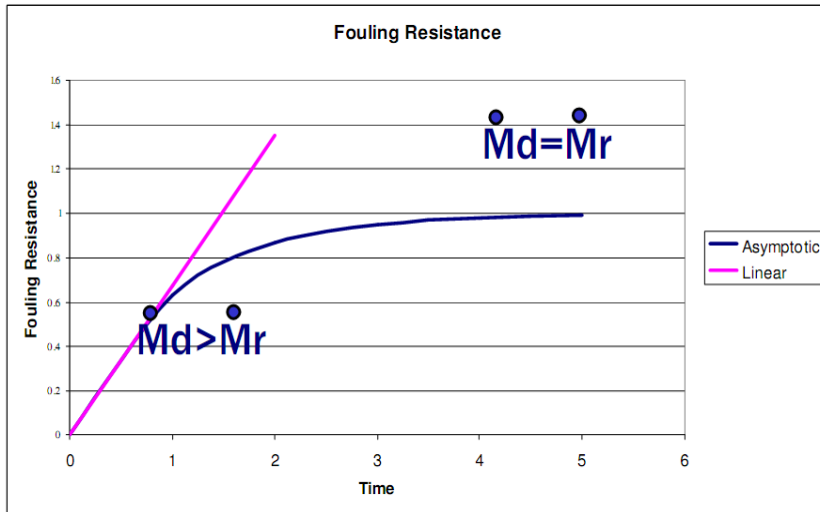
Figure 4.10 The behavior of fouling resistance inside of EGR cooler.
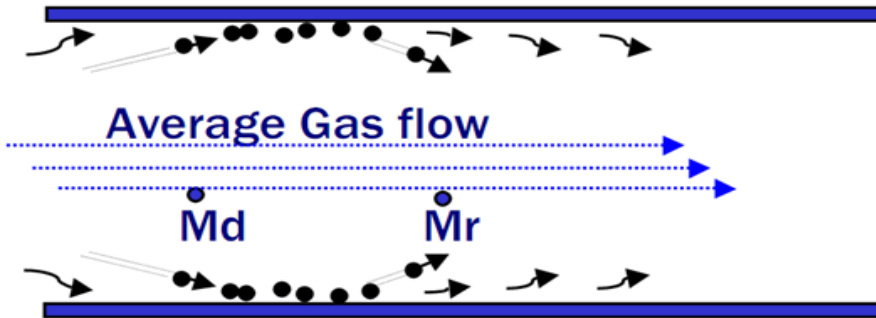
Figure 4.11 The local gas flow near the tube wall of EGR cooler.
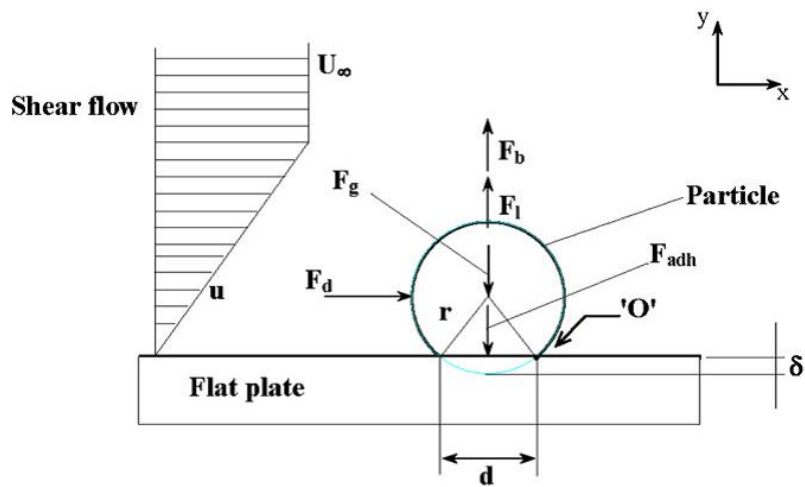
Figure 4.12 The forces acting on a particle lying on a flat surface and exposed to a shear flow [8].

4.3.2 The results of fouling resistance

The experiments were made for 4 kinds of EGR coolers, such as base specification #1(shell & tube ø8.0, I-flow type), modified specification #2(shell & tube ø7.5, I-flow type), base specification #3(shell & tube ø8.0, U-flow type) and modified specification #4(wavy fin, U-flow type) as shown in Figure 3.1 and 3.2.

The fouling resistances (R_f) and the effectiveness of EGR cooler (ε) are shown in Figure 4.13 ~ 4.20 as a function of the exhaust gas flow velocity.

In case of specification #1(shell & tube type ø8.0, I-flow type), it is shown from Figure 4.13 that the fouling resistance continuously increased with time during the experiments with gas velocity 10m/s and 30m/s, while for the gas velocity 50m/s a constant asymptotic fouling resistance was arrived after 2.5 hours of operation.

The fouling resistance including initial thermal resistance (R_c) and final thermal resistance (R_{final}) were determined and listed in table 4.4. The thermal resistance for exhaust gas velocity of 50m/s was increased from 1.14×10^{-3} m^{2}K/W at clean condition to 2.97×10^{-3} m^{2}K/W at fouled condition after 6 hours of operation. The value of thermal resistance for 50m/s is a little less than for 30m/s and exceedingly less than for 10m/s. The fouling resistance after 6 hours of operation test with gas velocity of 10m/s is 3.18 times bigger than for gas velocity of 30m/s, and 6.12 times bigger than for gas velocity of 50m/s. The initial fouling rate at the beginning of fouling test is determined by the tangent to the fouling resistance curve verses horizontal curve of time at t = 0 as shown in table 4.4. From these data we can see clearly the sensitivity of fouling rate and fouling resistance with regard to exhaust gas velocity. That is, the initial fouling rate for 10m/s is two times faster than for 30m/s and five times faster than for 50m/s.

The effectiveness of specification #1(shell & tube type ø8.0, I-flow type) was continuously decreased for gas velocity of 10m/s and 30m/s with elapsed time of operation, while for gas velocity of 50m/s it arrived at an asymptotic valve of 60% as shown in Figure 4.14.

In case of specification #2(shell & tube type ø7.5, I-flow type), it is shown from Figure 4.15 that the fouling resistance continuously increased with time during the experiments with gas velocity 10 m/s and 30m/s, while for the gas velocity 50m/s a constant asymptotic fouling resistance was arrived after 4 hours of operation.

The fouling resistance including initial thermal resistance (R_c) and final thermal resistance (R_{final}) were determined and listed in table 4.5. The thermal resistance for exhaust gas velocity of 50m/s was increased from 1.21×10^{-3} m^2K/W at clean condition to 5.23×10^{-3} m^2K/W at fouled condition after 6 hours of operation. The value of thermal resistance for 50m/s is somewhat less than for 30m/s and for 10m/s. The fouling resistance after 6 hours of operation test with gas velocity of 10m/s is 2.4 times bigger than for gas velocity of 30m/s, and 3.7 times bigger than for gas velocity of 50m/s. The initial fouling rate at the beginning of fouling test is determined by the tangent to the fouling resistance curve verses horizontal curve of time at t = 0 as shown in table 4.5. The initial fouling rate for 10m/s is 2.1times faster than for 30m/s and 4.6 times faster than for 50m/s.

The effectiveness of specification #2(shell & tube type ø7.5, I-flow type) was continuously decreased for gas velocity of 10m/s and 30m/s with elapsed time of operation, while for gas velocity of 50m/s it arrived at an asymptotic valve of 55% as shown in Figure 4.16.

In case of specification #3(shell & tube type ø8.0, U-flow type), it is shown from Figure 4.17 that the fouling resistance continuously increased with time

during the experiments with gas velocity 15 m/s, while for the gas velocity 60m/s a constant asymptotic fouling resistance was arrived after 4.5 hours of operation.

The fouling resistance including initial thermal resistance (R_c) and final thermal resistance (R_{final}) were determined and listed in table 4.6. The thermal resistance for exhaust gas velocity of 60m/s was increased from 1.57×10^{-3} m^{2}K/W at clean condition to 2.72×10^{-3} m^{2}K/W at fouled condition after 6 hours of operation. The value of thermal resistance for 60m/s is significantly less than for 15m/s. The fouling resistance after 6 hours of operation test with gas velocity of 15m/s is 20.1 times bigger than for gas velocity of 60m/s. The initial fouling rate at the beginning of fouling test is determined by the tangent to the fouling resistance curve verses horizontal curve of time at t = 0 as shown in table 4.6. The initial fouling rate for 15m/s is 4.3 times faster than for 60m/s.

The effectiveness of specification #3(shell & tube type ø8.0, U-flow type) was continuously decreased for gas velocity of 15m/s with elapsed time of operation, while for gas velocity of 50m/s it arrived at an asymptotic valve of 62% as shown in Figure 4.18.

In case of specification #4(Fin type, U-flow type), it is shown from Figure 4.19 that the fouling resistance continuously increased with time during the experiments with gas velocity 15 m/s, while for the gas velocity 60m/s a constant asymptotic fouling resistance was arrived after 4.5 hours of operation.

The fouling resistance including initial thermal resistance (R_c) and final thermal resistance (R_{final}) were determined and listed in table 4.7. The thermal resistance for exhaust gas velocity of 60m/s was increased from 1.57×10^{-3} m^{2}K/W at clean condition to 2.72×10^{-3} m^{2}K/W at fouled condition after 6 hours of operation. The value of thermal resistance for 60m/s is significantly less than for 15m/s. The fouling resistance after 6 hours of operation test with gas velocity of 15m/s is 20.1 times bigger than for gas velocity of 60m/s. The initial fouling rate at the beginning

of fouling test is determined by the tangent to the fouling resistance curve verses horizontal curve of time at t = 0 as shown in table 4.7. The initial fouling rate for 15m/s is 4.3 times faster than for 60m/s.

The effectiveness of specification #4(Fin type, U-flow type) was continuously decreased for gas velocity of 15m/s with elapsed time of operation, while for gas velocity of 50m/s it arrived at an asymptotic valve of 62% as shown in Figure 4.20.

Table 4.4 Fouling resistance of experiment performed in case of specification #1.

Exhaust gas velocity (m/s)	Overall thermal resistance R(m^2K/W)		Fouling resistance $R_f = R_{final} - R_c$	$\dfrac{R_{f,10m/s}}{R_f}$	$\dfrac{dR_f}{dt}\Big|_{t=0}$ (m^2K/W)
	R_c	R_{final}			
10	3.29×10^{-3}	1.45×10^{-2}	1.12×10^{-2}	1	5.57×10^{-5}
30	2.62×10^{-3}	6.14×10^{-3}	3.52×10^{-3}	3.18	2.79×10^{-5}
50	1.14×10^{-3}	2.97×10^{-3}	1.83×10^{-3}	6.12	1.11×10^{-5}

Table 4.5 Fouling resistance of experiment performed in case of specification #2.

Exhaust gas velocity (m/s)	Overall thermal resistance R(m^2K/W)		Fouling resistance $R_f = R_{final} - R_c$	$\dfrac{R_{f,10m/s}}{R_f}$	$\dfrac{dR_f}{dt}\Big|_{t=0}$ (m^2K/W)
	R_c	R_{final}			
10	3.32×10^{-3}	1.82×10^{-2}	1.49×10^{-2}	1	4.25×10^{-5}
30	2.66×10^{-3}	8.98×10^{-3}	6.32×10^{-3}	2.4	2.03×10^{-5}
50	1.21×10^{-3}	5.23×10^{-3}	4.02×10^{-3}	3.7	9.20×10^{-6}

Table 4.6 Fouling resistance of experiment performed in case of specification #3.

Exhaust gas velocity (m/s)	Overall thermal resistance R(m^2K/W)		Fouling resistance $R_f = R_{final} - R_c$	$\dfrac{R_{f,15m/s}}{R_f}$	$\dfrac{dR_f}{dt}\Big|_{t=0}$ (m^2K/W)
	R_c	R_{final}			
15	3.51×10^{-3}	2.67×10^{-2}	2.32×10^{-2}	1	5.60×10^{-5}
60	1.37×10^{-3}	2.72×10^{-3}	1.15×10^{-2}	2.0	1.33×10^{-5}

Table 4.7 Fouling resistance of experiment performed in case of specification #4.

Exhaust gas velocity (m/s)	Overall thermal resistance R(m^2K/W)		Fouling resistance $R_f = R_{final} - R_c$	$\dfrac{R_{f,15m/s}}{R_f}$	$\dfrac{dR_f}{dt}\Big|_{t=0}$ (m^2K/W)
	R_c	R_{final}			
15	3.73×10^{-3}	2.09×10^{-2}	1.72×10^{-2}	1	5.72×10^{-5}
60	1.43×10^{-3}	7.45×10^{-3}	6.02×10^{-3}	2.9	1.42×10^{-5}

Figure 4.13 Fouling resistance of EGR cooler, specification #1 (ø8.0).

Figure 4.14 Effectiveness of EGR cooler, specification #1 (ø8.0).

Figure 4.15 Fouling resistance of EGR cooler, specification #1 (ø7.5).

Figure 4.16 Effectiveness of EGR cooler, specification #1 (ø7.5).

Figure 4.17 Fouling resistance of EGR cooler, specification #3
(Shell & tube type).

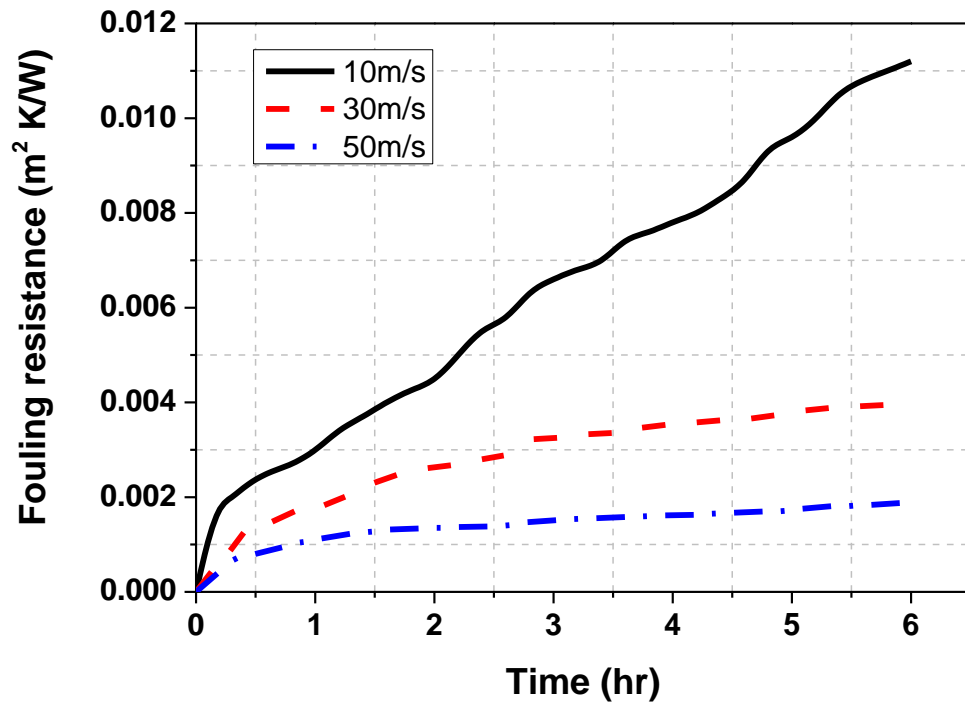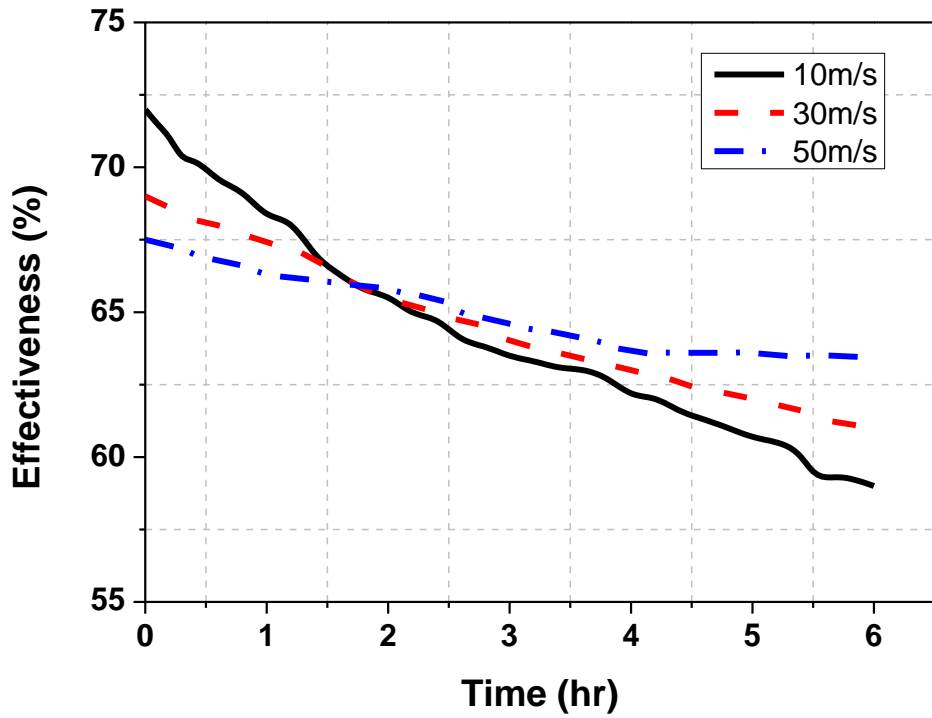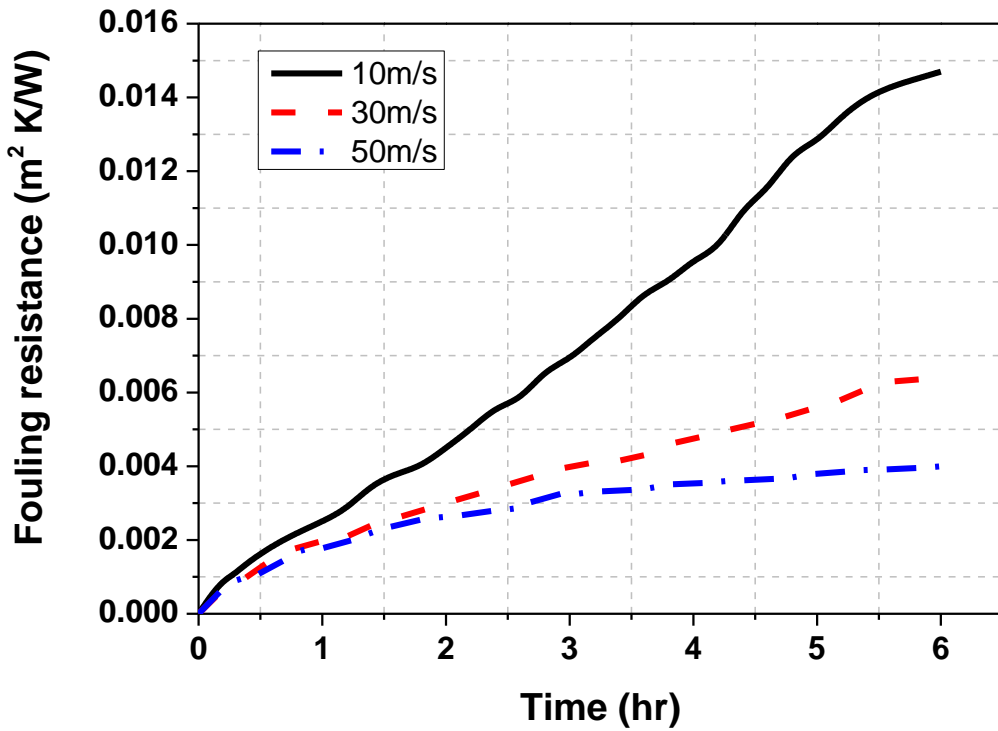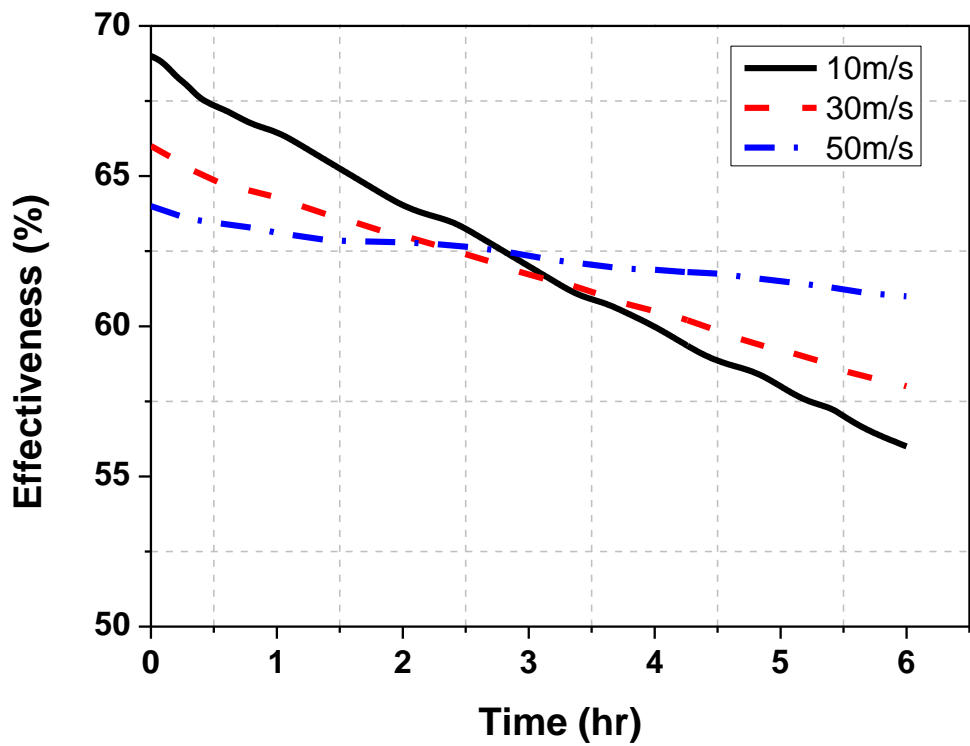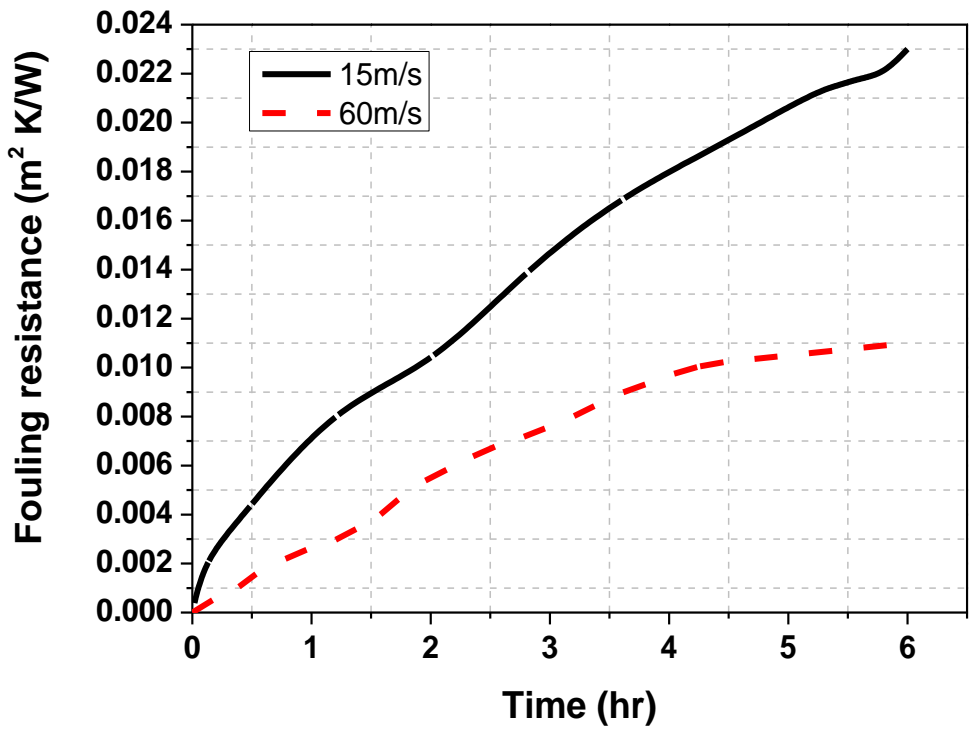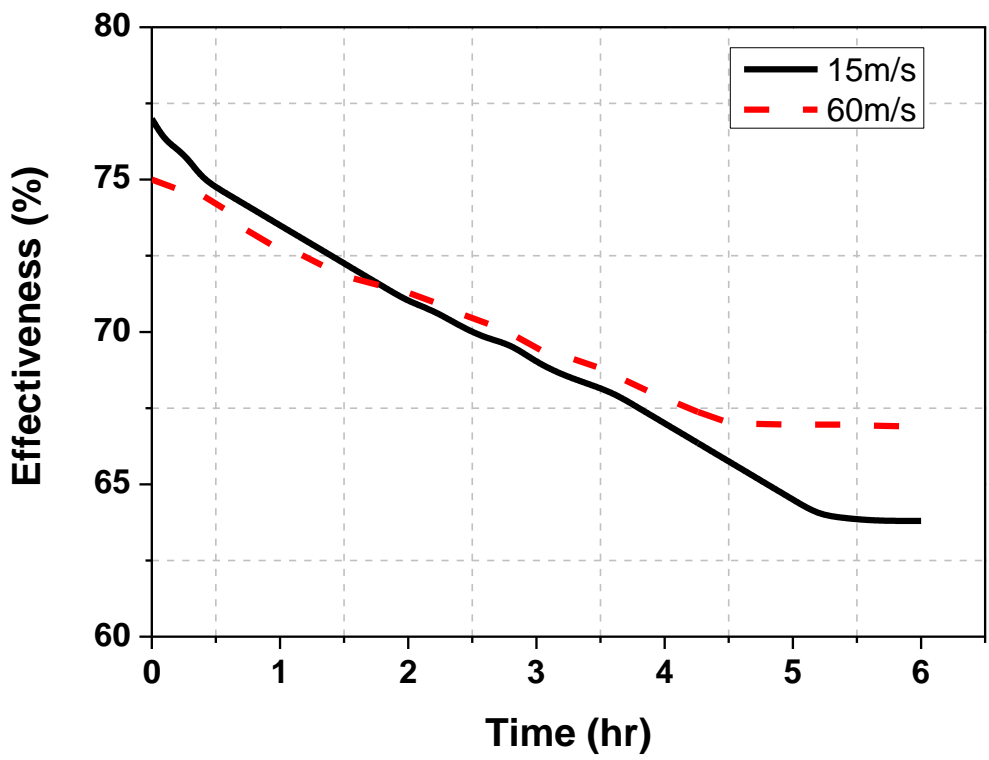Figure 4.18 Effectiveness of EGR cooler, specification #3 (Shell
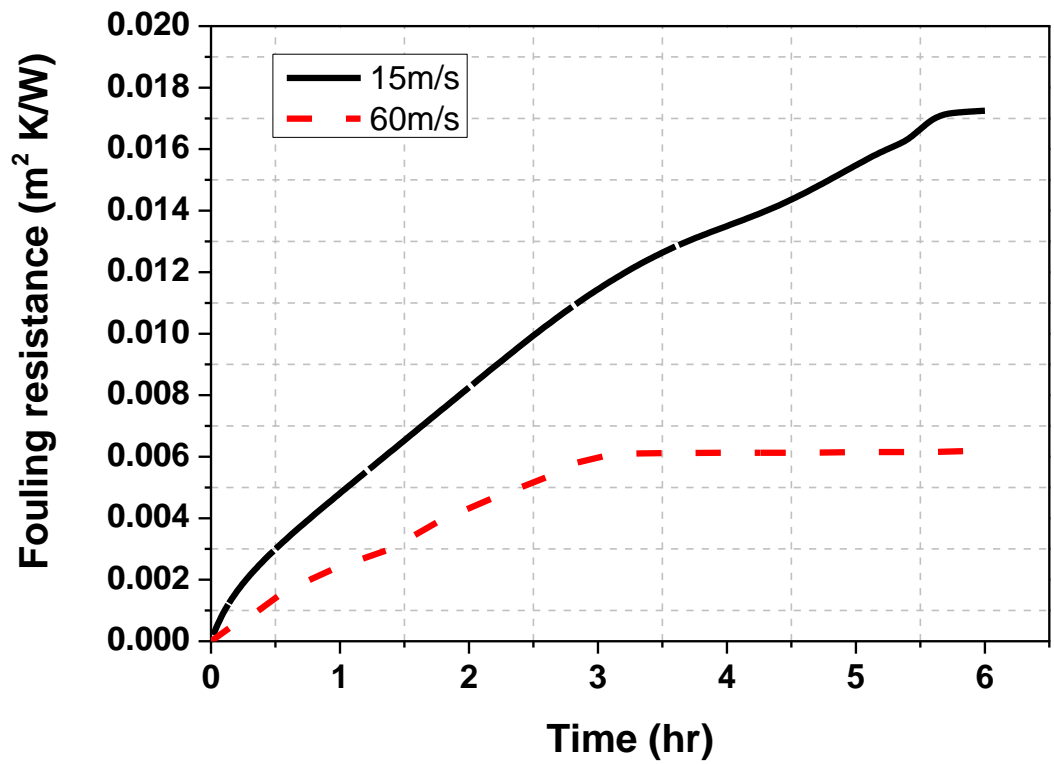& tube type).

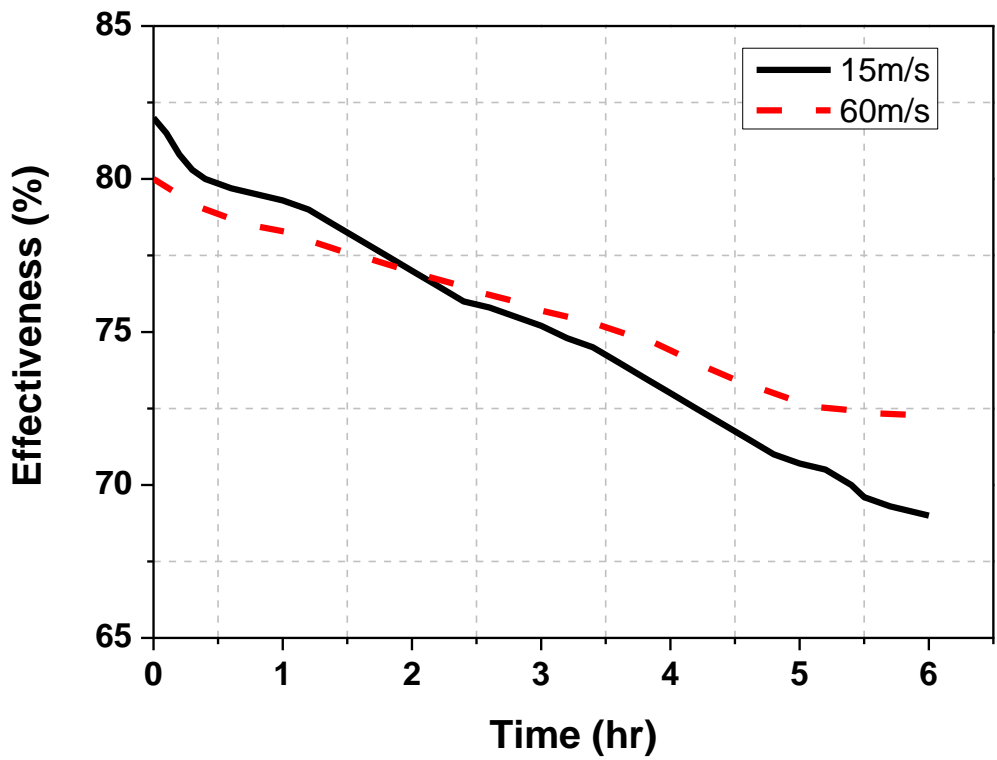Figure 4.19 Fouling resistance of EGR cooler, specification #4 (Fin type).

Figure 4.20 Effectiveness of EGR cooler, specification #4 (Fin type).

Chapter 5. Experimental test on an engine

5.1 Experimental setup

5.1.1 Experimental apparatus

The overall experimental apparatus on a dynamo cell consist of an engine with EGR cooler, a dynamometer and controller, exhaust gas analyzer, smoke meter and DMS 500 as shown in Figure 5.1.

A four-cylinder 2.2L and 1.6L direct injection Diesel engine as shown in Figure 5.2 and Figure 5.3 was used for experiment, respectively. These engines have a fuel injection equipment (FIE) including a piezo injector, a common rail, and a high pressure pump. Detailed specifications of engines and fuel injection equipments are shown in Table 5.1, Table 5.2 and Table 5.3, respectively. The test engine was connected to a 340 kW AC dynamometer which is able to operate both steady-state operations and transient state operations with the dynamometer controller. The specification of dynamometer is shown in Table 5.4. Oil and coolant temperature were controlled during the engine test using the PID controller, equipped in dynamometer control system. The quality of diesel was preserved from a large capacity fuel tank during the entire experiment period and fuel temperature was maintained to 40 ℃ using the fuel temperature controller. The temperature of the engine test cell was controlled by an air-conditioning system.

Exhaust gas composition of O_2 and CO_2 and NOx, THC, CO, and PM were measured during the test. NOx, THC, CO, CO_2, and O_2 were measured by the exhaust gas analyzer (HORIBA, MEXA-7100DEGR). All species were measured in volume fraction in wet condition. The measurement method of each emission is listed in Table 5.5. PM was measured by the smoke meter and DMS-500. The

specification of the smoke meter is shown in Table 5.6 and the specification of the DMS-500 is listed in Table 5.7. To monitor the AFR easily during the test, an AFR analyzer, as shown in Table 5.8, was installed at the exhaust manifold. It has an O_2 sensor and calculates AFR by the O_2 balance equation. AFR was calculated using measured O_2, CO_2, CO and THC from Spindt equation [73]:

$$AFR = \frac{(CO_2 \times 10000 + CO)}{(CO_2 \times 10000 + CO + THC)} \times (AA + BB) \qquad (5.1.1)$$

where,

$$AA = \frac{11.4919 \times FC \times (1 + \dfrac{CO/(CO_2 \times 10000)}{2} + \dfrac{O_2}{CO_2})}{\left(1 + \dfrac{CO}{(CO_2 \times 10000)}\right)} \qquad (5.1.2)$$

$$BB = \frac{119.8074 \times (1 - FC)}{\left(3.5 + \dfrac{CO}{(CO_2 \times 10000)}\right)} \qquad (5.1.3)$$

$$FC = \frac{12.011}{\left(12.011 + 1.008 \times HC\_ratio\right)} \quad . \qquad (5.1.4)$$

5.1.2 Experimental conditions

In this study, the engine was warmed up and the temperatures of coolant and oil were stabilized. To flow the exhaust gas into the EGR cooler, the bypass valve line was disconnected. The engine was operated at the conditions of 5 different operation points, such as 10, 20, 30, 40, and 50kg/h. The experiments were carried

out to evaluate the effectiveness and the pressure drop of EGR cooler in dynamometer. The schematic position of temperature sensors in EGR cooler were shown in Figure 5.4. The temperature of coolant was adjusted at 90℃. The temperature deviations were controlled within ±2℃.

The conditions illustrated in Figure 5.5 were utilized for the modified fouling test mode in engine dynamometer. These conditions were determined by combining the ESC-13 mode for emissions testing with the EGR cooler fouling procedure (76 hours) proposed by Modine, a manufacturer of EGR coolers as shown in Figure 5.6 and Figure 5.7, respectively [74-76]. The test conditions were designed to include a total of abbreviated 15 hours of engine operating time, with 5 hours of this period involving operating the engine at 1,100 rpm with no load and a high incidence of PM.

In the initial step of the fouling test, the engine was operated under the 3 conditions of 50, 80 and 120 kg/l of gas flow for a total of 1 hour at 25% engine load and 2,000 rpm. In the first step, the engine was operated for a total of 2 hours at 1,200 rpm under engine loads of 0, 20, 40, 60 and 80%. In the second step, the engine was operated for 5 hours at 0% engine load and 1,100 rpm. In the third step, the engine was operated for 1 hour at 1,200 rpm under engine loads of 20 and 80%. In the fourth step, the engine was operated for 3 hours at 75% engine load and 2,000 rpm. The fifth step was the same as the first step, and the final step was the same as the initial step. The engine was operated for a total of 15 hours to save the engine operating time and expenses.

Table 5.1   1.6L Engine specifications

Description	Specification
Engine type	In-line 4 cylinder 1.6 L
Max power(kW)/Torque(Nm)	94 / 259
Bore x Stroke (mm)	77.2 x 84.5
Compression ratio	17.3

Table 5.2   2.2L Engine specifications

Description	Specification
Engine type	In-line 4 cylinder 2.2 L
Max power(kW)/Torque(Nm)	147 / 436
Bore x Stroke (mm)	85.4 x 96.0
Compression ratio	16.0

Table 5.3 FIE specifications

Description	Specification
Fuel injector type	Piezoelectric type
Manufacturer	Bosch
No. of Nozzle Holes	8
Spray Angle	156 °
Nozzle Diameter (mm)	0.143

Table 5.4 Specifications of dynamometer

Description	Specification
Manufacturer	AVL ELIN
Model	MCA-231
Capacity	340kW
Type	AC
Cooling	Air cooling
Maximum rpm	7000

Table 5.5 The principle of measurement by the emission analyzer.

Emissions	Measurement principle
NOx	CLD
THC	FID
O_2, CO_2, CO	NDIR

Table 5.6 The specifications of the smoke meter.

Item	Specification
Manufacturer	AVL
Model	AVL 415S
Measurement range	0 ~ 10 FSN / 0 ~ 32,000 mg/m³
Resolution	0.001 FSN / 0.01 mg/m³
Repeatability (as standard deviation)	$\sigma \leq \pm$(0.005 FSN + 3 % of measured value)
Reproducibility (as standard deviation)	$\sigma \leq \pm$(0.005 FSN + 6 % of measured value)

Table 5.7 The specifications of the DMS-500

Item	Specification
Particle Size Range	5 nm – 1 µm (5 nm – 2.5 µm option)
Number of Electrometers	22
Size Classification	Electrical Mobility
Dilution Factor Range	1 – 3000
Maximum Primary Dilution Temperature	150 ºC
Sample Flow rate	8 slpm (1 µm range) at 0 ºC + 100 kPa
Instrument Zeroing	Automatic; internal HEPA filter
Spectral Elements	16 or 32/decade
Output Data Rate	10/sec – 1/min
Time Response	T 10–90 % 200 ms T 10–90 % 300 ms with 5m heated line
Calibrations: Non-agglomerate: Agglomerate (Diesel):	By NIST traceable PSL spheres & DMA size selected NaCl/H SO , comparison with standard electrometer DMA size selected soot, comparison with standard electrometer
Calibration Interval	12 months
Max Concentration	≈1011 dN/dlogD /cc (diluter on)

Table 5.8 The specifications of the AFR analyzer.

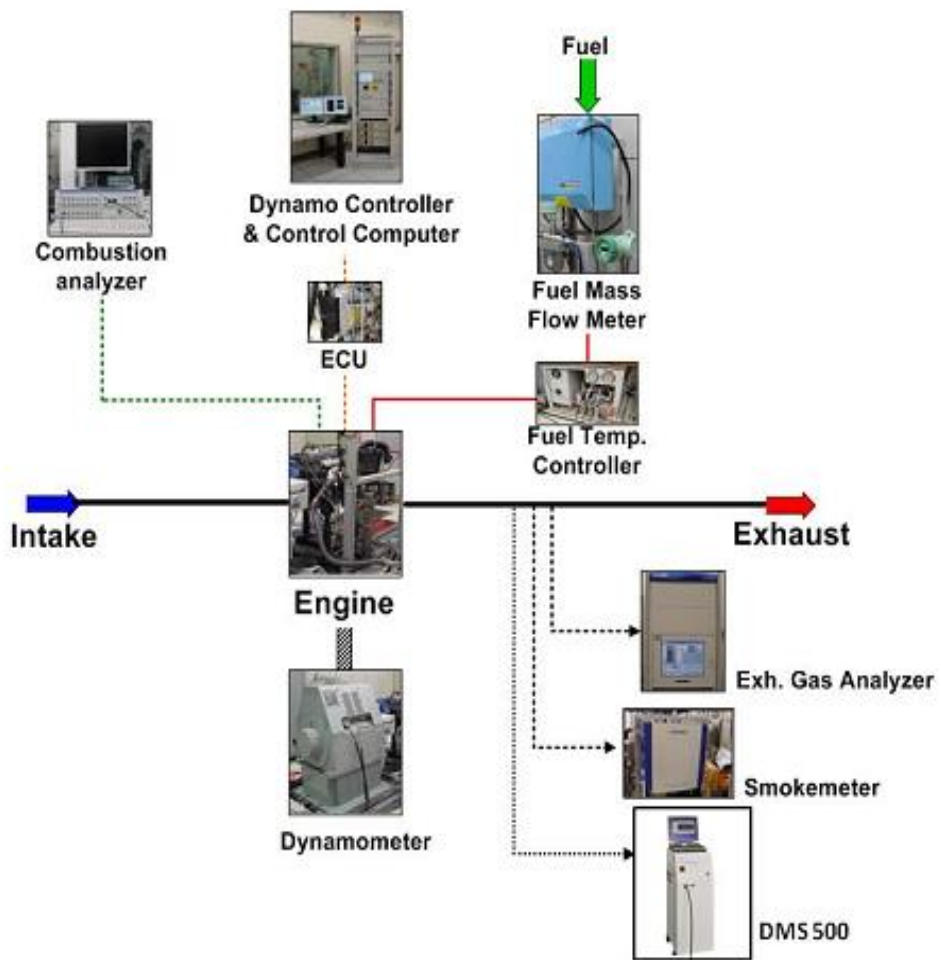| Item	Specification
Manufacturer	HORIBA
Model	MEXA-110λ
Measurement range (H/C = 1.85)	A/F 10.0 ~ 30.0
Accuracy (H/C = 1.85)	±0.3 A/F when 12.5 A/F ±0.1 A/F when 14.7 A/F ±0.5 A/F when 23.0 A/F
Exhaust gas temperature (℃)	-7 ~ 900 (recommend 200 ~800)

Figure 5.1 Schematic of engine test and measurement equipment

Figure 5.2 A four cylinder - 2.2Ldiesel engine.

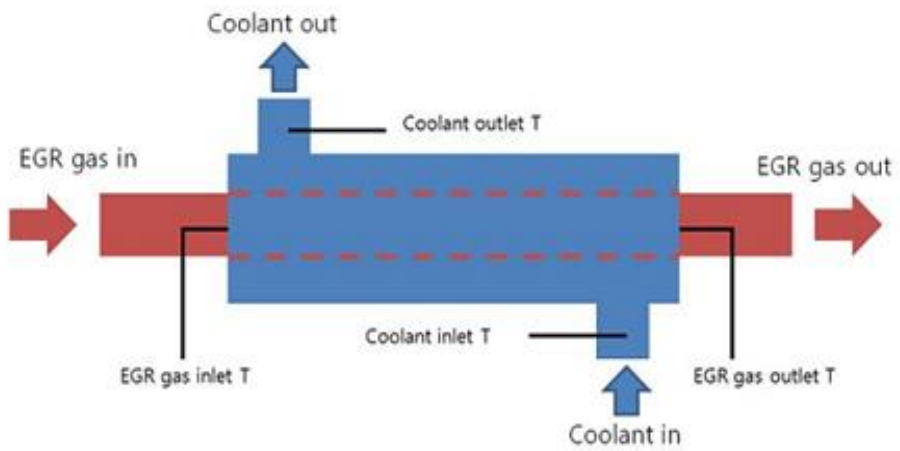Figure 5.3 A four cylinder - 1.6Ldiesel engine.

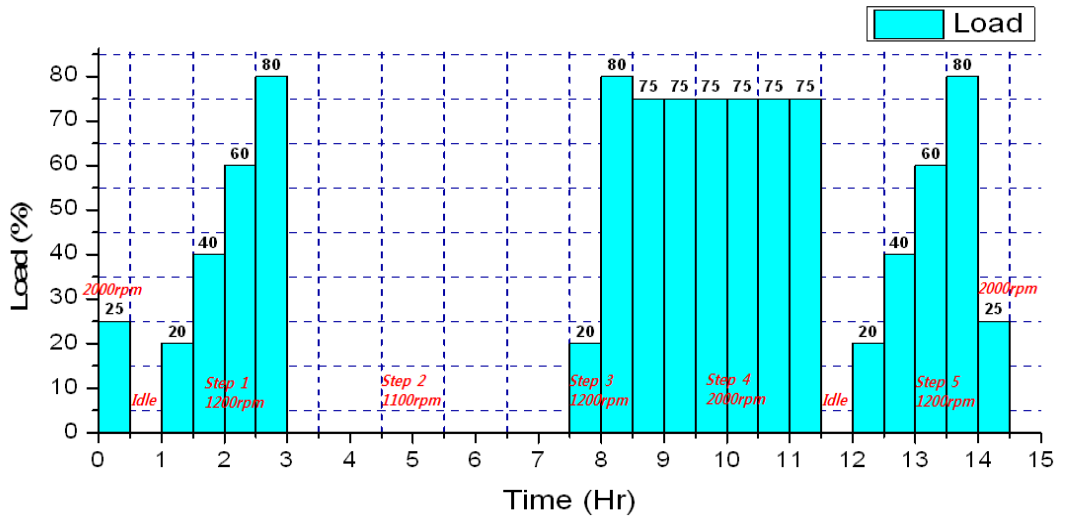Figure 5.4 Schematic position of temperature sensors in EGR cooler.
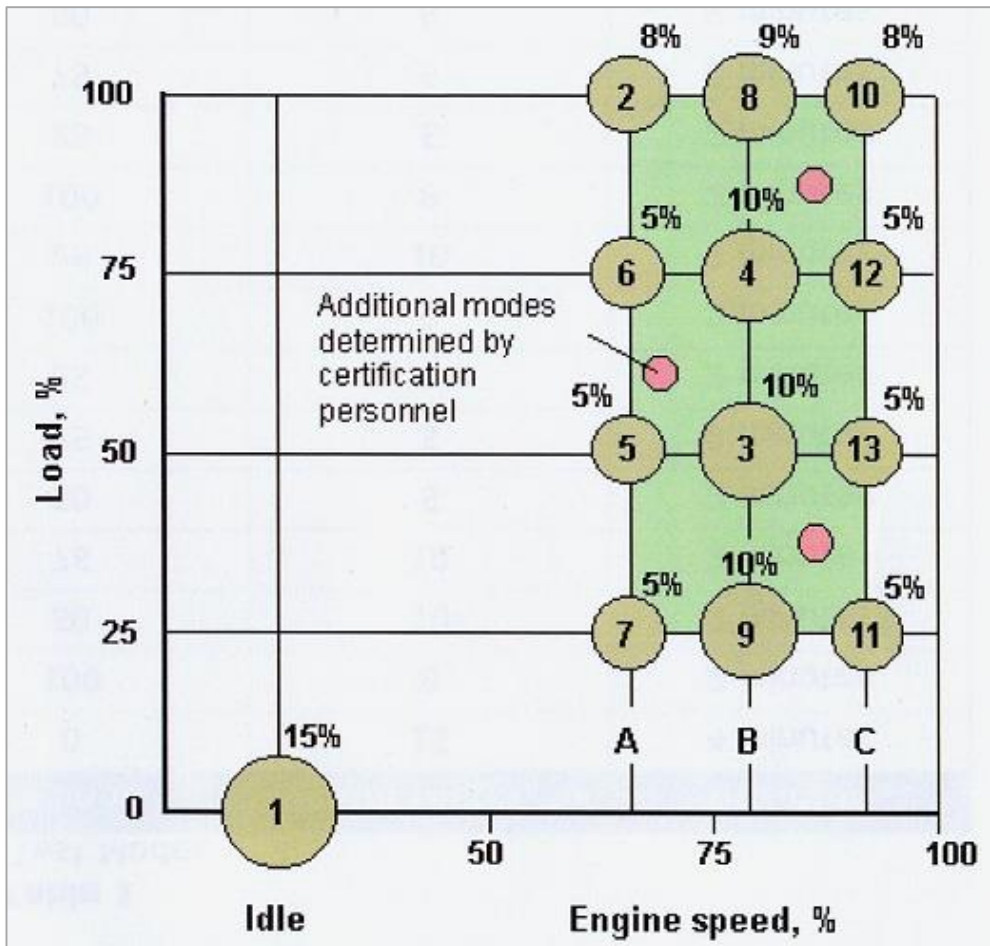
Figure 5.5 Modified fouling test mode.

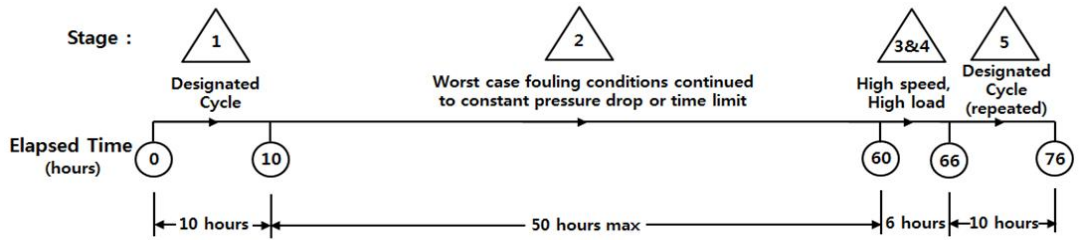Figure 5.6 ESC-13 mode for diesel engine test.

Figure 5.7 Fouling test mode of EGR cooler in Modine.

5.2 Experimental results

5.2.1 Effectiveness characteristics of I-flow EGR coolers

The experimental tests were performed to measure how PM fouling in I-flow EGR coolers changes the heat exchange effectiveness on engine dynamometer before and after fouling.

In case of specification #1(shell & tube type ø8.0, I-flow), the heat exchange effectiveness was decreased by max 14% after fouling as shown in Figure 5.8 and 5.11. The decreasing shapes are similar at both conditions. The outlet temperature of exhaust gas was increased, which have been caused by the PM deposited on the inner surface of the spiral tubes. The pressure drop between the inlet and the outlet of exhaust gas is the quantitative index of the PM deposited inside the EGR cooler. The accumulation of PM deposit raised enhanced thermal resistance because of the increased pressure drop. Accordingly, the pressure drop was increased by max 40%.

In case of specification #2(shell & tube type ø7.5, I-flow), the heat exchange effectiveness was decreased by max 17% as shown in Figure 5.9 and 5.11. The pressure drop was increased by max 54%.

In conclusion, the effectiveness of specification #1 was 5% and 9% higher than that of specification #2 before and after fouling, respectively. The pressure drops between two specifications were increased by 13% and 20% before and after fouling, respectively due to the difference of cross sectional areas as shown in Figure 5.10.

5.2.2 NO$_x$/PM characteristics of I-flow EGR coolers

According to EGR ratio, the emission level of NO$_x$ and PM were investigated [77]. In case of specification #1, depending on the EGR rate fluctuation, NO$_x$ decreases very largely, while PM increases slowly as shown in Figure 5.12. In case of specification #2, depending on the EGR rate fluctuation, the reduction rate of NO$_x$ and the increase rate of PM are large, respectively as shown in Figure 5.13. For both the specification #1 and #2, the emission level of NO$_x$ and PM were investigated according to EGR ratio after fouling as shown in Figure 5.14. This figure shows that the emission rate of NO$_x$ and PM of specification #1 is lower than that of specification #2.

The results converted to NO$_x$ change per unit EGR rate is shown in Figure 5. 15. NO$_x$ decreasing rate per unit EGR is about 4% larger in low EGR condition in case of specification #1 compared with specification #2. In addition, NO$_x$ decreasing rate per unit EGR is about 2% larger in high EGR condition in case of specification #1 compared with specification #2.

The results converted to PM change per unit EGR rate is shown in Figure 5. 16. PM increasing rate per unit EGR is about 6% larger in low EGR condition in case of spec. #2 compared with specification #1. PM increasing rate per unit EGR is about 3% larger in high EGR condition in case of specification #2 compared with specification #1.

In conclusion, specification #1 is superior to specification #2 in consideration of NO$_x$ and PM change characteristics.
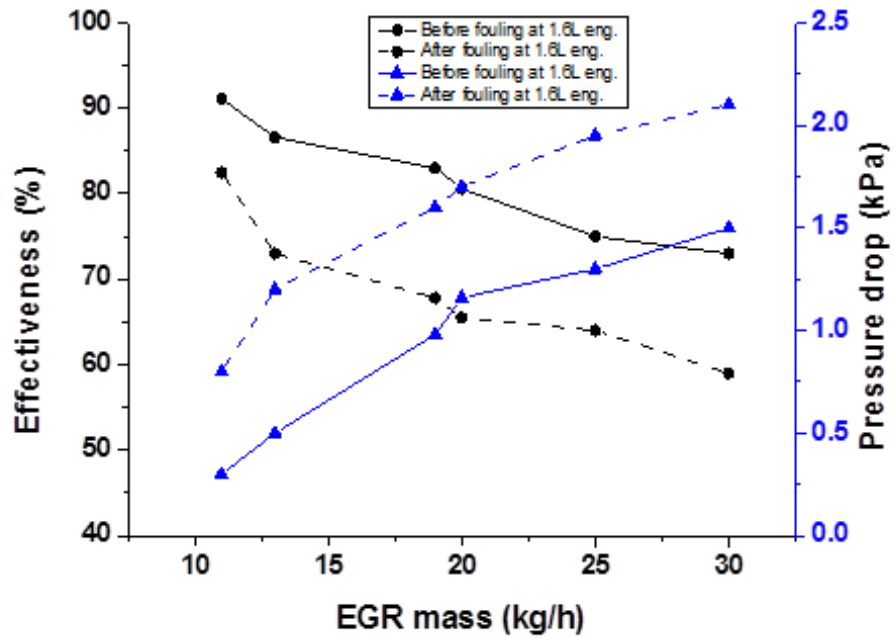
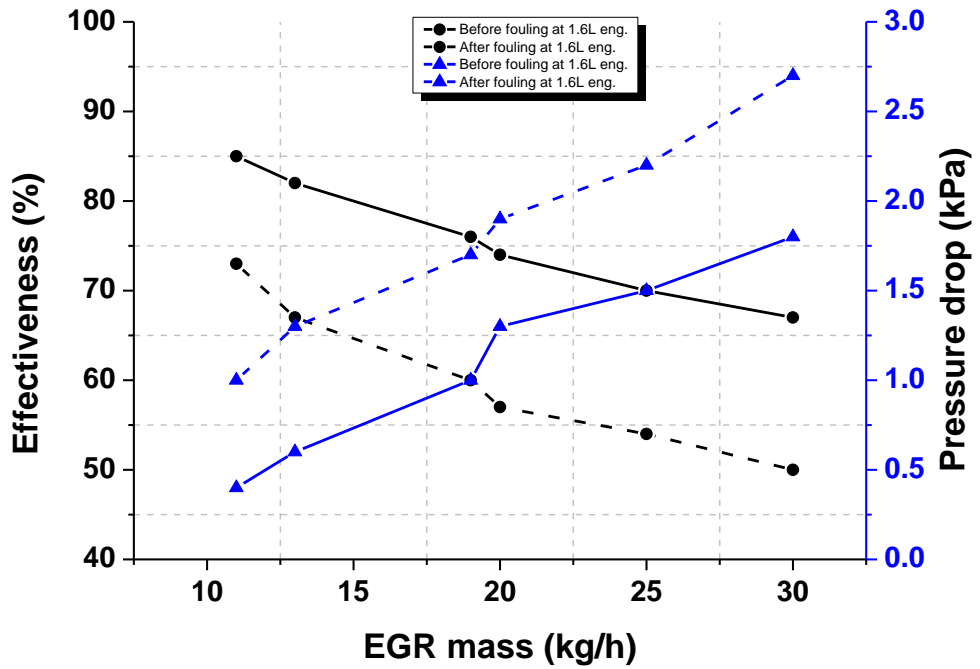Figure 5.8 Effectiveness and pressure drop of I-flow EGR cooler
(φ8.0 tube).

Figure 5.9 Effectiveness and pressure drop of I-flow EGR cooler
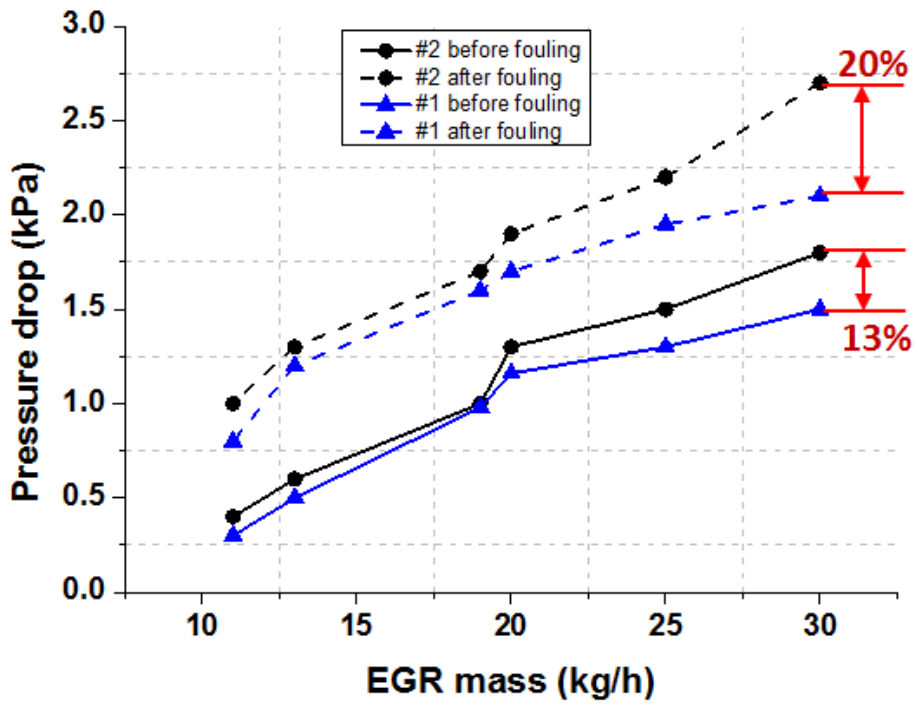(φ7.5 tube)

Figure 5.10 Pressure drop of I-flow EGR coolers (spec #1 and spec #2).

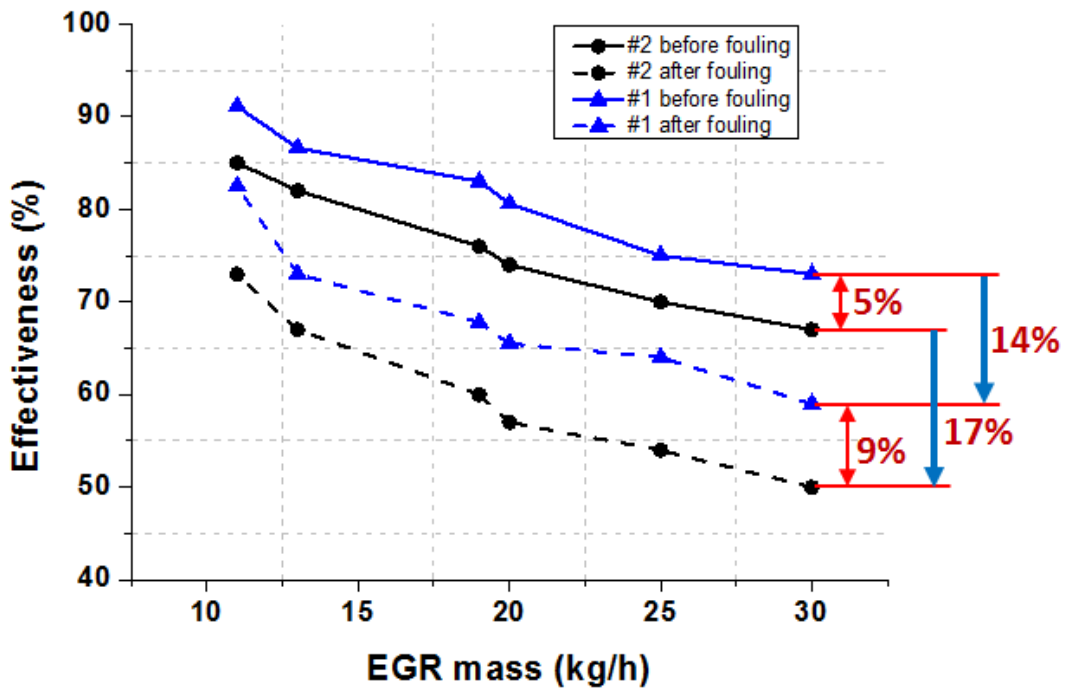Figure 5.11 Effectiveness of I-flow EGR coolers (spec #1 and spec #2).

Figure 5.12 NO$_x$ and PM change corresponding to EGR ratio
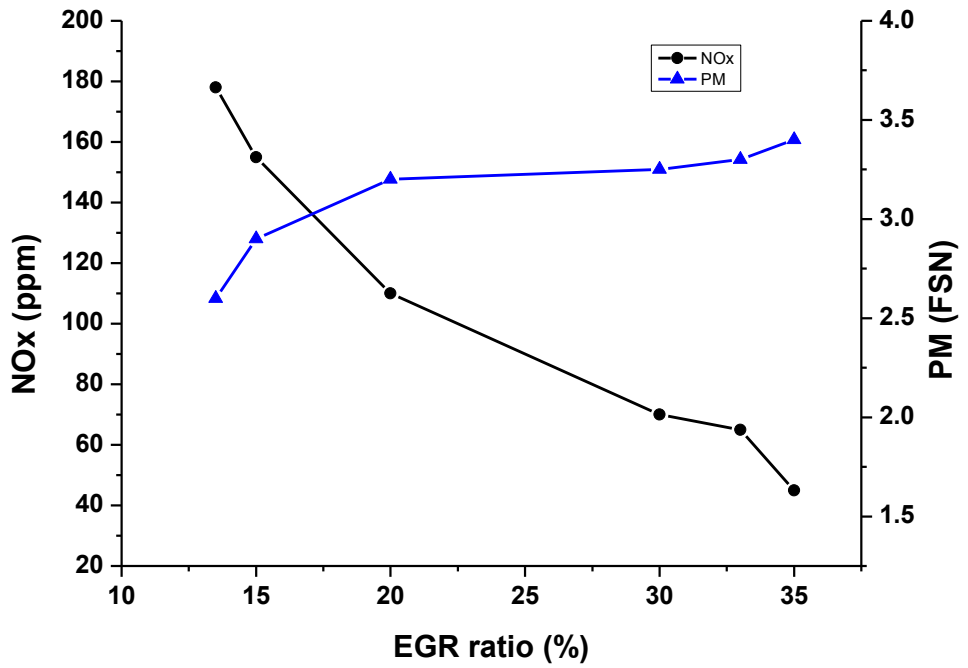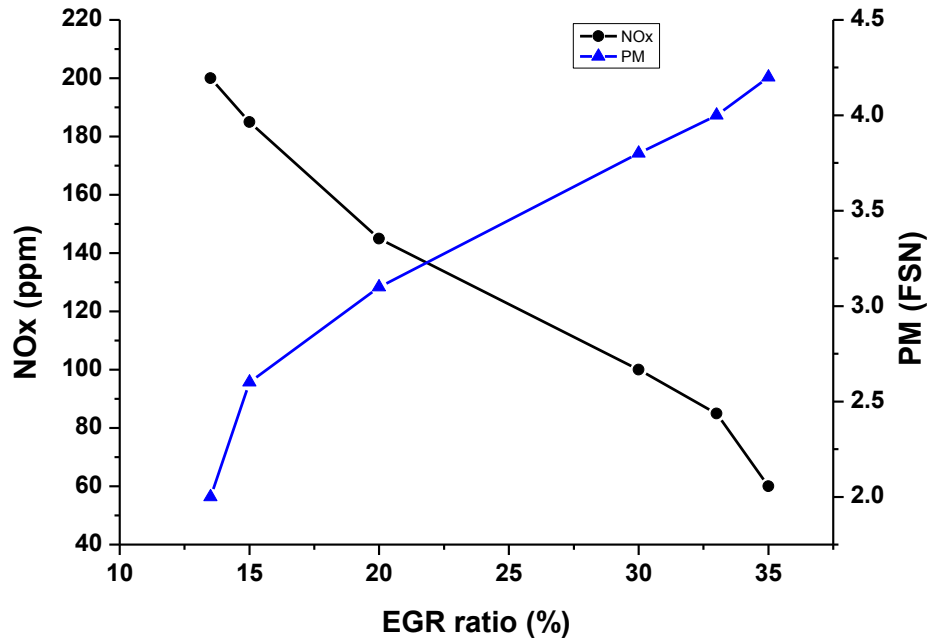of I-flow EGR cooler (ϕ8.0 tube).

Figure 5.13 NO_x and PM change corresponding to EGR ratio
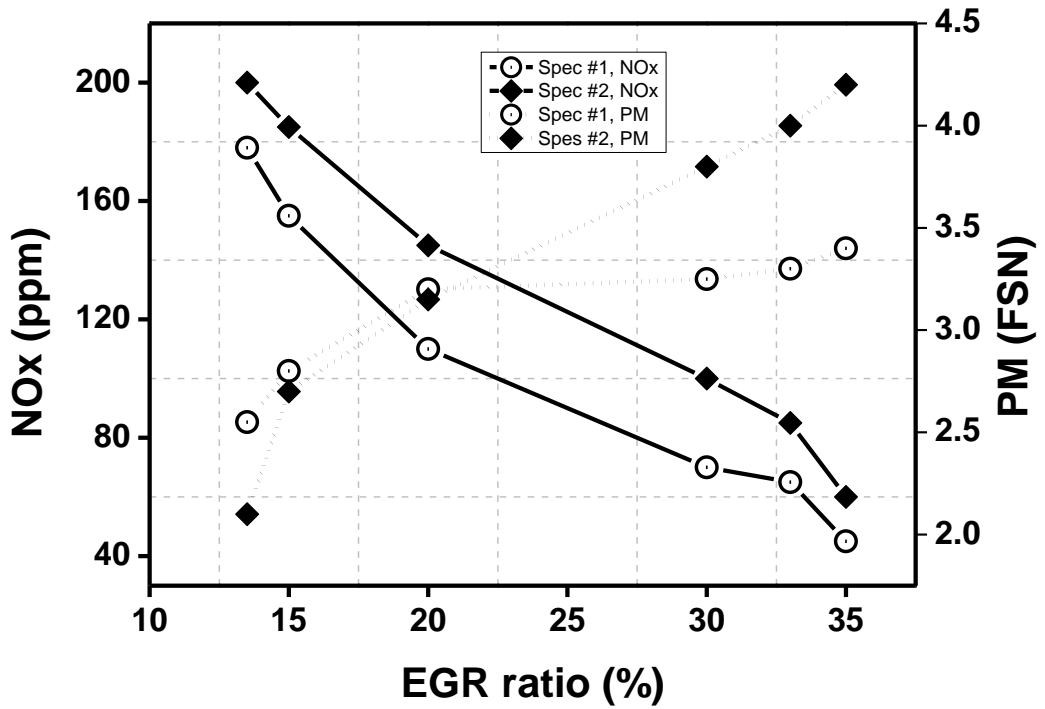of I-flow EGR cooler (φ7.5 tube).

Figure 5.14 NO$_x$ and PM change corresponding to EGR ratio
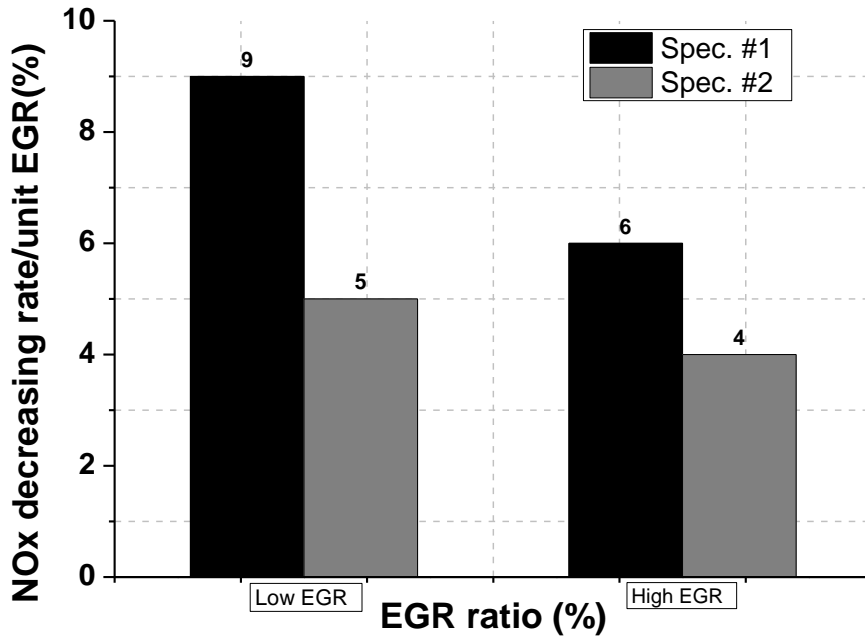of I-flow EGR cooler (spec. #1 and spec. #2).
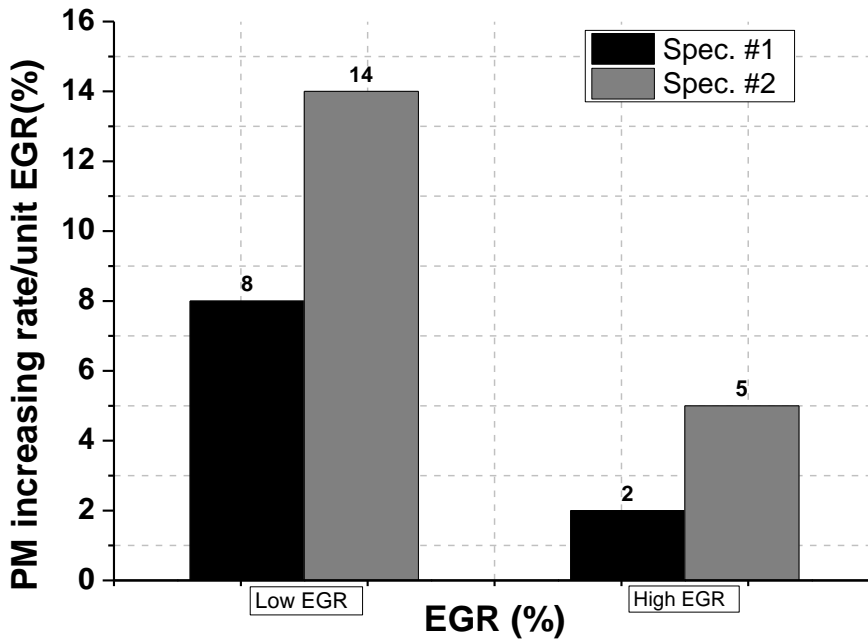
Figure 5.15 NO$_x$ change per unit EGR ratio.

Figure 5.16 PM change per unit EGR ratio.

5.2.3 Effectiveness characteristics of U-flow EGR coolers

The experimental tests were performed to measure how PM fouling in U-flow EGR coolers changes the heat exchange effectiveness on engine dynamometer before and after fouling.

In case of specification #3(shell & tube type ø8.0, U-flow), the heat exchange effectiveness was decreased by max 15% as shown in Figure 5.17 and 5.20. The pressure drop between the inlet and the outlet of exhaust gas is the quantitative index of the PM deposited inside the EGR cooler. The accumulation of PM deposit raised enhanced thermal resistance because of the increased pressure drop. Accordingly, the pressure drop was increased by max 16%.

In case of specification #4(Wavy-fin type, U-flow), the heat exchange effectiveness was decreased by max 10% as shown in Figure 5.18 and 5.20. The pressure drop was increased by max 17%.

In conclusion, the effectiveness of specification #4 was 4% and 9% higher than that of specification #3 before and after fouling, respectively. The pressure drop of specification #4 was nearly similar to that of specification #3.

5.2.4 NO$_x$/PM characteristics of U-flow EGR coolers

According to EGR ratio, the emission level of NO$_x$ and PM were investigated. In case of specification #3, depending on the EGR rate fluctuation, NO$_x$ decreases very largely, while PM increases slowly as shown in Figure 5.21. In case of specification #4, depending on the EGR rate fluctuation, the reduction rate of NO$_x$ and the increase rate of PM are similar to those of specification #3 as shown in Figure 5.22. For both the specification #3 and #4, the emission level of NO$_x$ and PM were investigated according to EGR ratio after fouling as shown in Figure 5.23.

This figure shows that the emission rate of NO_x of specification #3 is higher than that of specification #4. On the other hand, the emission rate of PM of specification #3 is similar to that of specification #4.

In order to observe the trend clearly, the results converted to NO_x change per unit EGR rate is shown in Figure 5. 24. NO_x decreasing rate per unit EGR is about 2% larger in low EGR condition in case of specification #4 compared with specification #3. In addition, NO_x decreasing rate per unit EGR is about 2% larger in high EGR condition in case of spec. #4 compared with specification #3.

The results converted to PM change per unit EGR rate is shown in Figure 5. 25. PM increasing rate per unit EGR is about 1% larger in low EGR condition in case of specification #3 compared with specification #4. PM increasing rate per unit EGR is about 0.5% larger in high EGR condition in case of specification #3 compared with specification #4.

In conclusion, specification #4 is somewhat superior to specification #3 in consideration of NO_x and PM change characteristics.
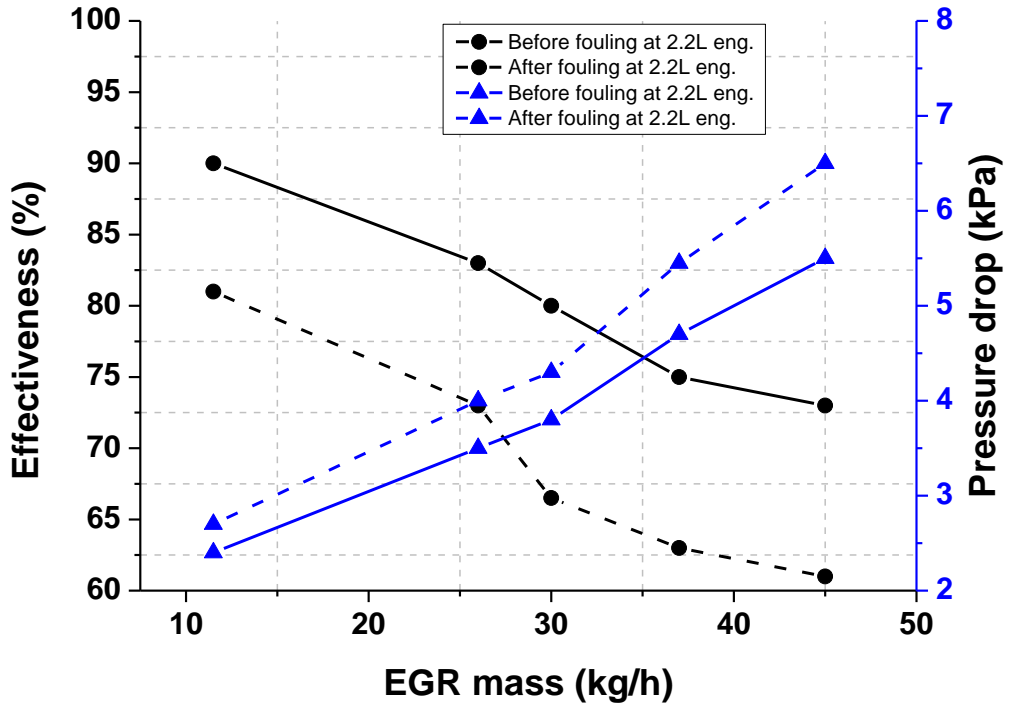
Figure 5.17 Effectiveness and pressure drop of U-flow EGR cooler
(φ8.0 tube).
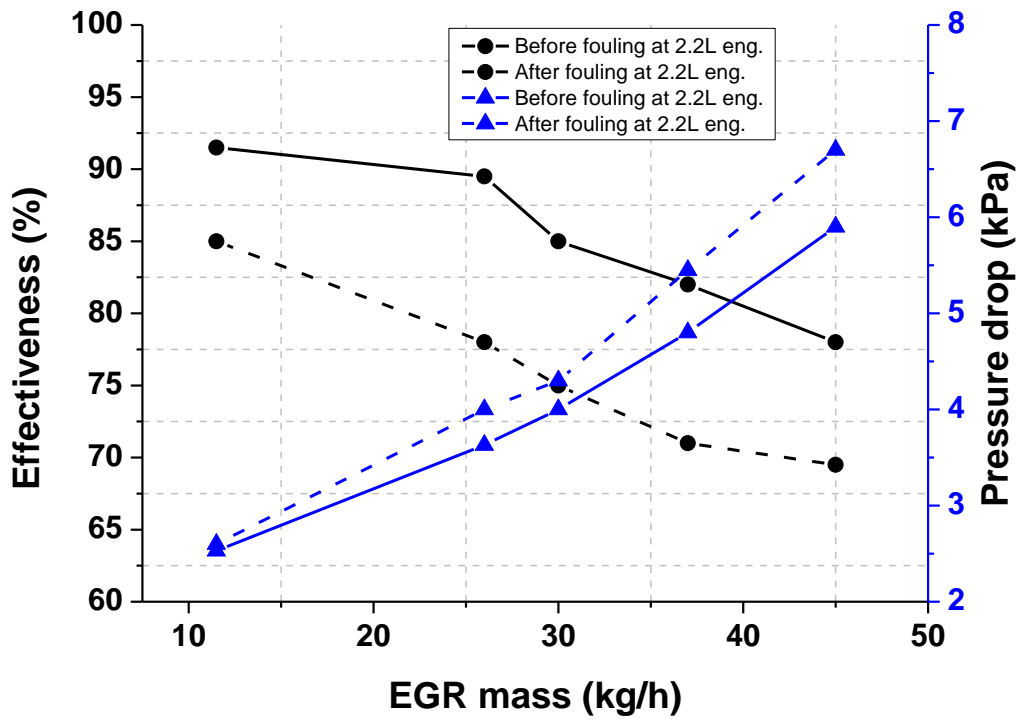
Figure 5.18 Effectiveness and pressure drop of U-flow EGR cooler

(Wavy fin).
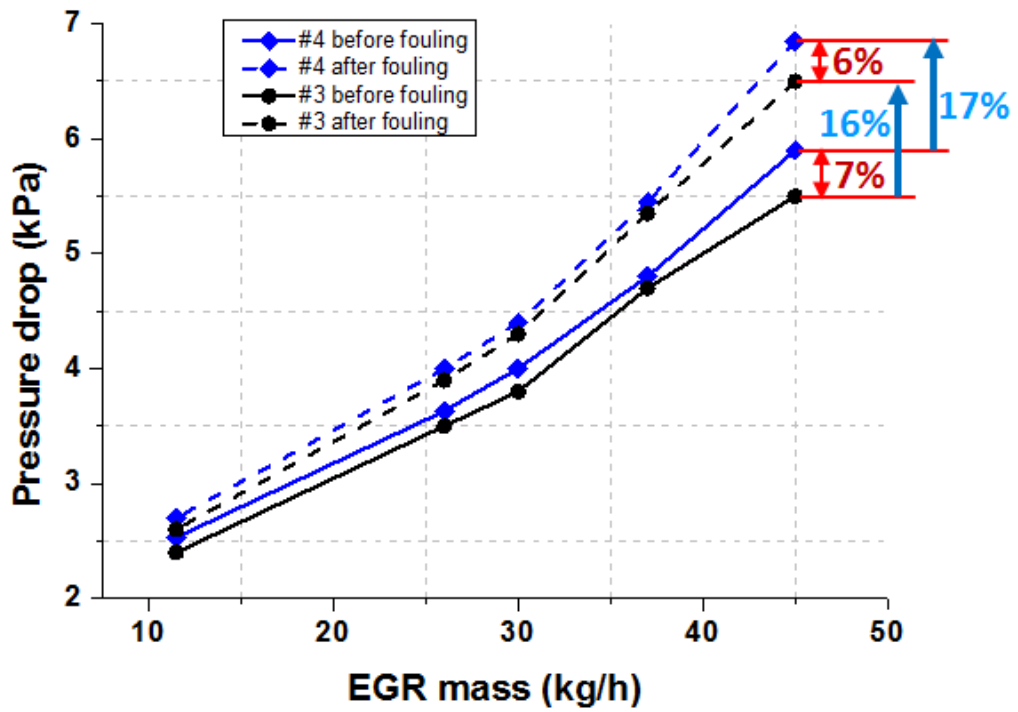
Figure 5.19 Pressure drop of U-flow EGR coolers (spec #3 and spec #4).
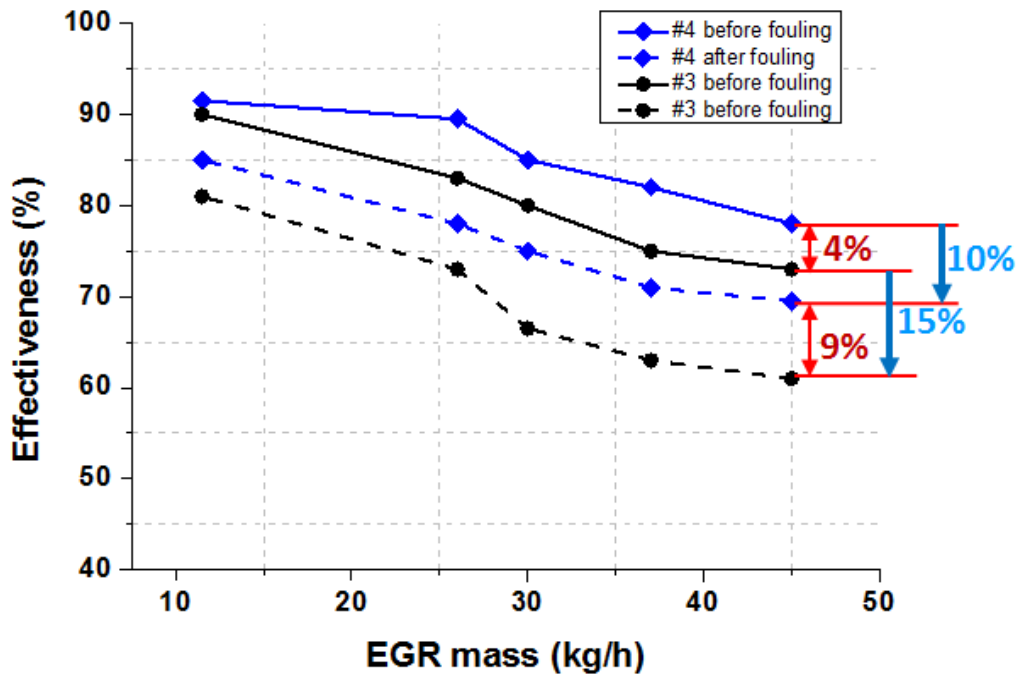
Figure 5.20 Effectiveness of UI-flow EGR coolers (spec #3 and spec #4).

Figure 5.21 NO$_x$ and PM change corresponding to EGR ratio

of U-flow EGR cooler (ϕ8.0 tube).

Figure 5.22 NO$_x$ and PM change corresponding to EGR ratio

of U-flow EGR cooler (Wavy fin).

Figure 5.23 NO$_x$ and PM change corresponding to EGR ratio
of I-flow EGR cooler (spec. #3 and spec. #4).

Figure 5.24 NO_x change per unit EGR ratio.

Figure 5.25 PM change per unit EGR ratio

5.2.5 PM characteristics of U-flow type at equivalent NO$_x$

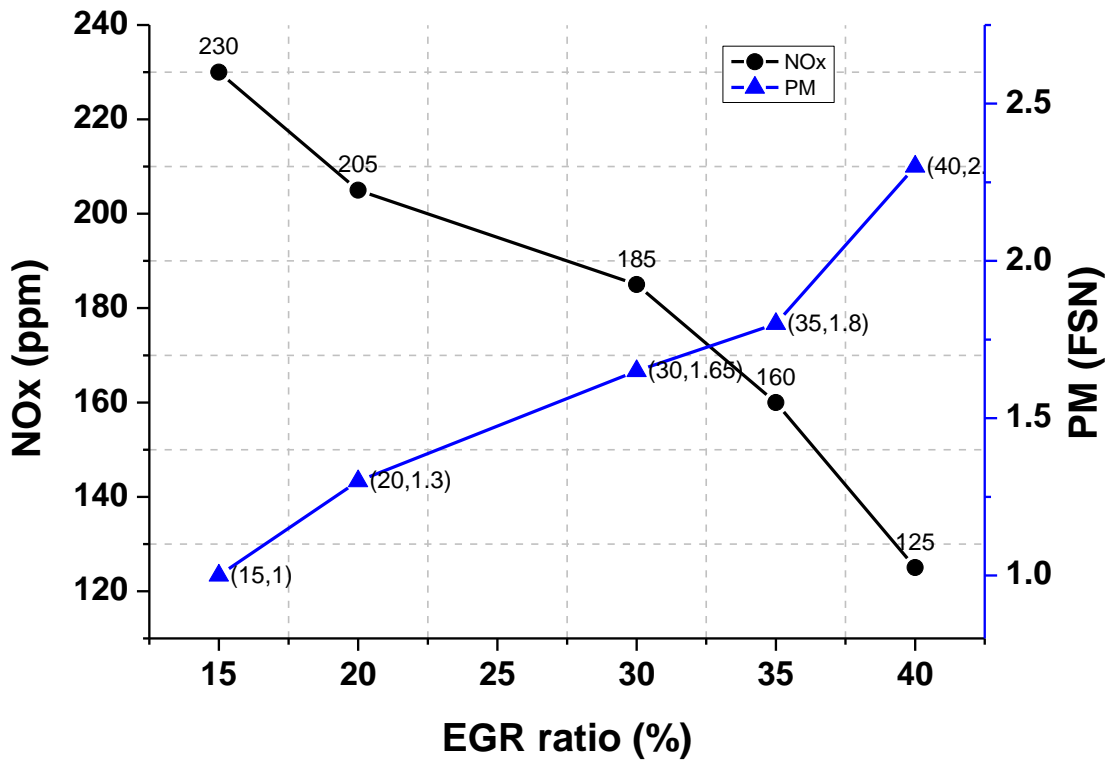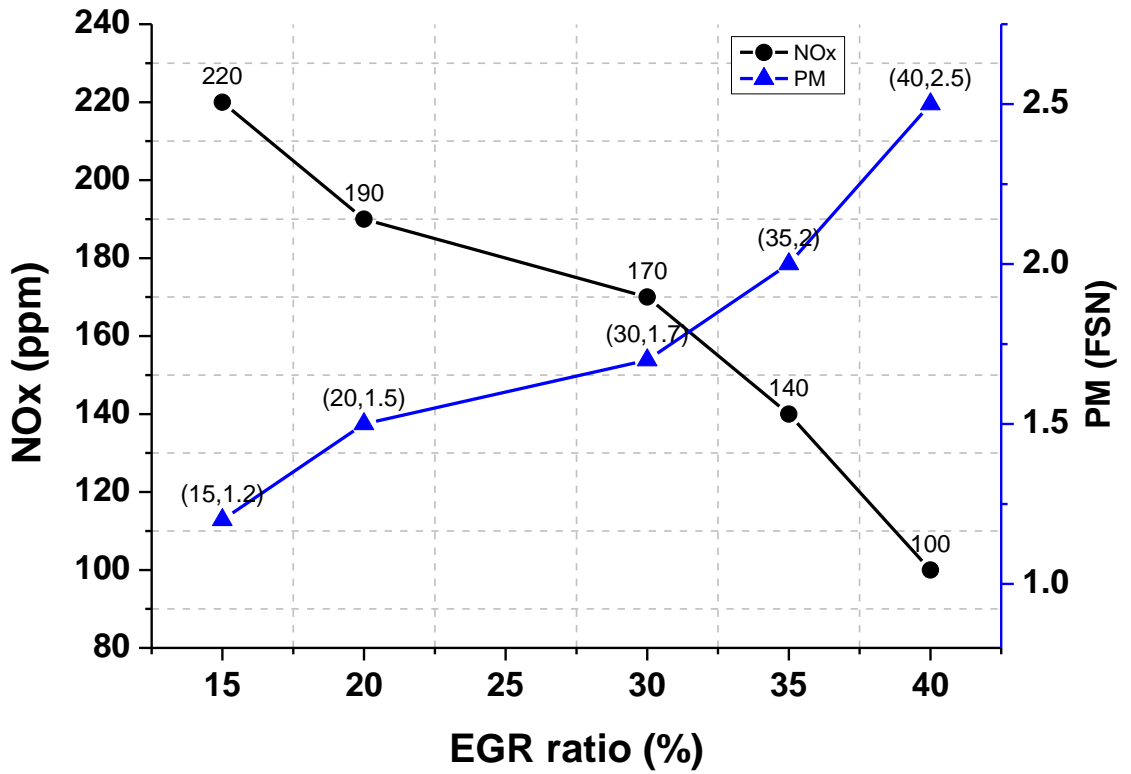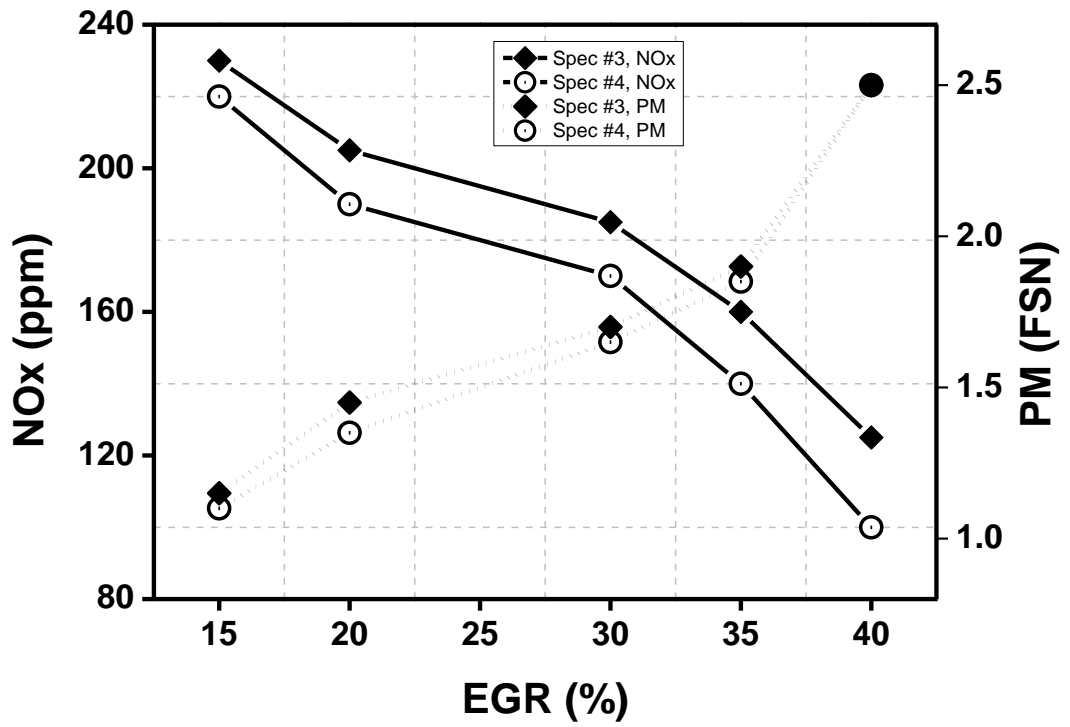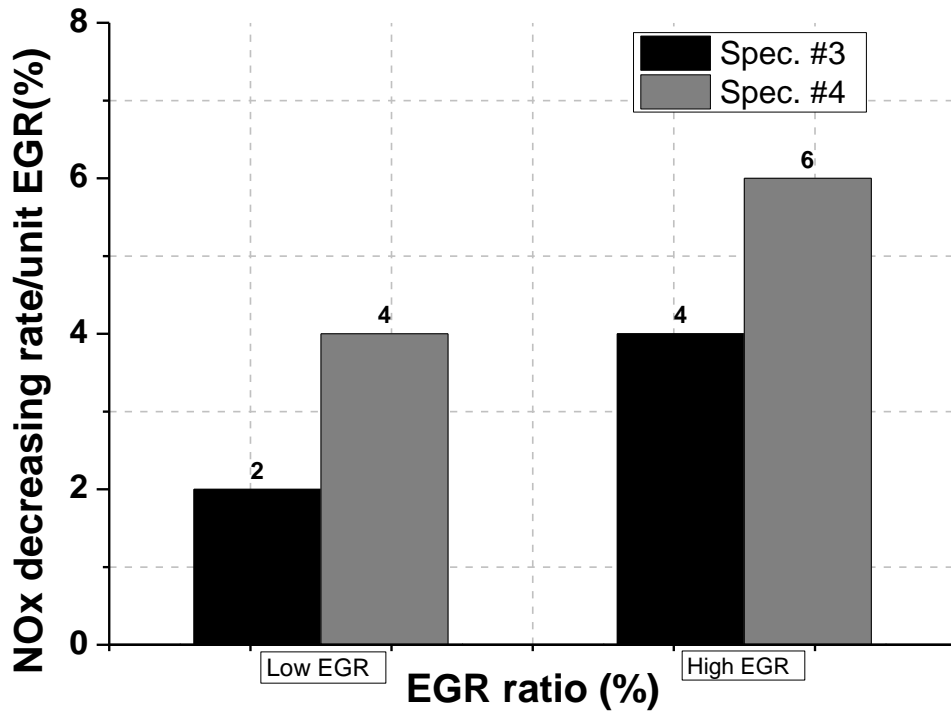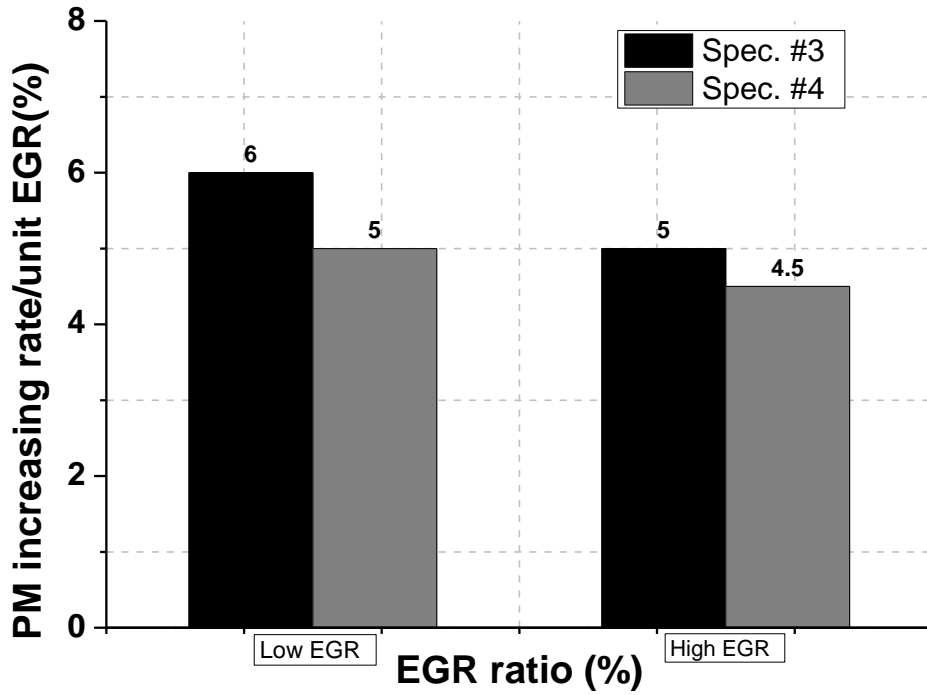When the emission levels of NO$_x$ are nearly equivalent for the specification #3 and #4, the PM size and numbers were investigated before and after fouling by using DMS-500 listed in table 5.7. The tests were performed at 2 kinds of conditions, such as 1250 rpm and 1750 rpm.

At 1250 rpm, the detail test conditions and PM characteristics for specification #3 at 24kg/h of EGR mass are shown in Figure 5.26. The detail test conditions and PM characteristics for specification #4 at 30kg/h of EGR mass are shown in Figure 5.27.

In case of specification # 3, there were no significant changes of the PM size and 5% decrease of the PM number before and after fouling.

In case of specification # 4, PM size in the range of 70~100nm were created mostly and the PM number were about 3.7E+08 before fouling. On the other hand, the PM size in the range of 65~85nm were created mostly and the PM number were about 2.2E+08 after fouling, which resulted in 41% decrease.

At 1750 rpm, the detail test conditions and PM characteristics for specification #3 at 45kg/h of EGR mass are shown in Figure 5.28. The detail test conditions and PM characteristics for specification #4 at 47kg/h of EGR mass are shown in Figure 5.29.

In case of specification # 3, there were no significant changes of the PM size and 7% decrease of the PM number before and after fouling.

In case of specification # 4, PM size in the range of 50~100nm were created mostly and the PM number were about 1.78E+08 before fouling. On the other hand, the PM size in the range of 50~85nm were created mostly and the PM number were about 1.26E+08 after fouling, which resulted in 29% decrease.

In conclusion, this result might be due to the superiority of heat transfer effectiveness of specification #4(fin type).

Base specification # 3 (S & T type) type : 24kg/h

Speed	BMEP	Fuel cons.	Int. Air
1250rpm	4bar	16.9mg/st	57.1kg/h

Figure 5.26 PM size distribution for equivalent NO_x emission at 24kg/h.

Modified specification # 4 (Fin type) : 30kg/h

Speed	BMEP	Fuel cons.	Int. Air
1250rpm	4bar	17.1mg/st	57.2kg/h
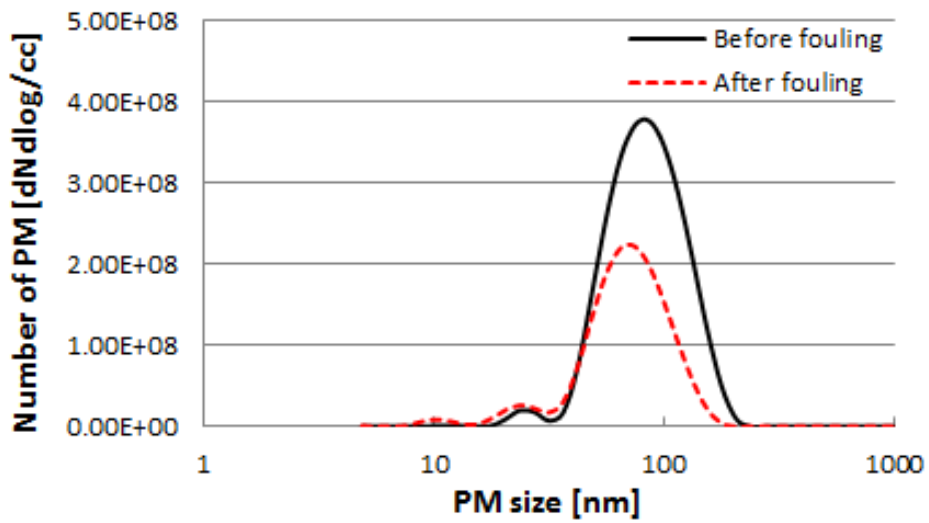
Figure 5.27 PM size distribution for equivalent NO$_x$ emission at 30kg/h.

Base specification # 3 (S & T type) type : 45kg/h

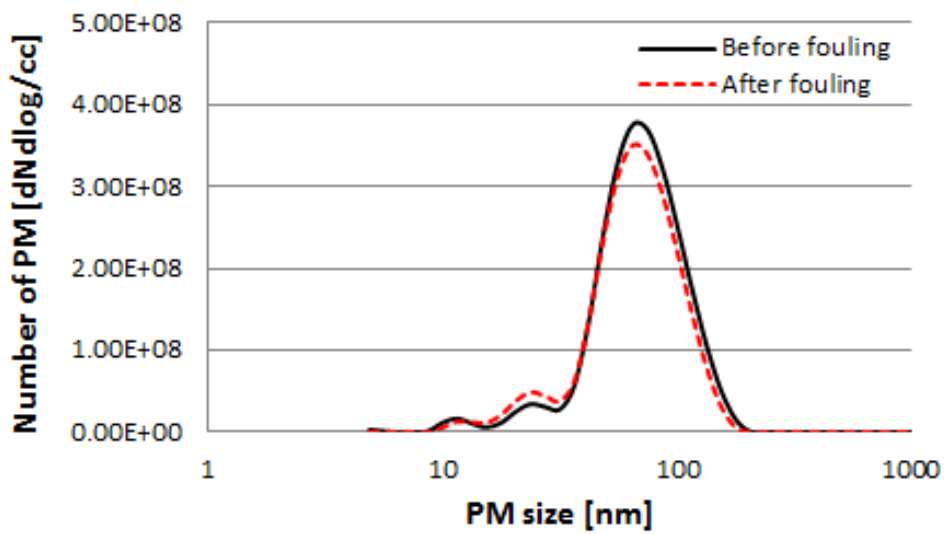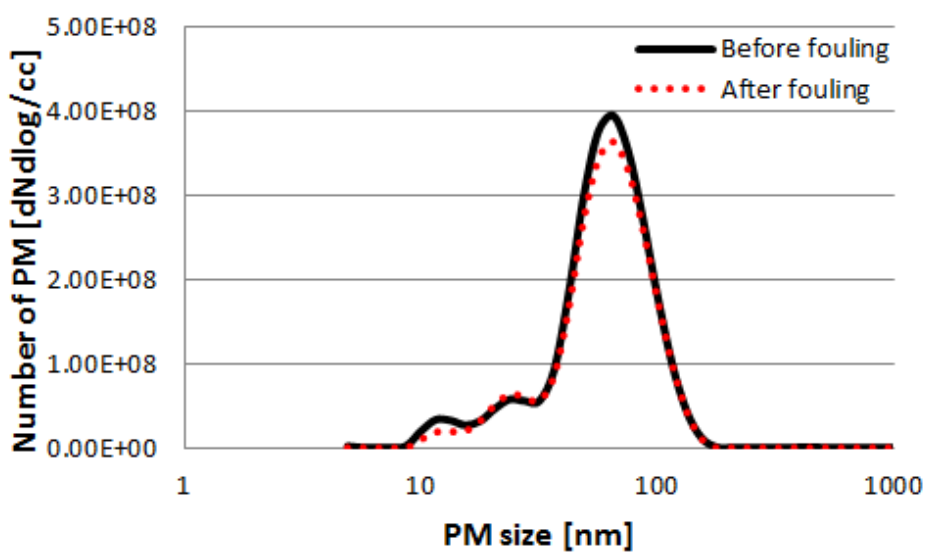| Speed	BMEP	Fuel cons.	Int. Air
1750rpm	4bar	16.8mg/st	88.3kg/h

Figure 5.28 PM size distribution for equivalent NO$_x$ emission at 45kg/h.

Modified specification # 4 (Fin type) : 47kg/h

Speed	BMEP	Fuel cons.	Int. Air
1750rpm	4bar	17.1mg/st	89.0kg/h
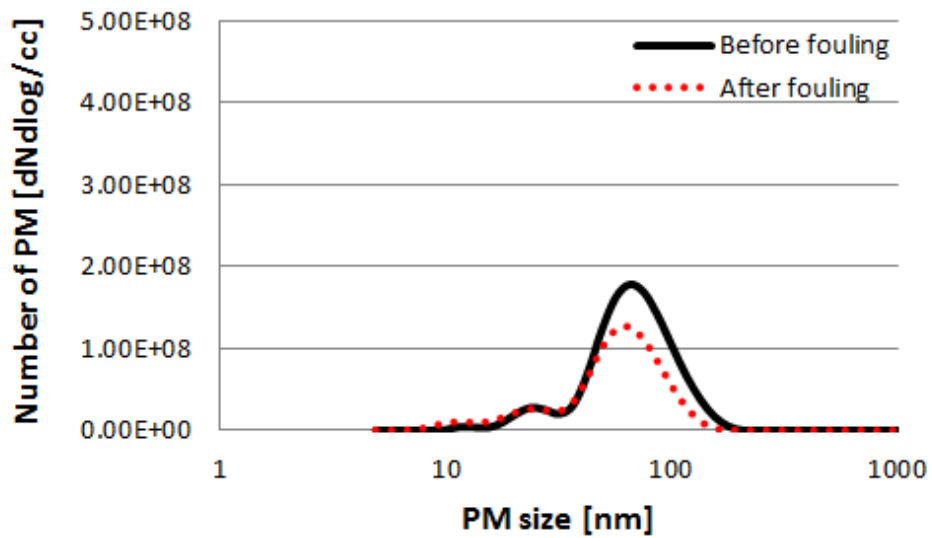
Figure 5.29 PM size distribution for equivalent NO$_x$ emission at 47kg/h.

5.2.6 Correlation of effectiveness between rig and engine

The correlation of thermal effectiveness of EGR cooler between test rig and real engine were analyzed before and after fouling.

Figure 5.30 shows the correlation of effectiveness of base specification #1 of I-flow EGR cooler (φ8.0 tube). At clean condition, there was effectiveness difference of 2.5% at 20kg/h. There was no significant effectiveness difference at other EGR mass even after fouling. Figure 5.31 shows the correlation of effectiveness of modified specification #2 of I-flow EGR cooler (φ7.5 tube).. At clean condition, there was reversal graph of effectiveness between rig and engine according to EGR mass increase. In general, the effectiveness differences were within max. 5%.

Figure 5.32 shows the correlation of effectiveness of base specification #3 of U-flow EGR cooler (φ8.0 tube). At clean condition, there was effectiveness difference of max. 5%. After fouling, there was effectiveness difference of max. 7% due to somewhat PM deposit. Figure 5.33 shows the correlation of effectiveness of modified specification #4 of U-flow EGR cooler (wavy fin). At clean and fouled conditions, the effectiveness differences were within max. 5%.

Figure 5.30 Base specification #1 of I-flow type (φ8.0 tube).
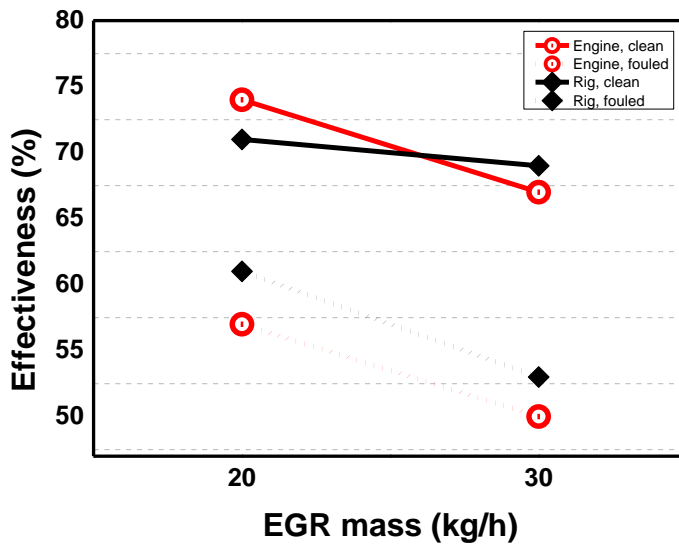
Figure 5.31 Modified specification #2 of I-flow type (φ7.5 tube).
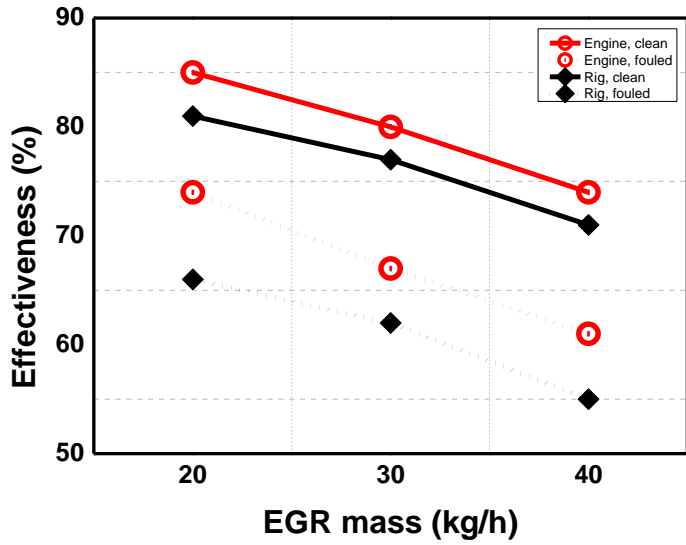
Figure 5.32 Base specification #3 of U-flow type (ϕ8.0 tube).
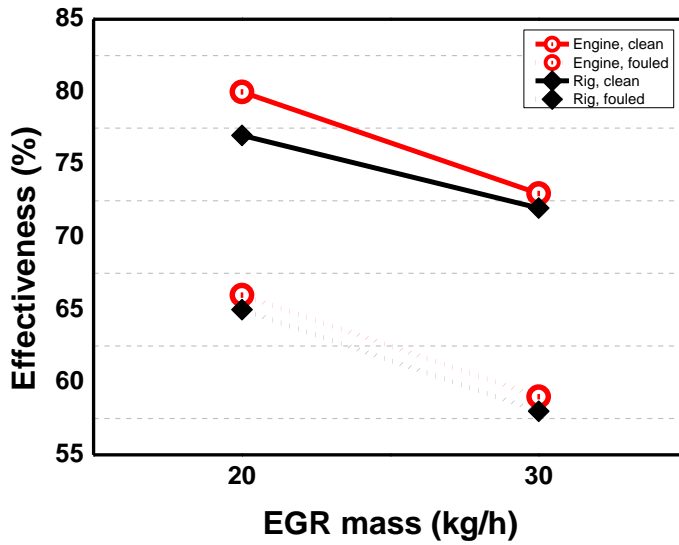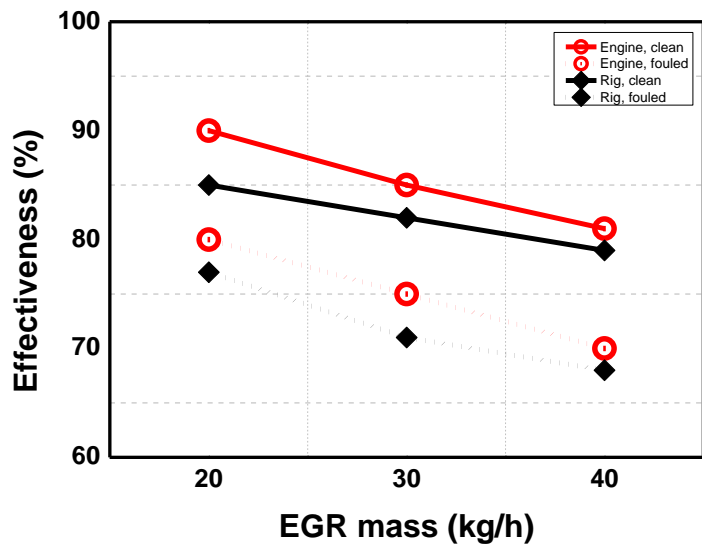

Figure 5.33 Base specification #3 of U-flow type (wavy fin).

Chapter 6. CFD analysis for virtual EGR cooler

6.1 Virtual modification of fin geometry

According to the research of Kim et al. [26], the modification of fin geometry, such as fin pitch and wave pitch in a small range of less than 10%, might be available in the improved thermal effectiveness despite a small increase in pressure drop. In order to confirm the better heat transfer effectiveness, the fin geometry of specification #4 was modified by CAD virtually for 8 cases as shown in Table 6.1 and CFD analysis were performed.

6.2 Results of CFD analysis

The input conditions of analysis are the same with base specification #4. Figure 6.2 shows the computational mesh of U-flow EGR cooler with virtually modified wavy fin. Figure 6.3 shows the temperature contours and pressure contours of exhaust gas flow in gas tubes for 8 cases.

As a result, Figure 6.4 shows the gas outlet temperatures, pressure drops and effectiveness of modified specifications. In conclusion, the optimal point for best thermal effectiveness corresponds to the case of fin pitch, 3.1mm and wave pitch, 8.6mm as shown in Figure 6.5.

Table 6.1 The virtual specifications of modified fin.

Case	Base	1	2	3	4	5	6	7	8
A (mm), Fin pitch	3.4	3.4	3.4	3.1	3.1	3.1	2.8	2.8	2.8
B (mm), Wave pitch	9.0	8.6	8.2	9.0	8.6	8.2	9.0	8.6	8.2
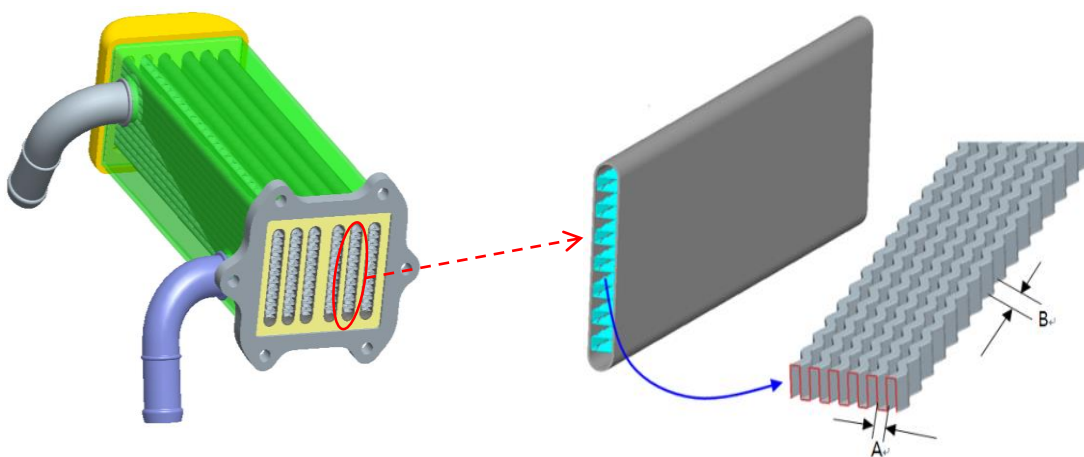
Figure 6.1 Virtual modification of fin geometry. .
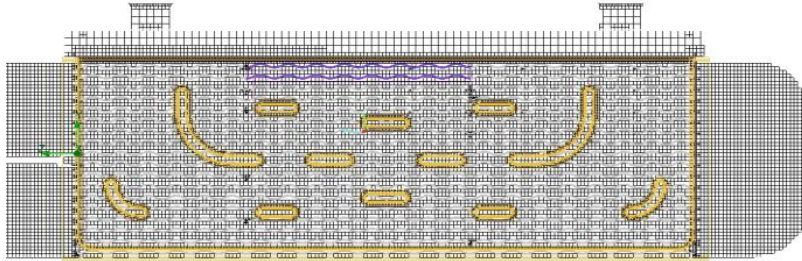
Figure 6.2 Computational mesh of EGR cooler (virtually modified Fin).
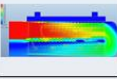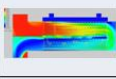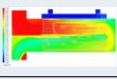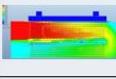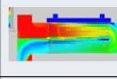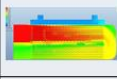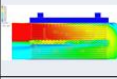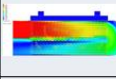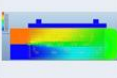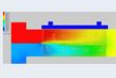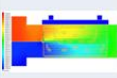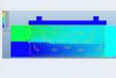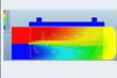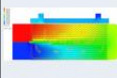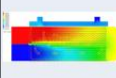
Case	1	2	3	4	5	6	7	8
Fin pitch, A (mm)	3.4	3.4	3.1	3.1	3.1	2.8	2.8	2.8
Wave pitch, B (mm)	8.6	8.2	9.0	8.6	8.2	9.0	8.6	8.2
Temperature contour								
Pressure contour								

Figure 6.3 CFD results based on fin geometry change.

Case	Base	1	2	3	4	5	6	7	8
Fin pitch, A (mm)	3.4	3.4	3.4	3.1	3.1	3.1	2.8	2.8	2.8
Wave pitch, B (mm)	9.0	8.6	8.2	9.0	8.6	8.2	9.0	8.6	8.2
Temperature, Gas outlet (℃)	139	133	144	137	128	139	148	144	151
Pressure drop (kPa)	4.9	5.1	5.4	5.1	5.3	5.9	6.0	6.3	6.5
Effectiveness (%)	86.0	88.0	85.0	87.0	89.5	86.0	84.0	85.0	83.0

Figure 6.4 Thermal effectiveness of CFD result.
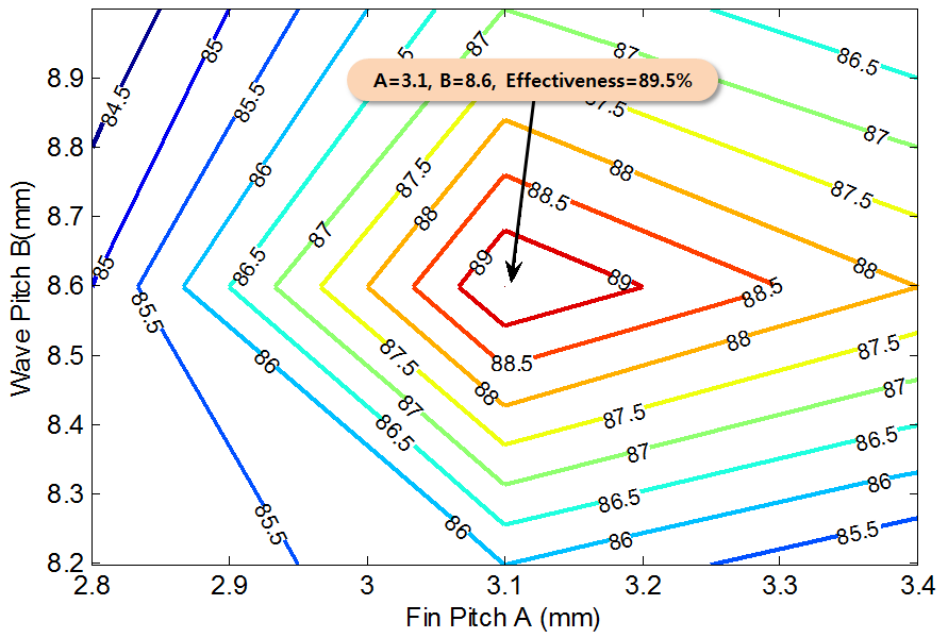
Figure 6.5 Optimal point for best effectiveness.

6.3 Validation process for the performance development of EGR cooler

There are 4 steps in validation process for performance of EGR cooler as shown in figure 6.6.

At first step, 3-D modeling is needed by using Auto-CAD or Pro-Engineer software. At next step, CFD analysis will be performed with 3-D model for the purpose of feasibility study to predict the performance of EGR cooler. Then, at third step, the EGR cooler will be tested in a test rig, which is a short term and cost saving process. However, the level of accuracy may be low and somewhat different from vehicle operating condition. At final step, the EGR cooler will be tested in an engine dynamometer, which is a long term and expensive process. The level of accuracy may be high and equivalent to vehicle operating condition. After completion of performance development, EGR cooler will be produced.
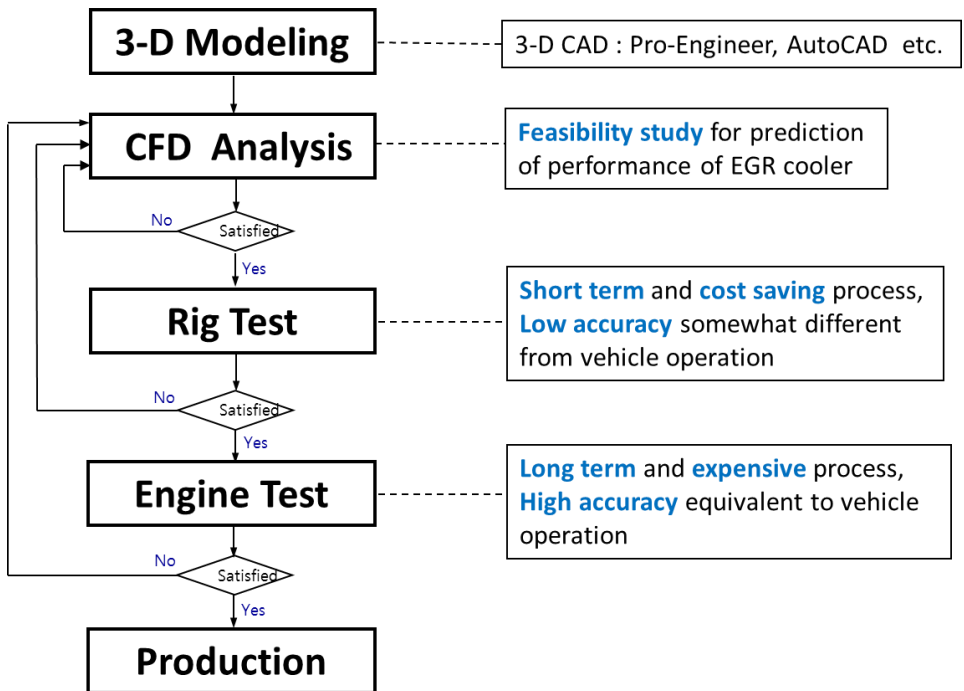
Figure 6.6 Validation process for the performance development of EGR cooler.

6.4 NO$_x$ trade-off as per improvement of effectiveness

There are positive and negative effects. For positive effect, the increase of surface area contacting coolant inside of EGR cooler enhances heat transfer and results in lowering gas outlet temperature and decreasing NO$_x$.

For negative effect, excessive increase of surface area contacting coolant inside of EGR cooler leads to narrow passage of gas and results in depositing PM inside tubes or fins and enhancing heat resistance. As a result, the pressure drop and gas outlet temperature will be increased and NO$_x$ will be emitted highly.

Further investigation of this trade-off relation will cause the optimization of EGR cooler design.

Chapter 7. Conclusions

In this study, the fouling characteristics which deteriorate the heat exchange effectiveness of EGR cooler was evaluated to cope with the recent stringent diesel emission regulations. Especially, there were no researches concerning the cross correlation on the fouling phenomena between a test rig and a real engine.

The design features of existing and modified EGR coolers were reviewed to maintain desired performance against fouling resistance. The behavior of fluid such as velocity vector, temperature and pressure contour of exhaust gases in an EGR cooler was analyzed through 3-D CFD. The results which consist of outlet temperatures, heat transfer effectiveness and pressure drops and so on were derived from using 2 kinds of EGR coolers in production and another 2 kinds of modified EGR coolers. These results were vital to predict the performance of EGR coolers. In case of I-flow EGR coolers, the effectiveness of base specification #1(ø8) is about 4% higher than that of modified specification #2(ø7.5). In case of U-flow EGR coolers, the effectiveness of base specification #3(shell & tube type) is about 3% lower than that of modified specification #4(fin type). In conclusion, the effectiveness of modified specification #4(fin type) is the best among them.

The characteristics of EGR coolers on a test rig were examined at clean and fouled conditions. Fouling resistances which are directly related to the thermal effectiveness were verified with gas velocities. The thermal effectiveness of 4 kinds of EGR coolers were investigated in test rig before and after fouling, respectively. Fouling resistance is also related with the deposit of PM. There is a threshold flow velocity which is about 30m/s to decrease fouling and stabilize the effectiveness. The velocity depends largely on the geometry design of tubes in EGR coolers.

In addition, the characteristics of EGR coolers on engine dynamometers were evaluated at clean and fouled conditions through the fouling test mode made from

ESC 13 procedure and proposal from an EGR cooler manufacturer. The thermal effectiveness of EGR coolers were also reviewed on the basis of test results.

The emission level of NOx and PM were investigated according to the EGR ratio. This work has the advantages to identify the changing rate of NOx and PM for the purpose of evaluation of EGR coolers.

Especially, when the emission levels of NO_x are nearly equivalent for specification #3 and specification #4, PM size and number of PM were measured in order to identify the superiority of heat transfer effectiveness of EGR cooler which resulted in increasing A/F by the cooling effect of an EGR cooler before and after fouling.

For the further confirmation, virtual modification of fin geometry through 3-D CAD was conducted. The virtual fin has 3.1mm of fin pitch and 8.6mm of wave pitch, which were decreased less than 10% compared with the specification #4. From the CFD analysis, the heat transfer effectiveness was confirmed about 3.5% higher than that of specification #4.

It can be concluded that fouling deposit layer on the wall surface of EGR cooler can have a huge impact on the performance and some important variables are summarized as follows,

- The stabilized thermal effectiveness against fouling resistance is driven by the removal forces which are a function of gas velocity near the wall

- The gas velocity may be higher than the critical flow velocity of 30m/s

- This velocity depends largely on the good geometry design of core parts, such as fin or shell and tube

It is found that the wavy fin type EGR cooler reveals the best effectiveness regarding heat transfer and fouling prevention. This study can suggest not only understanding for the fouling characteristics of EGR cooler but also validation for reduction of NO_x and PM.

Bibliography

[1] Benajes, J., Molina, S., Garcia, J. Influence of pre-and post-injection on the performance and pollutant emissions in a HD diesel engine. SAE paper, 2001-01-0526. 2001.

[2] Park, W., Choi, S., Chung, S., and Ha, J. A study on exhaust characteristics in HIDI diesel engine applied EGR cooler. Proceeding of KSAE 2003 Fall Conference, 2003; 393-397.

[3] Kakoi, K., Tsutsui, Y., Ono, N., Umezaya, K., and Kondo, N. Emission reduction technologies applied to high-speed direction injection diesel engine. SAE paper, 980173. 1988.

[4] Bond, M. Emission from heavy duty vehicles: Health and environmental implications and legislative remedies. 8th International Symposium on Heavy Vehicle Weights.2004; 1-13.

[5] Kouremenos, D. A, Hountalas, D. T., Binder, K. B. The effect of EGR on the performance and pollutant emission of heavy duty diesel engines using constant and variable AFR. In: proceedings of SAE 2001, 2001-01-0198.

[6] Kouremenos, D. A, Hountalas, D. T., Binder, K. B., Raab A., and Schnabel, M. H. Using advanced injection timing timing and EGR to improve DI diesel engine efficiency at acceptable NO and soot levels. In: proceedings of SAE 2001, 2001-01-0199.

[7] Maiboom, A., Tauzia, X., and Hetet, J. F. Influence of EGR unequal distribution from cylinder to cylinder on NOx–PM trade-off of a HSDI automotive Diesel engine. Applied Thermal Engineering; 29:2043-2050.

[8] Adb-Elhady, M.S., Zornek, T. et al. Influence of gas velocity on particulate fouling of exhaust gas recirculation coolers. International Journal of Heat and Mass Transfer. 2011;54:838-846.

[9] Mori, K., Matsuo, S., Nakayama, S., Shiino, S., Kawatani, T., Nakashima, K. et al. Technology for environmental harmonization and future of the diesel engine. SAE Paper, 2009-01-0318. 2009.

[10] Moon, B., Oh, Y., Oh, S.,Kang, K., and Ahn, K. A study on heavy-duty diesel engine

performance with CR-DPF and cooled-EGR. Trans. KSAE 2006;14(3):75-80.

[11] Hoard, J., Abarham, M., Styles, D., Giuliano, J. M., Sluder, C. S., Storey, J. Diesel EGR cooler fouling. SAE paper, 2008-01-2475. 2008.

[12] Zhang, F., Nieuwstadt, M. Adaptive EGR cooler pressure drop estimation. SAE paper, 2008-01-0624. 2008.

[13] Bobba, M. K., Genzale, C. L., and Musculus P. B. Effect of iginition delay on in-cylinder soot characteristics of a heavy duty diesel engine operating at low temperature conditions. SAE paper, 2009-01-0946. 2009.

[14] Kumar, R., and Zheng, M. Fuel efficiency improvement of low temperature combustion diesel engine. SAE paper, 2008-01-0841. 2008.

[15] Cong, S., McTaggart-Cowan, G., and Garner, C. Effects of fuel injection parameters on low temperature diesel combustion stability. SAE paper, 2010-01-0611. 2010.

[16] Collura, S., Chaoul, N., Azambre, B. et al. Influence of the soluble organic fraction on the thermal behavior, texture and surface chemistry of diesel exhaust soot. Carbon. 005; 43:605-613.

[17] Muller, J. O., Su, D. S., Jentoft, R. E., Wild, U., and Schlogl, R. Diesel engine exhaust emission: Oxidative behavior and microstructure of black smoke soot particulate. Environmental Science and Techlonogy. 2006; 40: (4) 1231-1236.

[18] Neer, A., Koylu, U. M. Effect of operating conditions on the size, morphology, and concentration of submicrometer particulates emitted from a diesel engine. Combustion and Flame. 2006; 146: 142-154.

[19] Maiboom A, Tauzia X, Hétet JF. Influence of high rates of supplemental cooled EGR on NOx and PM emissions of an automotive HSDI diesel engine using an LP EGR loop. International Journal of Energy Research. 2008;32(15):1383-98.

[20] Ladommatos N, Abdelhalim S, Zhao H, Hu Z. The Dilution, Chemical, and Thermal Effects of Exhaust Gas Recirculation on Diesel Engine Emissions-Part 4: Effects of Carbon Dioxide and Water Vapour (971660). PROGRESS IN TECHNOLOGY. 2002;89:173-92.

[21] Nitu B, Singh I, Zhong L, Badreshany K, Henein N, Bryzik W. Effect of EGR on autoignition, combustion, regulated emissions and aldehydes in DI diesel engines. SAE

paper, 2002-01-1153. 2002.

[22] Jacobs T, Assanis D, Filipi Z. The impact of exhaust gas recirculation on performance and emissions of a heavy-duty diesel engine. SAE paper, 2003-01-1068. 2003.

[23] Maiboom A, Tauzia X, Hétet JF. Influence of high rates of supplemental cooled EGR on NOx and PM emissions of an automotive HSDI diesel engine using an LP EGR loop. International Journal of Energy Research. 2008;32(15):1383-98.

[24] Grillot, J. M., Icart, G. Fouling of a cylinderical probe and a finned tube bundle in a diesel exhaust environment. Experimental Thermal and Fluid Science. 1997; 14: 442-454.

[25] Storey, J. M. E., Sluder, C. S., and Michael, J.L. Exhaust gas recirculation cooler fouling in diesel application: Fundamental studies of deposit properies and microstructure. Heat Transfer Engineering. 2013; 34: 655-664.

[26] Kim, H. M., Park, S. K., Choi, K. S., Wang, D. H., Lee, D. H., Lee, D. K., Cha, Y. S., Lee, J. S., and Lee, J. Investigation on the flow and heat transfer characteristics of diesel engine EGR coolers. International Journal of Automotive Technology. 2008; 9(2):149-153.

[27] Zhang, R., Charles, F., Ewing, D., Chang, J. S., Cotton, J. S. Effect of diesel soot deposition on the performance of exhaust gas recirculation cooling devices. SAE paper, 2004-01-0122. 2004.

[28] Zahn, R., Eakle, S. T., Miller, J. W. EGR system fouling control. SAE paper, 2008-01-0066. 2008.

[29] www.dieselnet.com.

[30] www.seekingalpha.com.

[31] Cabrejos, F. J., Klinjing, G. F. Incipient motion of solid particles in horizontal pneumatic conveying. Power Technol. 1992; 72: 51-61.

[32] Halow, J. S. Incipient rolling, sliding and suspension of particles in horizontal and inclined turbulent flow. Chem. ENG. Science. 1973; 28: 1-12.

[33] Abd-Elhady, M. S., Malayeri, M. R., and Muller-Steinhagen, H. Fouling problems in exhaust gas recirculation coolers in the automotive industry. Heat Transfer Engineering. 1990; 11: 73-107.

[34] Chenoweth, J. M. Final report of HTRI/TEMA joint committee to review the fouling section of the TEMA standards. Heat Transfer Engineering. 2011; 32: 248-257.

[35] Kumar, N., Krishnan, S., and Thasan, N. Effects of fouling in EGR coolers in automobiles-a review study. IJIR in science, Engineering and Technology. 2013; 2: 3024-3032.

[36] Talbot, L. et al., Thermophoresis of particles in a heated boundary layer. Journal of Fluid Mechanics. 1980; 01 (4):737-758.

[37] Sluder, C. S., Storey, J., Lewis, D., Styles, D., Giuliano, J., and Hoard, J. Hydrocarbons and particulate matter in EGR cooler deposits: Effect f gas flow rate, coolant temperature, and oxidation catalyst. SAE paper, 2008-01-2467. 2008.

[38] Girard, J. W., Gratz, L. D., Johnson, J. H., Bagley, S. T., and Leddy, D. G. A study of the character and deposition rates of sulfur species in the EGR cooling system of a heavy-duty diesel engine. SAE paper, 1999-01-3566. 1999.

[39] Warey, A., Balestrino, S., Szymkowicz, P., and Malayeri, M. R. A one dimensional model for particulate deposition and hydrocarbon condensation in exhaust gas recirculation coolers. Aerosol Science and Technology. 2012; 46:198-213.

[40] Kakac, S., Bergles, A. E., and Mayinger, F. Heat exchangers, Hemisphere Publishing, New York, 1981.

[41] Kakac, S., Shah, R. K., Bergles, A. E. Low Reynolds number flow heat exchangers, Hemisphere Publishing, New York, 1983.

[42] Kays, W. M., London, A. L. Compact heat exchangers, 3rd ed., McGraw-Hill, New York, 1984.

[43] Digiovanni, M. A., Webb, R. L. Heat Transfer Engineering. 1989; 10: 61.

[44] Webb, R. L. Heat Exchanger Design Handbook, Section 3.9. New York, 2002.

[45] Incropera, Frank P., Dewitt, David P. et al. Introduction to heat transfer. 5th ed. 2005.

[46] Incropera, Frank P., Dewitt, David P. et al. Heat and mass transfer. 5th ed. 2005.

[47] Holman JP. Heat transfer. 9th edn. McGraw-Hill. 2002. Experimental Thermal and Fluid science. 2013; 44: 275-284.

[48] Liu, L., Ling, X., and Peng, H. Analysis on flow and heat transfer characteristics on oler helical baffled cooler with spiral corrugated tubes.

[49] Abarham, M., Zamankhan, P., Hoard, J. W. and et. al. CFD analysis of a particle transport in axi-symmetric tube flows under the influence of thermophoretic force. Internal journal of heat and mass transfer. 2013; 61: 94-105. EGR co

[50] Paterson, J., Larpent, S., Fernandez, N., Kunel, W., Lang, C., Brotz, F., and Heckenberger, T. Transient CFD simulation of exhaust gas recirculation coolers for further structural analyses. SAE paper, 2009-01-1228. 2009.

[51] Duraisamy, s., Bhaleghare, S. S., Sundaralingam, S. et al. Optimization of an Exhaust Gas Recirculation Cooler using CFD Technique. ISCA J. Engineering Sciences. 2012; 01: 62-67.

[52] Millo, F., Giacominetto, P. F., and Bernardi, M. G. Analysis of different exhaust gas recirculation architectures for passenger car diesel engines. Applied energy. 2012; 98: 79-91

[53] Nagendra, K., Tafti, D. K., and Viswanathan, A. K. Modeling of soot deposition in wavy-fin exhaust gas recirculator coolers. International J. Heat and Mass Transfer. 2011; 64: 1671-1681.

[54] Yang, Y. S. et al. Thermodynamic performance simulation of diesel EGR cooler with finned tube. Advanced Materials Research. 2010; 97-101: 3345-3348.

[55] Mon, M. S., Gross, U. Numerical study of fin-spacing effects in annular-finned tube heat exchangers. International J. Heat and Mass Transfer. 2004; 47: 1953-1963.

[56] Chen, H. T., Chou, J. C. Investigation of natural-convection heat transfer coefficient on a vertical square fin of finned-tube heat exchangers. International J. Heat and Mass Transfer. 2006; 49: 3034-3044.

[57] Li, Z., Davidson, J.H., and Mantell, S.C. Heat transfer enhancement using shaped polymer tubes fin analysis. International J. Heat Transfer. 2004; 126: 211-218.

[58] Wentzel, M. Gorzawski, H. et al. Transmission electron microscopic and aerosol dynamical characterization of soot aerosols. J. Aerosol Science. 2003; 34(10): 1347-1370.

[59] White, F. M. Fluid mechanics (5th ed.). McGraw-Hill. 2003.

[60] Yaws, C. L. Yaw's transport properties of chemicals and hydrocarbons (Electronic ed.), Knpvel, New York. 2010.

[61] Yung, B. P. K., Merry, H., and Bott, T. R. The role of turbulent bursts in particle re-entrainment in aqueous systems. Chem. Eng. Sci. 1989; 44(4); 873-882.

[62] Yung, B. P. K., Merry, H., and Bott, T. R. Effects of particle-surface interaction on deposition and re-entrainment of a particle fouling system. Geothermics. 1989; 18; 327-335.

[63] Epstein, N. Elements of particle deposition onto nonporous surfaces parallel to suspension flows. Experimental Thermal and Fluid Science. 1997; 14(4): 323-334.

[64] Gokoglu, S. A., Rosner, D. E. Thermophoretically augmented mass transfer rates to solid wall across laminar boundary layers. American I. Aeronautics J.1986; 24:172-179.

[65] Bohnet, M. Fouling of heat transfer surfaces. Chem. Eng. Technology. 1987; 10: 113-125.

[66] Paz, C., Suarez, E., Eiris, A., and Porteiro, J. Experimental evaluation of the critical local wall shear stress around cylindrical probes fouled by diesel exhaust gases. Exp. Thermal and Fluid Science. 2012; 38: 85-93.

[67] Soltani, M., Ahmadi, G. On particle adhesion and removal mechanisms in turbulent flows. J. Adhesion Science and Technology. 1994; 8: 763-785.

[68] Rabinovich, E., Kalman, H. Incipient motion of individual particles in horizontal particle–fluid systems. Powder Technology. 2009; 192: 326-338.

[69] Stevenson, P., Thorpe, R. B., and Davidson, J. F. Incipient motion of small particle in the viscous boundary layer at a pipe wall. Chemical Engineering Science. 2002; 57: 4505-4520.

[70] Sharma M.M., Chamoun H., sarma D., Schechter R. S. Factors controlling the hydrodynamic detachment of particles from surfaces. Colloid Interface Sci. 1992; 149: 121-134.

[71] Hubbe M. A. Theory of detachment of colloidal particles from flat surfaces exposed to flow. Colloid Surface. 1984; 12: 151-178.

[72] Zhang F., Busnaina A. A., Fury M. A., Wang S. Q. The removal of deformed submicon particles from silicon wafer by spin rinse and megasonics. J. Electron. Mater. 2000; 29: 199-204.

[73] Heywood JB. Internal combustion engine fundamentals. 1988.

[74] Love, N. D., Szybist, J. P., and Sluder, C. S. Effect of heat exchanger material and fouling on thermoelectric exhaust heat recovery. Applied Energy. 2012; 89: 322-328.

[75] Sluder, C., Storey, J., and Youngquist, A. ULSD and B20 hydrocarbon impacts on EGR cooler performance and degradation. SAE paper, 2009-01-2802. 2009.

[76] Hausberger, S., Rexeis, M. Emission behaviour of modern heavy duty vehicles in real world driving. International Journal of Environment and Pollution. 2004; 22: 275-286.

[77] Osada, H., Aoyagi, Y., Shimada, K., Goto, Y. et al. Reduction of NOx and PM for a Heavy Duty Diesel Using 50% EGR Rate in Single Cylinder Engine. SAE paper, 2010-01-1120. 2010.

초 록

최근 수년 동안, 고속 직접분사식 디젤엔진이 양호한 연비, 높은 열효율과 매우 낮은 이산화탄소배출 등에 기인하여 RV, SUV 및 승용차에 많이 적용되어 오고 있다. 그러나, 지구온난화와 같은 세계적인 환경문제로 인하여 승용디젤차량에 대한 배기가스규제, 특히 질소산화물(NOx)과 입자상 물질(PM)에 대한 강화가 선도되고 있다. 예를 들어, 2014 년부터 적용되는 Euro-6 배기규제는 현행 Euro-5 배기규제보다 NOx를 56% 더 저감해야만 한다.

배기재순환(EGR)장치는 엔진 본체의 큰 변경 없이 NOx 를 줄이기 위해 디젤엔진에 널리 적용되어 오고 있다. EGR 의 기본 원리는 연소실 내의 화염온도와 작동유체의 산소 농도를 낮추어 NOx 를 저감한다. EGR 밸브를 사용하여 배기가스를 재순환시키는 기존의 시스템은 NOx 를 저감시키기는 하지만 PM 을 증가시킴으로써 그 효율성에 변화가 요구된다. 그러므로, 이런 단점을 보완하기 위해 시스템변경이 필요하다. 최근, 새로운 EGR cooler 시스템에 의해 NOx 를 저감시키면서 동시에 PM 과 연비악화의 단점을 극복할 수 있는 다양한 연구들이 활발히 진행되고 있다.

엄격한 Euro-6 의 NOx 규제를 만족하기 위해서 높은 EGR 율을 사용하는 것이 보다 중요하다. 높은 EGR 율을 적용하면 PM 은 불가피하게 증가된다. 실제로, 배기가스 내에 PM 농도가 증가하면 EGR cooler 의 내부표면에 PM 퇴적이 비교적 용이해진다. 이것이 EGR cooler 의 열전달 효율을 떨어뜨리고 압력강하를 증가시키는 이른바, 파울링(fouling)이다. 결과적으로 NOx 저감율과 엔진성능이 저하된다. 한편, 저온연소 및 초고압 연료분사장치와 같은 고속 직접분사식 디젤엔진에 사용되고 있는 최근 연소기술은 EGR cooler 의 내부표면에 보다 더 작은 입자들의 퇴적으로 인해 심각한 파울링 현상을 초래하고

있다. 따라서, EGR cooler 의 파울링에 대하여 많은 연구가 되고 있으나, 리그시험과 실 엔진간의 파울링 현상에 대한 상관성 연구는 거의 없었다.

본 연구에서는 파울링 저항에 대한 바람직한 열전달 성능을 유지하기 위하여 기존 및 사양 변경한 EGR cooler 들의 설계 특징을 평가하였다. 3 차원 전산유체해석을 통해 EGR cooler 내 가스의 속도벡터, 온도 및 압력 구배 등을 분석하였다. 그 결과, 생산 중인 2 종과 사양 변경한 2 종의 EGR cooler 에 대하여 출구온도 및 열전달 효율을 예측하였다.

리그시험기로 파울링 전, 후 상태에서 EGR cooler 들의 특성을 조사하였다. 이 단계에서 열 전달효율에 직접 관련된 파울링 저항들을 가스속도 별로 평가하였다. 그리고, 엔진 동력계에서 EGR cooler 들의 특성을 조사하였다. 파울링 시험모드는 ESC-13 모드와 EGR cooler 제조사의 자료에 근거하여 정하였다. 배기가스 유량에 따라 열전달 효율 및 압력강하 특성을 검토하였다. EGR 율에 따른 NO_x 및 PM 의 배출수준에 대한 분석 작업도 추가로 수행하였다. 이 분석은 EGR cooler 의 평가를 위하여 NO_x 및 PM 의 변화를 확인할 수 있는 장점을 가지고 있다.

이상과 같이 설계평가, 리그 및 엔진 시험의 각 단계별로 EGR cooler 들의 파울링 특성을 평가하였다. 이 결과를 토대로, 개선된 설계사양에 대한 전산유체해석을 통하여 효율성을 검증하였다. 이러한 연구에 의해, 파울링에 우수한 특성을 갖는 EGR cooler 의 적절한 설계방안을 제안할 수 있게 되었다.

주요어: 배기재순환, 고속직접분사식 디젤엔진, 질소산화물, 입자상 물질, 배기재순환 냉각기, 파울링, 열전달효율

학번: 2011-30207